

# Quantum doubles in symmetric blockade structures

Hans Peter Büchler,<sup>\*</sup> Tobias F. Maier, Simon Fell, and Nicolai Lang<sup>†</sup>

*Institute for Theoretical Physics III and Center for Integrated Quantum Science and Technology,  
University of Stuttgart, 70550 Stuttgart, Germany*

(Dated: November 7, 2025)

Exactly solvable models of topologically ordered phases with non-abelian anyons typically require complicated many-body interactions which do not naturally appear in nature. This motivates the “inverse problem” of quantum many-body physics: given microscopic systems with experimentally realistic two-body interactions, how to design a Hamiltonian that realizes a desired topological phase? Here we solve this problem on a platform motivated by Rydberg atoms, where elementary two-level systems couple via simple blockade interactions. Within this framework, we construct Hamiltonians that realize topological orders described by non-abelian quantum double models. We analytically prove the existence of topological order in the ground state, and present efficient schemes to prepare these states. We also introduce protocols for the controlled adiabatic braiding of anyonic excitations to probe their non-abelian statistics. Our construction is generic and applies to quantum doubles  $\mathcal{D}(G)$  for arbitrary finite groups  $G$ . We illustrate braiding for the simplest non-abelian quantum double  $\mathcal{D}(S_3)$ .

The ground state phase diagrams of quantum many-body systems at zero temperature can be extremely rich. Of special interest are quantum phases with properties that are unique to quantum systems. One of the most intriguing examples are topologically ordered phases of two-dimensional systems which are characterized by their pattern of long-range entanglement [1–4]. It is the entanglement structure of these gapped ground states which entails anyonic statistics of excitations and robust ground state degeneracies on topologically non-trivial manifolds. While topological phases with abelian anyonic excitations have useful applications as quantum error correction codes [5–7], phases with non-abelian excitations are of special interest due to their higher-dimensional braid group representations, which makes them potential substrates for topological quantum computing [8–10]. While there is general consensus that some fractional quantum Hall states are natural examples of topological orders with abelian anyons [11, 12], the appearance and realization of non-abelian phases in fractional quantum Hall states or artificial matter is much more challenging [9, 13, 14]. Especially the experimental detection of their characteristic entanglement structure (e.g., by probing the anyonic braiding statistics) is still an open problem. Meanwhile, on the theory side, there are thoroughly explored models that give rise to a large variety of topological orders with non-abelian anyons. Examples are Chern-Simon theories for fractional quantum Hall states [15–17], Kitaev’s quantum double models [5], and string-net condensates [18, 19], as well as other minimalistic models [20, 21]. Unfortunately, most of these models rely on non-trivial multi-body interactions which do not naturally appear in nature – a major roadblock to experimentally explore these topological orders. This motivates the inverse problem of

quantum many-body physics: provided a platform with experimentally realistic interactions and tunability of elementary degrees of freedom, is it possible – and if so how – to engineer quantum systems that naturally realize interesting quantum many-body ground states? In this paper, we consider systems characterized by a two-body blockade interaction and show how these can be used to systematically engineer microscopic models that realize a large class of non-abelian topological orders.

In recent years, a major goal has been to realize and probe topological phases in artificial matter. In condensed matter settings,  $p$ -wave superconductors are promising for the realization of Majorana zero modes, either on the boundaries of wires [22, 23] or in the core of vortices [24, 25], while recent progress with two-dimensional van der Waals materials opens a pathway towards fractional Chern insulators [26–29]. The framework of quantum simulation provides another promising approach, where a variety of systems based on cold atomic and molecular gases have been put forward. First theoretical proposals focused on the realization of Kitaev’s honeycomb model [20] in optical lattices [30] or using a spin toolbox realized by polar molecules [31]. Other proposals target the realization of fractional quantum Hall states with rotating gases [32], Majorana modes in double wires [33] and  $p$ -wave superfluids [34], and bosonic fractional Chern insulators with polar molecules [35] and Rydberg atoms [36]. In particular Rydberg atoms have emerged as promising platform to study topological phases, with the first experimental observation of a symmetry protected topological phase in one-dimension [37], and attempts to probe a  $\mathbb{Z}_2$  spin liquid with toric code topological order [38, 39]. (Although the experimentally observed signatures are most likely due to dynamical state preparation, rather than ground state properties of the engineered Hamiltonian [40, 41].) The advantage of the Rydberg platform is the high flexibility to arrange atoms in arbitrary two- [42–44] and three-dimensional geometries [45], local optical access to individual atoms, a large freedom to select inter-

<sup>\*</sup> [hans-peter.buechler@itp3.uni-stuttgart.de](mailto:hans-peter.buechler@itp3.uni-stuttgart.de)

<sup>†</sup> All authors contributed equally to the theoretical analysis and the writing of this manuscript.

nal states to engineer microscopic Hamiltonians, as well as strong van der Waals and dipolar exchange interactions between different Rydberg levels [46–48]. Notably, the strong van der Waals coupling can often be modeled by a simple blockade interaction [44, 49–55]: a strong (infinite) interaction on distances shorter than a (tunable) blockade radius, and a vanishing interaction on larger distances. The simplicity of this coupling makes Rydberg atoms a versatile platform for the bottom-up design of artificial quantum matter.

In this paper, we use a framework inspired by the Rydberg platform to design microscopic Hamiltonians with ground states that are in the topological phase of Kitaev’s paradigmatic quantum double models (of which the toric code is the simplest example [5]). The latter are characterized by a finite group  $G$  and, for non-abelian groups, their topological order supports non-abelian anyonic excitations. Our framework is based on microscopic two-level systems, arranged in a periodic two-dimensional structure, with local detunings, local transverse fields, and simple two-body blockade interactions. The approach presented here is the natural extension to arbitrary groups  $G$  of the construction presented in Ref. [56] for the abelian group  $\mathbb{Z}_2$ . The main idea is that blockade interactions can be abstractly described by vertex-weighted *blockade graphs*, and the design of these graphs can be guided by two crucial insights. First, ground states map to *maximum-weight independent sets* and satisfy local constraints that are encoded in the topology of these graphs. And second, blockade graphs can feature *local graph automorphisms* that translate to local unitary symmetries of the Hamiltonian, which, in turn, enforce strong quantum fluctuations within the subspace of states that satisfy the local constraints. While closely related models with local symmetries have been recently proposed [57–61], the Hamiltonians introduced here allow for a rigorous proof that their ground state is in the topological phase of the prescribed quantum double  $\mathcal{D}(G)$  for weak transverse fields. Furthermore, a spectral gap to flux anyons can be proved in the thermodynamic limit, while a finite charge gap is expected as well, but much more challenging to show rigorously [62]. Leveraging this framework, we propose an efficient scheme to adiabatically prepare these ground states, together with a controllable procedure to prepare states with localized anyonic excitations. Finally, we propose an efficient protocol for the adiabatic braiding of anyons to experimentally probe their non-abelian statistics. While our construction is generic and works for arbitrary groups  $G$ , we illustrate the braiding protocol for the simplest non-abelian quantum double  $\mathcal{D}(S_3)$ . The proposed construction and protocols pave the way towards probing non-abelian topological orders in artificial matter with realistic two-body interactions. While our approach is inspired by the Rydberg platform, our formulation is platform-agnostic and allows for alternative realizations, e.g., with polar molecules in optical tweezers [63] or superconducting qubits connected by microwave cavities acting as a bus to mediate blockade interactions [64].

## I. THE MODEL

We consider extensive *blockade structures*  $\mathcal{G}$  of two-level systems arranged in space. We denote the total Hilbert space of such a structure by  $\mathcal{H}_{\mathcal{G}}$ . The two-level systems  $i$  are subject to a uniform transverse field  $\Omega$  and local detunings  $\Delta_i$ , and interact via an isotropic Blockade potential [44, 49–55]; i.e., their interaction vanishes at large distances and saturates at a value  $U_0$  on distances shorter than a blockade radius  $r_B$ :

$$U(r) := \begin{cases} 0 & \text{for } r > r_B, \\ U_0 & \text{for } r \leq r_B. \end{cases} \quad (1)$$

Note that in the context of blockade interactions,  $U_0$  is often set to infinity. Here we keep it as free but large parameter which has no effect on our results but makes rigorous statements easier to prove. The simplicity of the blockade potential (1) suggests encoding the spatial arrangement of a structure  $\mathcal{G}$  by a *vertex-weighted blockade graph*  $\mathcal{G} \equiv (V, E, W)$ : The two-level systems  $i \in V$  form the *vertices*  $V$  of the graph, so that the Hilbert space of the structure has the form  $\mathcal{H}_{\mathcal{G}} = (\mathbb{C}^2)^{\otimes |V|}$ . The detunings are interpreted as the *weights*  $W \equiv \{\Delta_i\}$  of the vertices, and the *edges*  $e = \{i, j\} \in E$  of the graph denote pairs of two-level systems that are in blockade (i.e., are separated by less than the blockade radius  $r_B$ ).

With these conventions, the Hamiltonian associated to a blockade structure/graph  $\mathcal{G}$  has the form

$$H_{\mathcal{G}} = H_{\mathcal{G}}^0 + \Omega \sum_{i \in V} \sigma_i^x$$

with  $H_{\mathcal{G}}^0 = U_0 \sum_{\{i,j\} \in E} n_i n_j - \sum_{i \in V} \Delta_i n_i,$  (2)

where  $\sigma_i^\alpha$  denotes the Pauli matrices for each two-level system and  $n_i = (1 - \sigma_i^z)/2$  is the projector onto the state  $|1\rangle_i$ . The summation of the interaction term in (2) runs over all pairs  $\{i, j\} \in E$  of sites which are connected by an edge of the blockade graph  $\mathcal{G}$ . Clearly there exists a one-to-one correspondence between Hamiltonians of the form (2) and vertex-weighted graphs  $\mathcal{G}$  for every transverse field  $\Omega$ . However, note that not every abstract graph can be realized as blockade graph of a spatial structure in two or three dimensions. The Hamiltonian (2) belongs to the class of transverse field Ising models in the presence of a site dependent longitudinal field  $\Delta_i$ . The complexity and versatility of this family of Hamiltonians (e.g., to realize non-abelian topological phases) is hidden in the spatial arrangement of the two-level systems, and therefore the choice which pairs of two-level systems are in blockade.

We now present a generic construction of a family of blockade graphs  $\mathcal{G}$  such that the ground states of the corresponding Hamiltonians (2) realize all topological phases of Kitaev’s quantum double models [5, 65–69], defined on a honeycomb lattice with trivalent sites (Fig. 1). These models are derived from a finite group  $G$  of order  $N = |G|$ . To each element  $g \in G$  a quantum state  $|g\rangle$

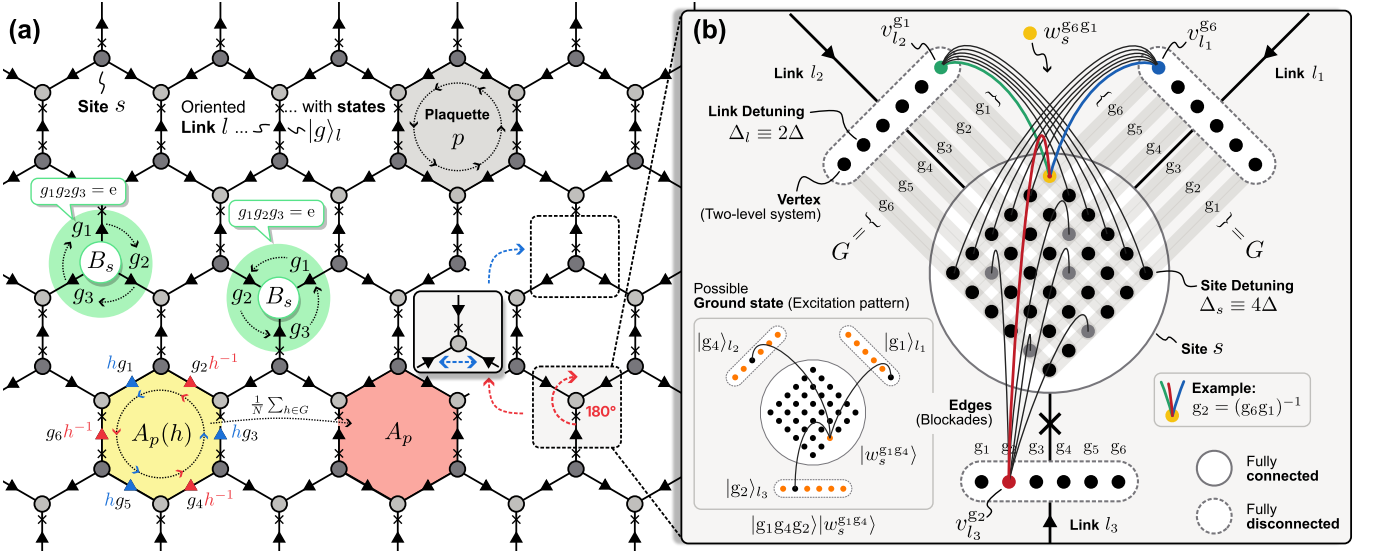


**Figure 1. Conventions and Construction.** (a) We construct quantum doubles (3) for a finite group  $G$  on the trivalent and bipartite honeycomb lattice. By convention, the links of the lattice are assigned an orientation (solid arrows). Every link  $l$  is associated with a  $N = |G|$ -dimensional quantum system with one state  $|g\rangle_l$  for each group element  $g \in G$ . Each plaquette  $p$  is assigned a counter-clockwise orientation (dotted arrows). With this convention, a plaquette  $p$  is on the left (right) of a bounding link  $l$  [write  $l \in p \uparrow$  ( $l \in \uparrow p$ )], if the link's orientation is parallel (antiparallel) to the orientation of the plaquette. On each site  $s$ , we define a projector  $B_s$  that singles out states that satisfy the no-flux condition  $g_1 g_2 g_3 = e$ , where  $e \in G$  denotes the identity and the multiplication sequence depends on the sublattice (two green sites). On each plaquette, there are operators  $A_p(h)$  that act by left/right multiplication on the group elements on the bounding links (blue/red).  $A_p(h)$  acts by left (right) multiplication if the plaquette orientation aligns (counter-aligns) with the link orientation. This construction ensures that  $A_p(h)$  commutes with all site constraints  $g_1 g_2 g_3 = e$  enforced by  $B_s$ . Summing over all group elements yields the projector  $A_p$ . (b) Microscopically, the quantum double is realized by a blockade Hamiltonian (2) encoded by a blockade graph  $\mathcal{G} = (V, E, W)$ . Depicted is an example for  $N = 6$  with group elements  $g_i$  for  $i = 1, \dots, 6$  and exemplary group product  $g_2 = (g_6 g_1)^{-1}$ . Note that roman symbols like  $g_2$  label *specific group elements*, whereas italic symbols like  $g_3$  are used as *variables*. For the construction it is convenient to mark one of the three edges at each site (crosses); this choice has no physical consequence. Then one places  $N$  two-level systems (vertices) on each link  $l$  which are not in blockade which each other; each is assigned a group element and labeled by  $v_l^g$ . Additionally, there are  $N^2$  two-level systems on the site labeled by pairs of group elements and denoted by  $w_s^{g_1 g_2}$ ; these site systems are all in blockade which each other (blockades not shown). The crucial part is how the link vertices are connected by edges (blockades) with the site vertices (solid arcs, only a few are shown). This construction is explained in the text and depends on the orientation of the site (= the sublattice) and the marked edge (crosses). The inset shows an exemplary classical ground state  $|g_1 g_4 g_2\rangle |w_s^{g_1 g_4}\rangle$  that satisfies all blockades and realizes the state with constraint  $g_1 g_4 g_2 = e$ . Note that there is only one two-level system excited on the site and all but one on each link. Although the construction seems to break the three-fold rotation symmetry of a site (via the edge marked with a cross), the cyclic symmetry of the constraint  $g_1 g_2 g_3 = e$  ensures that the constructed blockade graph is completely symmetric under rotations by  $120^\circ$ . To obtain the blockade graph on the other sublattice, one can rotate the shown site by  $180^\circ$  and swap two of the three edges, thereby inverting the orientation of the multiplication around the vertex.

is assigned on every *link* of the lattice; thus the Hilbert space of the quantum double on a periodic honeycomb lattice with  $L$  unit cells is  $\mathcal{H}_G = (\mathbb{C}^N)^{\otimes 3L}$ . In addition, we assign an orientation to each link; it is convenient to choose all links incoming (outgoing) on alternating lattice sites, see Fig. 1 (a). Then, the Hamiltonian of the quantum double model can be written as

$$H_G = -J_s \sum_{\text{Sites } s} B_s - J_p \sum_{\text{Faces } p} \underbrace{\frac{1}{N} \sum_{h \in G} A_p(h)}_{A_p} \quad (3)$$

with  $J_s > 0$  and  $J_p > 0$ . (Note that we are using the convention of Simon [69] – which is formulated on the *dual* lattice of the original model introduced by Kitaev [5].)

The *site operators*  $B_s$  are local projectors onto configurations where the three states  $|g_1\rangle$ ,  $|g_2\rangle$  and  $|g_3\rangle$  on the links adjacent to site  $s$  obey the “no-flux” constraint  $g_1 g_2 g_3 = e$  with  $e \in G$  the identity of the group  $G$ . Note that in general the group  $G$  is non-abelian and therefore the order of multiplication is important – here we follow the convention with clockwise multiplication on sites with outward pointing arrows, and counter-clockwise multiplication on sites with inward pointing arrows [Fig. 1 (a)]. The *plaquette operators*  $A_p(h)$  flip between such configurations by changing each state  $|g_l\rangle$  on links  $l \in p$  bounding plaquette  $p$  to  $|h g_l\rangle$  or  $|g_l h^{-1}\rangle$ : if the arrow on the link is parallel to the counter-clockwise orientation of the loop surrounding the plaquette, the action is  $|h g_l\rangle$  on this link

(= the plaquette is on the left of the link arrow); otherwise, the action is  $|g_l h^{-1}\rangle$  (= the plaquette is on the right of the link arrow), see Fig. 1 (a). The sum  $A_p$  of  $A_p(h)$  over all group elements  $h \in G$  defined in Eq. (3) is then again a projector.

It is straightforward to show that the projectors  $B_s$  and  $A_p$  all commute with each other, and the ground state of Hamiltonian (3) on a planar patch with open boundaries (with suitable boundary conditions) is the (unique) *equal-weight superposition* of all configurations that satisfy the local constraints imposed by the site terms  $B_s$ . For the abelian group  $G = \mathbb{Z}_2$ , this model yields the toric code on a honeycomb lattice, whereas for a general group  $G$ , the ground state is the fixpoint wave function of a topological phase characterized by the quantum double  $\mathcal{D}(G)$  of the group  $G$  [5, 70, 71]. Notably, for non-abelian groups  $G$ , these topological phases feature non-abelian anyonic excitations and can be used for universal topological quantum computation [66].

Our next goal is to describe a construction  $G \mapsto \mathcal{G}$  of a blockade graph  $\mathcal{G}$  for an arbitrary finite group  $G$ , such that the ground state of the associated blockade Hamiltonian (2) for weak  $\Omega \ll \Delta_i$ ,  $U_0$  is in the topological phase of the quantum double Hamiltonian (3). We first explain the rationale of our approach and then describe the detailed construction below. We start with  $\Omega = 0$  and construct a blockade graph  $\mathcal{G} = (V, E, W)$  such that there is a one-to-one correspondence between the degenerate ground states of  $H_{\mathcal{G}}$  and  $H_G$  for  $J_p = 0$  (this ground state manifold is extensively degenerate). Crucially, the construction of  $\mathcal{G}$  ensures the existence of a group of local graph automorphisms that translate to local symmetries of the Hamiltonian  $H_G$ . The generators of this local symmetry act on the ground state space of  $H_G$  exactly like the operators  $A_p(h)$  act on the ground states space of  $H_G$  (for  $J_p = 0$ ). Then we turn on a weak field  $\Omega$  and show that the (now unique) ground state of  $H_G$  exhibits topological order and is in the same phase as the ground state of the quantum double  $H_G$  for finite  $J_p > 0$ . Thus the core idea for this realization of Kitaev's quantum double models is to implement the site terms  $B_s$  via diagonal two-body interactions, while the terms  $A_p(h)$  appear as a local symmetry of the microscopic Hamiltonian. Together with a uniform transverse field  $\Omega$ , the latter implies the perturbative generation of terms  $A_p(h)$  in the low-energy effective Hamiltonian of the system. Note that for  $G = \mathbb{Z}_2$  this approach leads to the model presented in Ref. [56], and large parts of the proof of topological order presented there can be straightforwardly transferred to the general construction for arbitrary groups  $G$  presented here.

We now describe the construction of the graph  $\mathcal{G}$  for the Hamiltonian  $H_G$  in detail. To this end, we consider a finite group  $G$  with  $N = |G|$  elements. As shown in Fig. 1 (b), we distinguish between two-level systems placed on the *links* to implement the logical states  $|g\rangle_l$ , and two-level systems on the *sites* to realize the site constraints. For simplicity, we start with the construction of a blockade graph  $\mathcal{G}_s$  for a single site  $s$  of the honeycomb lattice and

its three adjacent links, see Fig. 1 (b). On the links we place  $N$  two-level systems ( $N$  *vertices* in graph language). To each vertex on link  $l$  we associate a unique group element  $g \in G$  and denote this vertex by  $v_l^g$ . This yields a Hilbert space of dimension  $2^N$  on each link and we identify the states  $|g\rangle_l$  of the quantum double as basis of an  $N$ -dimensional subspace spanned by

$$|g\rangle_l \equiv |11\dots 0\dots 11\rangle_l, \quad (4)$$

$\uparrow$   
 Vertex  $v_l^g$

i.e., all two-level systems on the link are excited to state  $|1\rangle$  except for vertex  $v_l^g$  which is in the de-excited state  $|0\rangle$ . There are no edges (= blockades) connecting the vertices on the links among themselves, and we choose the detunings uniformly  $\Delta_l \equiv \Delta_i = \Delta$  on all vertices of the link. Next, we place  $N^2$  two-level systems with detuning  $\Delta_s \equiv \Delta_i = 4\Delta$  on the *site*, such that every pair has a distance smaller than the blockade radius  $r_B$ . Hence the blockade graph on a site with  $N^2$  vertices is *fully connected* and has uniform weight.

The last and most important step is to define the edges of the blockade graph that connect the  $3 \times N$  vertices on the three links with the  $N^2$  vertices on their common site. To this end, we label the three links adjacent to site  $s$  by  $l_1, l_2, l_3$  with order as indicated in Fig. 1 (a), i.e., clockwise for outgoing arrows and anti-clockwise for incoming arrows. Furthermore, we assign to each (ordered!) pair of group elements  $g_1, g_2 \in G$  a unique vertex on the site  $s$  and denote it by  $w_s^{g_1 g_2}$ . Then the vertex  $v_{l_1}^{g_1}$  on the first link connects to the  $N$  vertices  $w_s^{g_1 h}$  for all  $h \in G$ , while the vertex  $v_{l_2}^{g_2}$  on the second link connects to all vertices  $w_s^{h g_2}$  for  $h \in G$ . Finally, the vertex  $v_{l_3}^{g_3}$  on the third link connects to all vertices  $w_s^{g_1 g_2}$  which satisfy the condition  $g_3 = (g_1 g_2)^{-1}$ . Note that for every  $g_3 \in G$  there are exactly  $N$  vertices on the site that satisfy this condition. In summary, each vertex  $w_s^{g_1 g_2}$  on a site has an edge with one vertex on each adjacent link:  $v_{l_1}^{g_1}$ ,  $v_{l_2}^{g_2}$ , and  $v_{l_3}^{g_3}$ , with the three group elements satisfying  $g_1 g_2 g_3 = e$ . It is important to point out that this construction is invariant under cyclic permutations of the links since  $g_1 g_2 g_3 = g_2 g_3 g_1 = g_3 g_1 g_2$ , i.e., the construction is invariant under the choice of labeling. In particular, the (apparent) distinction of one of the three links [Fig. 1 (b)] is an artefact of the construction and not reflected in the graph. Furthermore, a mapping between sites with incoming arrows and sites with outgoing arrows is possible by exchanging the labeling between two links.

For such a single site with three adjacent links, the ground states of the Hamiltonian  $H_{G_s}^0$  (with  $U_0 > \Delta_s$ ) are characterized by a single vertex  $w_s^{g_1 g_2}$  in state  $|1\rangle$  and all other vertices on the site in state  $|0\rangle$  due to the on-site blockade interactions; we denote this state by  $|w_s^{g_1 g_2}\rangle$ . Meanwhile, on each adjacent link, the (unique) vertex connected to the excited vertex  $w_s^{g_1 g_2}$  is in state  $|0\rangle$  due to the blockade, while all other vertices on the link are in state  $|1\rangle$ . Therefore each link is in state  $|g_l\rangle_l$  with the constraint  $g_1 g_2 g_3 = e$ . Hence all states in the

degenerate ground state manifold of a single site can be written as  $|g_1, g_2, g_3\rangle |w_s^{g_1 g_2}\rangle$  with  $g_1 g_2 g_3 = e$ , and there is a one-to-one correspondence to the eigenstates of the projection operator  $B_s$  with eigenvalue  $+1$  of the quantum double (3). The ground state energy of  $H_{\mathcal{G}_s}^0$  for a single site with three links is  $E = -(3N + 1)\Delta$ . It is important to stress that here the full Hilbert space of a site with three links is  $2^{3N+N^2}$ -dimensional and therefore much larger than the Hilbert space of a quantum double model with dimension  $N^3$ . In particular the one-to-one mapping is only valid for *ground states*, while our blockade model has a much richer excitation structure.

Before we extend this analysis to the full honeycomb lattice, we discuss the *graph automorphisms* of such a single site (and its three adjacent links). Automorphisms of vertex-weighted graphs are permutations of vertices that map adjacent vertices to adjacent vertices with the same weights. The set of all automorphisms of a graph forms its *automorphism group* (with concatenation of automorphisms as multiplication). Due to the high symmetry of the construction, the automorphism group of the graph  $\mathcal{G}_s$  turns out to be  $(G \times G) \rtimes \text{Aut}(G)$  with  $\text{Aut}(G)$  the group of group automorphisms of  $G$ . In the following, we focus on an important subgroup of these graph automorphisms, a discussion of the full automorphism group can be found in Appendix A.

Since each vertex on a link is associated with a unique group element  $g \in G$ , the group  $G$  induces a permutation  $\varphi_l(h, k)$  of vertices on link  $l$  via

$$\varphi_l(h, k) : v_l^g \mapsto v_l^{hgk^{-1}} \quad \text{for every } h, k \in G. \quad (5)$$

Note that these permutations map the states  $|g\rangle_l$  on link  $l$  to the states  $|hgk^{-1}\rangle_l$  on the same link. Correspondingly, there is a permutation  $\phi_s(h_1, h_2, h_3)$  of the vertices on site  $s$  defined via

$$\phi_s(h_1, h_2, h_3) : w_s^{g_1 g_2} \mapsto w_s^{h_1 g_1 h_2^{-1} h_2 g_2 h_3^{-1}} \quad (6)$$

for every triple  $h_1, h_2, h_3 \in G$ . The permutations (5) and (6) allow us to define a permutation  $\Phi_s$  which acts on the vertices of site  $s$  and all three adjacent links, and turns out to be a graph automorphism of  $\mathcal{G}_s$  parametrized by three group elements:

$$\begin{aligned} \Phi_s(h_1, h_2, h_3) := & \varphi_{l_1}(h_1, h_2) \cdot \varphi_{l_2}(h_2, h_3) \cdot \varphi_{l_3}(h_3, h_1) \\ & \times \phi_s(h_1, h_2, h_3). \end{aligned} \quad (7)$$

Crucially, the automorphism  $\Phi_s$  leaves the constraint  $g_1 g_2 g_3 = e$  invariant. Note that every permutation of vertices (two-level systems) induces a unitary operator on the Hilbert space; by abuse of notation, we denote permutations and induced unitaries with the same symbol. Then the (unitary action of)  $\Phi_s$  maps ground states of  $H_{\mathcal{G}_s}^0$  onto each other. In addition, these operations generate a single *orbit*, i.e., starting from an arbitrary ground state  $|g_1, g_2, g_3\rangle |w_s^{g_1 g_2}\rangle$  one can reach any other ground state by applying these graph automorphisms. According to the definition put forward in Ref. [56], this makes the

blockade structure  $\mathcal{G}_s$  *fully-symmetric*, a special feature that ensures that the ground states of  $H_{\mathcal{G}_s}$  for  $\Omega \neq 0$  contain *equal-weight superpositions* of the degenerate ground states of  $H_{\mathcal{G}_s}^0$ . Of special interest in the following are graph automorphism  $\Phi_s(h) \equiv \Phi_s(e, h, e)$  with two elements  $h_i$  equal to the identity  $e$ . Under these permutations, the state  $|g\rangle_{l_3}$  on one link (here  $l_3$ ) remains invariant, whereas the other two links (here  $l_1$  and  $l_2$ ) transform as  $\Phi_s(h) |g\rangle_{l_1} = |gh^{-1}\rangle_{l_1}$  and  $\Phi_s(h) |g\rangle_{l_2} = |hg\rangle_{l_2}$ , respectively. These automorphisms allow us to construct local *plaquette automorphisms* below.

We close this section by constructing the blockade graph  $\mathcal{G}$  on the full honeycomb lattice. The most important aspect is that the orientation of the sites of the honeycomb lattice alternates between *clockwise* (outgoing arrows) and *anti-clockwise* (incoming arrows), Fig. 1 (a). The construction of both types of sites follows the recipe detailed above: For each site, we label the adjacent links according to its orientation, and connect the vertices on the links to the vertices on the site as explained above. The site graphs are then joined by identifying the vertices on common links. To ensure that this construction leads to a gapped ground state manifold that realizes the intended constraints on every site, one adds up the detunings of vertices that are shared between sites. This leads to the link detunings  $\Delta_l = 2\Delta$  in the bulk of the honeycomb lattice. A mathematically rigorous discussion of this construction (dubbed *amalgamation*) can be found in Ref. [55]. Note that for *open* boundaries, the above procedure leads to link detunings  $\Delta_l = 2\Delta$  in the bulk, but only  $\Delta_l = 1\Delta$  for dangling links on the boundary.

In summary, this construction provides the required graph  $\mathcal{G}$  describing the Hamiltonian  $H_{\mathcal{G}}$  in Eq. (2). The remainder of this paper is dedicated to studying the ground state properties of  $H_{\mathcal{G}}$  and discussing local modifications needed for braiding anyons.

## II. GROUND STATE PROPERTIES

The graph  $\mathcal{G}$  on a honeycomb lattice with periodic boundary conditions and  $A$  units cells contains  $|V| = (3N + 2N^2)A$  vertices, so that the Hilbert space  $\mathcal{H}_{\mathcal{G}}$  of our model is  $2^{|V|}$ -dimensional. The ground state manifold  $\mathcal{H}_{\mathcal{G}}^0$  of  $H_{\mathcal{G}}^0$  for  $U_0 > 4\Delta$  is characterized by a state  $|g_l\rangle_l$  on each link, and a state  $|w_s^{g_i g_j}\rangle$  on each site, such that the group elements on the links  $\mathbf{g} \equiv \{g_l\}$  satisfy the constraints of the projectors  $B_s$  for all sites (namely  $g_1 g_2 g_3 = e$  for the three links connected to a site). We denote states which satisfy this constraint on all sites as  $|\mathbf{g}\rangle$ ; they span the ground state manifold  $\mathcal{H}_{\mathcal{G}}^0$ . States in the orthogonal complement  $\mathcal{H}_{\mathcal{G}}^\perp \equiv (\mathcal{H}_{\mathcal{G}}^0)^\perp$  are denoted by  $|\mathbf{n}\rangle$ . This demonstrates the one-to-one mapping between  $\mathcal{H}_{\mathcal{G}}^0$  and the degenerate ground states of the quantum double Hamiltonian  $H_{\mathcal{G}}$  for  $J_p = 0$ . Note that all states  $|\mathbf{n}\rangle \in \mathcal{H}_{\mathcal{G}}^\perp$  exhibit an excitation gap of at least  $2\Delta$ .

Next, we show the existence of local graph automorphisms on each plaquette (Fig. 2). For each group element

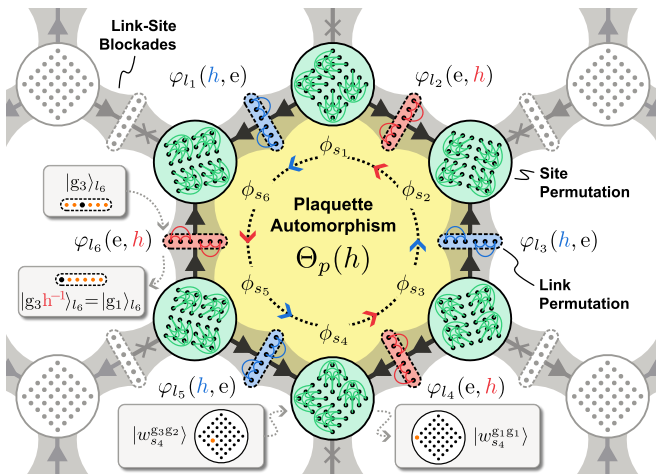


Figure 2. **Plaquette automorphisms.** The blockade graph  $\mathcal{G}$  (shaded gray) constructed in Fig. 1 allows for local automorphisms  $\Theta_p(h)$  for each  $h \in G$  that affect only the vertices on links and sites bounding a single plaquette  $p$ . The automorphism decomposes into a product of permutations of vertices  $\varphi_l$  and  $\phi_s$  on links  $l \in p$  and sites  $s \in p$ , respectively. The link permutations depend on whether the link orientation is parallel (anti-parallel) to the orientation of the plaquette (blue and red arrows). The definition of these permutations is given in the text. Describing the site permutations  $\phi_s$  is most convenient if the site vertices are labeled by the pairs of group elements of the two adjacent edges that bound the plaquette. (To apply the construction detailed in Section I, the radial edge on every site of the plaquette is identified with  $l_3$  [marked by a cross]; this is indicated by rotated and mirrored arrays of site vertices.) As a blockade graph automorphism,  $\Theta_p(h)$  induces a symmetry of the blockade Hamiltonian  $H_{\mathcal{G}}$  on the full Hilbert space. As such, the ground state manifold remains invariant, and the representation induced by the link permutations acts by left and right group multiplications on the ground states  $|\mathbf{g}\rangle$  in  $\mathcal{H}_{\mathcal{G}}^0$ . The insets show exemplary actions of the permutations on states (black vertices:  $|0\rangle$ , orange vertices:  $|1\rangle$ ). Note that links (and sites) that are not adjacent to  $p$  are unaffected by the automorphism (gray).

$h \in G$  we can define a permutation  $\Theta_p(h)$  of vertices that belong to the links and sites surrounding a single plaquette  $p$ . To define  $\Theta_p(h)$ , we choose a labeling for each affected site  $s$  such that  $l_3$  is the link that points outwards (is not part of the plaquette). Then the permutation is defined via the permutations (5) and (6) as

$$\Theta_p(h) := \prod_{l \in \uparrow_p} \varphi_l(e, h) \prod_{l' \in \uparrow_p} \varphi_{l'}(h, e) \prod_{s \in p} \phi_s(e, h, e), \quad (8)$$

where  $\uparrow_p$  ( $\uparrow_p$ ) labels the links with the plaquette to the right (left) of the arrow, and  $s \in p$  denotes sites on the boundary of plaquette  $p$ . It is easy to convince oneself that this permutation is a local graph automorphism of  $\mathcal{G}$  for every  $h \in G$ . To see this, recall that every *single* site graph  $\mathcal{G}_s$  has automorphisms  $\Phi_s(e, h, e)$  which leave one link ( $l_3$ ) invariant.  $\Theta_p(h)$  is the result of chaining six of these permutations along common links bounding a plaquette. Hence we refer to  $\Theta_p(h)$  as *plaquette au-*

*tomorphisms.* Remarkably, plaquette automorphisms on different plaquettes commute with each other – in analogy to the operators  $A_p(h)$  of the quantum double model (3). Since  $\Theta_p(h)$  are automorphisms of  $\mathcal{G}$ , the induced unitary representations [which we also denote by  $\Theta_p(h)$ ] give rise to local symmetries of the blockade Hamiltonian  $H_{\mathcal{G}}^0$ , i.e.,

$$\Theta_p(h)H_{\mathcal{G}}^0 = H_{\mathcal{G}}^0\Theta_p(h) \quad \text{for all plaquettes } p \text{ and } h \in G.$$

As a consequence, all  $\Theta_p(h)$  leave the ground state manifold  $\mathcal{H}_{\mathcal{G}}^0$  invariant and act on ground states  $|\mathbf{g}\rangle$  exactly like the operators  $A_p(h)$  act on the corresponding ground states of the quantum double model (3) for  $J_p = 0$ . However, in contrast to the operators  $A_p(h)$ , the operators  $\Theta_p(h)$  affect not only states on links but also states on sites, and furthermore act non-trivially on excited states  $|\mathbf{n}\rangle \in \mathcal{H}_{\mathcal{G}}^{\perp}$ .

We can now discuss the ground state of the full Hamiltonian  $H_{\mathcal{G}}$  with finite transverse field  $\Omega \neq 0$ . Note that for uniform  $\Omega$  [recall Eq. (2)] the operators  $\Theta_p(h)$  remain symmetries of the full Hamiltonian  $H_{\mathcal{G}}$ . When a finite patch of the honeycomb lattice is embedded on a topologically trivial surface with open boundaries (and “dangling” edges), the plaquette automorphisms  $\Theta_p(h)$  map all states  $|\mathbf{g}\rangle$  in the ground state manifold  $\mathcal{H}_{\mathcal{G}}^0$  onto each other. This follows from the analogous property of Kitaev’s quantum double models [5]. Thus the graph automorphisms  $\Theta_p(h)$  generate a single orbit and the complete blockade structure described by  $\mathcal{G}$  is fully symmetric. This allows us to apply Theorem 1 from Ref. [56] which states that in this case the ground state  $|\Omega\rangle$  of  $H_{\mathcal{G}}$  is unique and has the form

$$|\Omega\rangle = \lambda(\Omega) \sum_{|\mathbf{g}\rangle \in \mathcal{H}_{\mathcal{G}}^0} |\mathbf{g}\rangle + \sum_{|\mathbf{n}\rangle \in \mathcal{H}_{\mathcal{G}}^{\perp}} \eta_{\mathbf{n}}(\Omega) |\mathbf{n}\rangle. \quad (9)$$

The first term describes an equal-weight superposition of all product basis states  $|\mathbf{g}\rangle$  in  $\mathcal{H}_{\mathcal{G}}^0$ , while the second term describes admixtures of additional states due to the coupling by the transverse field. Note that the ground state (9) is in the subspace  $\mathcal{H}_{\mathcal{G}}^S$  (*symmetric sector*) of all states with eigenvalue +1 for all symmetries  $\Theta_p(h)$ , i.e.,

$$|\Omega\rangle \in \mathcal{H}_{\mathcal{G}}^S = \{ |\psi\rangle \mid \forall p, h : \Theta_p(h) |\psi\rangle = |\psi\rangle \} \subset \mathcal{H}_{\mathcal{G}}. \quad (10)$$

Note that for *periodic* boundary conditions, there is also a unique ground state in the symmetric sector. However, equal-weight superpositions of states in  $\mathcal{H}_{\mathcal{G}}^0$  are only guaranteed within the orbits generated by plaquette automorphisms [72].

We stress that due to the admixtures in Eq. (9), one cannot immediately conclude that  $|\Omega\rangle$  is topologically ordered. However, for weak  $\Omega \ll \Delta$ , we can follow the arguments from Ref. [56] to show that the state (9) is topologically ordered and characterized by the quantum double model  $\mathcal{D}(G)$ . The rigorous proof for  $G = \mathbb{Z}_2$  is given in Ref. [56] and its extension to arbitrary groups  $G$  is detailed in Appendix D. Here we only sketch the gist of

the proof. It requires periodic boundary conditions and makes use of the extended auxiliary Hamiltonian

$$\begin{aligned} \tilde{H}_G(\Omega, \omega) := & H_G^0 + \Omega \sum_{i \in V} \sigma_i^x \\ & + \omega \sum_{\text{Faces } p} \left[ \mathbb{1} - \overbrace{\frac{1}{|G|} \sum_{h \in G} \Theta_p(h)}^{\text{Projector } \Theta_p} \right]. \end{aligned} \quad (11)$$

For  $\omega = 0$  and  $\Omega = 0$  we recover the extensive ground state degeneracy of  $\mathcal{H}_G^0$  (now with topological degeneracies). In a first step, we turn on  $\omega$  with  $0 < \omega < \Delta$ . This lifts the extensive degeneracy and the ground states become equal-weight superpositions of states  $|g\rangle$  in the orbits generated by plaquette symmetries  $\Theta_p(h)$ . The new ground state manifold  $\mathcal{H}_G^\omega = \mathcal{H}_G^0 \cap \mathcal{H}_G^S$  has only topological degeneracies and is separated by a finite excitation gap of order  $\omega$  from excited states. The ground states in  $\mathcal{H}_G^\omega$  can be mapped by local unitaries to the ground states of Kitaev's quantum double model (3) and are therefore topological ordered; note that they are also in the symmetric sector  $\mathcal{H}_G^S$  since  $\Theta_p(h)\Theta_p = \Theta_p$  for all  $h \in G$ . The ground state manifold  $\mathcal{H}_G^\omega$ , together with the Hamiltonian  $\tilde{H}_G(0, \omega)$ , shows that the latter is *frustration-free* and satisfies a condition called *local topological quantum order* [73–75]. Given these features, it can be shown that its gap is stable in the thermodynamic limit against arbitrary small, local perturbations [74], which implies that the ground state manifold remains in the same gapped topological phase [76]. In particular, we can turn on a small transverse field  $\Omega \ll \omega, \Delta$  and the new ground state manifold  $\mathcal{H}_G^{\Omega, \omega}$  of the Hamiltonian  $\tilde{H}_G(\Omega, \omega)$  remains topologically ordered. (Note that the topological ground state degeneracy can be lifted by finite size effects.) Using the arguments from above, we know that  $H_G$  has a unique ground state  $|\Omega\rangle$  in the symmetric sector  $\mathcal{H}_G^S$ . Since  $H_G$  commutes with  $\tilde{H}_G(\Omega, \omega)$  and  $|\Omega\rangle$  is annihilated by the positive-semidefinite auxiliary term in Eq. (11),  $|\Omega\rangle$  must also be the (unique) ground state of  $\tilde{H}_G(\Omega, \omega)$ , i.e.,  $|\Omega\rangle \in \mathcal{H}_G^{\Omega, \omega}$ . This demonstrates that the ground state  $|\Omega\rangle$  of  $H_G$  for small enough  $\Omega \ll \Delta$  is in the same topological phase as Kitaev's quantum double model (3).

The gap stability argument above also implies an excitation gap of order  $\Delta$  to all states in the symmetric sector  $\mathcal{H}_G^S$  (this includes “flux excitations” of the quantum double, see Section III below). Consequently, the ground states are protected by a gap against any perturbation which respects the plaquette symmetries  $\Theta_p(h)$ . An important question is whether the Hamiltonian  $H_G$  also exhibits a gap between states in the symmetric sector  $\mathcal{H}_G^S$  and its complement  $(\mathcal{H}_G^S)^\perp$  (this includes “charge excitations”). Such a gap is at least suggested by a (heuristic) Schrieffer-Wolff transformation [77] that predicts an effective Hamiltonian within the manifold  $\mathcal{H}_G^0$  of the form

$$H_{\text{eff}} \sim -\Delta_c \sum_p \sum_{h \in G \setminus \{e\}} \Theta_p(h) \quad (12)$$

with coupling  $\Delta_c \sim \Delta \left(\frac{\Omega}{\Delta}\right)^K$  and  $K$  the number of two-level systems that flip their state under the action of  $\Theta_p(h)$  (i.e.,  $K = 24$  for the honeycomb lattice). However, a rigorous proof of the existence of a finite charge gap is technically challenging and deferred to an upcoming paper [62].

### III. FLUX ANYONS AND WILSON LOOPS

The types of anyonic excitations of the quantum double  $\mathcal{D}(G)$  are classified by the irreducible representations of the Drinfeld double [5, 78]. A systematic characterization of the anyons is given by the following construction [69, 70]. First, one picks a conjugacy class  $C$  of the group  $G$  with an arbitrary representative  $r_C \in C$ , i.e.,  $C = \{gr_Cg^{-1} \mid g \in G\}$ . Next, one considers the centralizer  $Z_G(r_C) = \{g \in G \mid gr_C = r_Cg\}$  of this representative, i.e., the subgroup of  $G$  of all elements that commute with  $r_C$ . The different anyon types of the quantum double  $\mathcal{D}(G)$  can then be labeled by pairs  $[C, R]$  of a conjugacy class  $C$  and an irreducible representation  $R$  of its centralizer  $Z_G(r_C)$ . (Note that the irreducible representations are independent of the representative  $r_C$  since centralizers of different representatives are isomorphic via conjugation.) The quantum dimension  $d_{[C, R]}$  of an anyon turns out to be the product of the number of elements in the conjugacy class  $C$  and the dimension  $d_R$  of the irreducible representation  $R$ :  $d_{[C, R]} = |C|d_R$ . Following the nomenclature of a lattice gauge theory, one distinguishes *flux anyons*  $[C, E]$  given by a conjugacy class  $C$  and the trivial representation  $E$ , and *charge anyons*  $[C_e, R]$  given by an irreducible representation  $R$  of the group  $G = Z_G(e)$  and the conjugacy class  $C_e \equiv \{e\}$  of the identity; anyons  $[C, R]$  with  $C \neq C_e$  and  $R \neq E$  carry flux and charge and are referred to as *dyons*.

The Hamiltonian  $H_G$  with its blockade graph  $\mathcal{G}$  (defined via the site graphs  $\mathcal{G}_s$ ) enforces the zero-flux constraint  $g_1g_2g_3 = e$  on every site by construction. This means that flux excitations (which violate this constraint) are energetically penalized. In the following, we present a straightforward generalization of the site graph  $\mathcal{G}_s$  that allows for the preparation of states with an arbitrary flux anyon trapped on site  $s$ , while maintaining a well-defined excitation gap to other flux sectors (and the vacuum). As explained above, flux anyons  $[C, E]$  are characterized by a conjugacy class  $C$  of the group  $G$ . One can create such a localized flux on a given site  $s$  by enforcing the modified constraint  $g_1g_2g_3 \in C$  on the three links connecting to this site. In the following, we describe a generalization  $\mathcal{G}_s[\Delta]$  of the site graph  $\mathcal{G}_s$  which allows for the preparation of any flux anyon  $[C, E]$  on site  $s$  in the ground state. Instead of  $N^2 = |G|^2$  two-level systems on the site, we now need  $N^3$  two-level systems, all of which are in blockade, so that the induced graph is fully connected and only one of these two-level systems can be excited at any time; we label these vertices by  $w_s^{g_1g_2r}$  with  $g_1, g_2, r \in G$ . Next, we choose detunings  $\Delta \equiv \{\Delta_C\}$  for all conjugacy classes  $C$

of  $G$ ; these determine by how much the energy of a flux anyon  $[C, E]$  on this site is lowered, and therefore play the role of site-local chemical potentials for flux anyons. To this end, we set the detuning of vertex  $w_s^{g_1 g_2 r}$  to  $\Delta_C$  where  $C$  is the conjugacy class of  $r$  (i.e.  $r \in C$ ), such that for every conjugacy class  $C$  there are  $|C|N^2$  vertices with the same detuning  $\Delta_C$ . We can now define the edges of the graph  $\mathcal{G}_s[\Delta]$  that connect the vertices on the adjacent links to the vertices on the site. Each vertex  $v_{l_1}^{g_1}$  on link  $l_1$  is connected to the  $N^2$  vertices  $w_s^{g_1 h r}$  on the site, while each vertex  $v_{l_2}^{g_2}$  on link  $l_2$  is connected to the  $N^2$  vertices  $w_s^{h g_2 r}$ . Finally, we connect every vertex  $w_s^{g_1 g_2 r}$  on the site to the vertex  $v_{l_3}^{g_3}$  on link  $l_3$  with  $g_3 = (g_1 g_2)^{-1} r$ . As a consequence, each configuration which satisfies the constraint  $g_1 g_2 g_3 \in C$ , with  $C$  a conjugacy class of  $G$ , has the same energy contribution  $-\Delta_C$ . To prepare a specific flux anyon  $[C_r, E]$  on such a site, one sets  $\Delta_{C_r} = 4\Delta$  and  $\Delta_C = -1$  for all  $C \neq C_r$ . This lowers the energy of the flux anyon  $[C_r, E]$  and separates it by a gap from all other flux excitations (and the vacuum). It is crucial that this site graph respects all local graph automorphisms of  $\mathcal{G}_s$  discussed in Section I, and a Hamiltonian  $H_{\tilde{\mathcal{G}}}$  derived from a graph  $\tilde{\mathcal{G}}$  that uses the generalized site graph  $\mathcal{G}_s[\Delta_s]$  on some sites (with potentially different detunings  $\Delta_s$ ) is still symmetric under the local plaquette automorphisms  $\Theta_p(h)$  introduced in Section II. Only global symmetries derived from outer automorphisms of  $G$  are modified by this construction; for details see Appendix A.

By construction, the ground states of the Hamiltonian  $H_{\tilde{\mathcal{G}}}^0$  in the symmetric sector  $\mathcal{H}_{\tilde{\mathcal{G}}}^S$  are described by flux anyons trapped on the sites with a generalized site graph  $\mathcal{G}_s[\Delta_s]$ , and their energy can be tuned by the detunings  $\Delta_s$ . It is important to point out that the ground state manifold of a system with non-trivial flux anyons can have a topological ground state degeneracy even on topologically trivial surfaces. Furthermore, there is a finite excitation gap to states within the symmetric sector  $\mathcal{H}_{\tilde{\mathcal{G}}}^S$ . Therefore, this construction can be used to prepare states with a preferred flux pattern on the lattice as *ground states* of the blockade Hamiltonian  $H_{\tilde{\mathcal{G}}}^0$ . We will use this feature in Section IV to implement the braiding of flux anyons. Note that the above construction can be significantly simplified if the goal is to trap a *specific* flux anyon  $[C_r, E]$ . In this case, one can omit all site vertices except the  $|C_r|N^2$  vertices that belong to the relevant conjugacy class (and, if required, the  $N^2$  vertices for the vacuum  $C_e$ ).

Following the discussion in Section II on the robustness of topological order for a finite transverse field  $\Omega \neq 0$  in a flux-free state on a torus, we expect that the topological properties and ground state degeneracy of the modified Hamiltonian  $H_{\tilde{\mathcal{G}}}$  in the symmetric sector  $\mathcal{H}_{\tilde{\mathcal{G}}}^S$  are again robust in the presence of a small but finite transverse field  $\Omega \neq 0$ , even in the presence of imprinted flux anyons. In this case, the splitting of the ground state degeneracy is exponentially suppressed in the distance between the flux

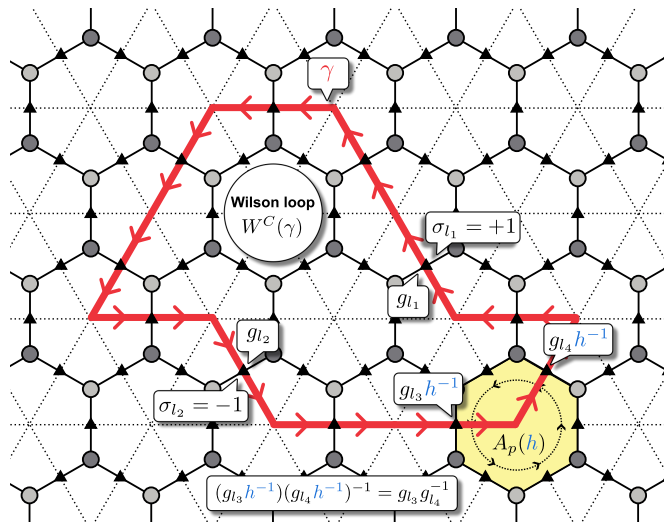


Figure 3. **Wilson loops.** Wilson loop operators  $W^C(\gamma)$  are defined on closed, oriented loops  $\gamma$  (red) on the dual lattice (dotted). For the evaluation of  $W^C(\gamma)$  in the product basis  $|\mathbf{g}\rangle \in \mathcal{H}_G$ , the product of all group elements  $g_l^{\sigma_l}$  on links  $l$  crossed by  $\gamma$  is needed (with multiplication order from left to right along the loop's orientation); here  $\sigma_l = +1$  ( $\sigma_l = -1$ ) if the crossed edge  $l$  points to the left (right) of  $\gamma$  when following its orientation. This construction ensures that  $W^C(\gamma)$  commutes with the plaquette operators  $A_p(h)$  (plaquette in the bottom right corner).

anyons (instead of the system size) and therefore requires that flux anyons are far apart.

In analogy to lattice gauge theories, the flux anyons are conveniently probed and characterized by *Wilson loops*. In the case of quantum doubles, Wilson loops are closely related to closed charge-like *Ribbon operators* which probe the enclosed flux [5, 69]. Wilson loop operators are associated to a closed, oriented loop  $\gamma$  on the *dual* lattice, see Fig. 3. In the product basis  $|\mathbf{g}\rangle \in \mathcal{H}_G$  of the quantum double model (3), they are defined by

$$W^R(\gamma) := \chi_R \left( \prod_{l \in \gamma} g_l^{\sigma_l} \right) \quad (13)$$

with  $R$  an irreducible representation of the group  $G$  and  $\chi_R$  its character. The product runs over all links crossed by the closed loop  $\gamma$  (with multiplication order from left to right along the loop's orientation). The exponents  $\sigma_l \in \{-1, 1\}$  are defined such that  $\sigma_l = +1$  ( $\sigma_l = -1$ ) if the arrow of the crossed link points left (right) when following the loop along its orientation. This convention ensures that  $W^R(\gamma)$  commutes with all plaquette operators  $A_p(h)$  (Fig. 3).

For fixpoint ground states of a quantum double model – which in our case correspond to the ground states of  $\tilde{H}_{\tilde{\mathcal{G}}}(0, \omega)$  or, equivalently, the ground states of  $H_{\tilde{\mathcal{G}}}^0$  in the symmetric sector – the Wilson loops (13) are independent of the shape of the loop, and only depend on the enclosed flux. For example, a loop  $\gamma$  that encloses a flux  $[C, E]$



yields  $\langle W^R(\gamma) \rangle = \chi_R(r_C)$  with  $r_C \in C$ , i.e., the measurement over all irreducible representations  $R$  uniquely determines the enclosed flux. This property can be made explicit by taking the discrete Fourier transform of the Wilson loop  $W^R(\gamma)$  over the group  $G$ ,

$$W^C(\gamma) := \frac{1}{|G|} \sum_R \sum_{r \in C} \chi_R^*(r) W^R(\gamma) \quad (14a)$$

$$= \begin{cases} 1 & \text{if } \prod_{l \in \gamma} g_l^{\sigma_l} \in C, \\ 0 & \text{otherwise,} \end{cases} \quad (14b)$$

and therefore  $\langle W^{C'}(\gamma) \rangle_C = \delta_{C,C'}$  where  $\langle \bullet \rangle_C$  denotes a state with flux  $C$  enclosed by  $\gamma$ ; see Appendix E for details.

However, in general there are fluctuations of flux excitations. In this case it is known from pure gauge theories in  $2+1$  dimensions [79] that the Wilson loop in the trivial phase decays with an area law, whereas in the topological phase it decays with a perimeter law

$$\langle W^R(\gamma) \rangle \sim e^{-|\gamma|/\xi_R}, \quad (15)$$

where  $|\gamma|$  denotes the length of  $\gamma$ . Hence the expectation values of Wilson loops can be used to probe two properties: Varying the loop  $\gamma$  and verifying the perimeter law demonstrates the topological character of the phase, and the expectation value for a fixed loop yields information about the enclosed flux.

However, for our implementation of quantum doubles via a Hamiltonian  $H_{\tilde{G}}$  with finite transverse field  $\Omega \neq 0$ , we cannot necessarily associate a group element  $g_l$  to each link, since the full Hilbert space of a link is much larger than  $\mathcal{H}_l^G \equiv \text{span}\{|g\rangle_l \mid g \in G\}$ . To solve this problem, we modify the Wilson loop operator,

$$\mathbb{W}^R(\gamma) := W^R(\gamma) \prod_{l \in \gamma} \mathbb{P}_l^G, \quad (16)$$

where  $\mathbb{P}_l^G$  is the projector on link  $l$  onto the subspace  $\mathcal{H}_l^G$ . This modification guarantees that the Wilson operator  $\mathbb{W}^R(\gamma)$  is well defined on the full Hilbert space  $\mathcal{H}_{\tilde{G}}$  of the blockade structure  $H_{\tilde{G}}$ . To understand the effect of this projector, we consider a simplified model where each link is with probability  $p < 1$  in a state in  $\mathcal{H}_l^G$ . Then the projector  $\prod_{l \in \gamma} \mathbb{P}_l^G$  leads to an additional contribution  $p^{|\gamma|}$  to the perimeter law. This suggests that the modified Wilson loop (16) can still distinguish between the trivial and the topological phase, as this additional factor is consistent with a perimeter law. Furthermore, we expect that one can factor out this additional contribution by evaluating the ratio between two Wilson loops with irreducible representation  $R$  and trivial representation  $E$ , respectively:

$$\frac{\mathbb{W}^R(\gamma)}{\mathbb{W}^E(\gamma)} := \frac{\langle W^R(\gamma) \rangle}{\langle W^E(\gamma) \rangle} \approx \frac{1}{|\mathcal{I}_G|} \sum_{\mathbf{g}_\gamma \in \mathcal{I}_G} \chi_R \left( \prod_{l \in \gamma} g_l^{\sigma_l} \right). \quad (17)$$

Here  $\mathbf{g}_\gamma \equiv (g_l)_{l \in \gamma}$  denotes measurement outcomes of one experimental sample for links along the loop  $\gamma$ . The last

equality shows that it is convenient for an experiment to evaluate the expectation value by only taking into account the post-selected measurements  $\mathcal{I}_G$  where all links along the loop  $\gamma$  are in a state in  $\mathcal{H}_l^G$ .

Finally, we point out that if perturbations of the Hamiltonian  $H_{\tilde{G}}$  slightly break the local symmetries  $\Theta_p(h)$ , charges are also allowed to fluctuate. To identify the topological phase in this case, it is necessary to use Fredenhagen-Marcu order parameters [80, 81].

#### IV. ADIABATIC STATE PREPARATION AND ANYON BRAIDING

A remarkable property of the Hamiltonian  $H_G$  (and  $H_{\tilde{G}}$ ) [Eq. (2)] is that it can be generalized to *local* transverse fields  $\Omega_s$  and  $\Omega_l$  on sites  $s$  and links  $l$  without violating the local plaquette symmetries  $\Theta_p(h)$ . The only constraint is that  $\Omega_s$  ( $\Omega_l$ ) and  $\Delta_s$  ( $\Delta_l$ ) are equal for all two-level systems that are permuted by these local automorphisms, i.e., transverse fields and detunings must be uniform on each site  $s$  and link  $l$  respectively, but can vary between sites and links. This allows us to locally control the system with time dependent parameters  $\Omega_s(t)$  and  $\Delta_s(t)$  on sites [ $\Delta_s(t)$  for generalized sites], and  $\Omega_l(t)$  and  $\Delta_l(t)$  on links. In a first step, we leverage this control to propose a protocol for the adiabatic preparation of the flux-free topological quantum many-body ground state of  $H_G$ . Later, we extend this protocol to realize controlled braiding of flux anyons using  $H_{\tilde{G}}$ .

For the adiabatic preparation of the ground state of  $H_G$  on a patch of the honeycomb lattice (Fig. 4), we start with  $\Omega_i = 0$  and  $\Delta_i = -\Delta < 0$  on all vertices, and prepare these two-level systems in the unique ground state  $|\psi_0\rangle = \bigotimes_{i \in V} |0\rangle_i$ . This state is obviously in the symmetric sector,  $|\psi_0\rangle \in \mathcal{H}_{\tilde{G}}^S$ , so that the symmetry sector is completely fixed by this initial state. The main idea for an efficient adiabatic preparation is to *grow* the topological phase, starting from a single site  $s$ . On this site, we first adiabatically turn on the transverse field  $\Omega_s \sim \Delta$ , then ramp the detuning from  $\Delta_s = -\Delta < 0$  to its final value  $\Delta_s = 4\Delta > 0$ , and finally adiabatically turn off the transverse field again, see Fig. 4 (a). Due to the strong blockade interaction on the site, only a single vertex can be excited to  $|1\rangle$ , but since  $\Omega_s$  acts uniformly on all vertices on  $s$ , this protocol results in an equal-weight superposition of all possible single-excitation states:

$$|\psi_1\rangle = \mathcal{N} \left[ \bigotimes_{i \notin s} |0\rangle_i \right] \left[ \sum_{g_1, g_2 \in G} |w_s^{g_1 g_2}\rangle \right], \quad (18)$$

with normalization  $\mathcal{N} = 1/|G|$ . Recall that  $|w_s^{g_1 g_2}\rangle$  denotes the state with vertex  $w_s^{g_1 g_2}$  on site  $s$  excited to  $|1\rangle$  and all other vertices on the site in state  $|0\rangle$ . During this adiabatic ramping procedure, the system always exhibits a gap of order  $\max\{|\Delta_s|, \Omega_s|G|\}$ . Note that the transverse field exhibits a collective enhancement due to the blockade interaction, so that for optimal ramping  $\Omega_s \sim \Delta/|G|$  and the preparation can be achieved on the time scale  $\hbar/\Delta$ .

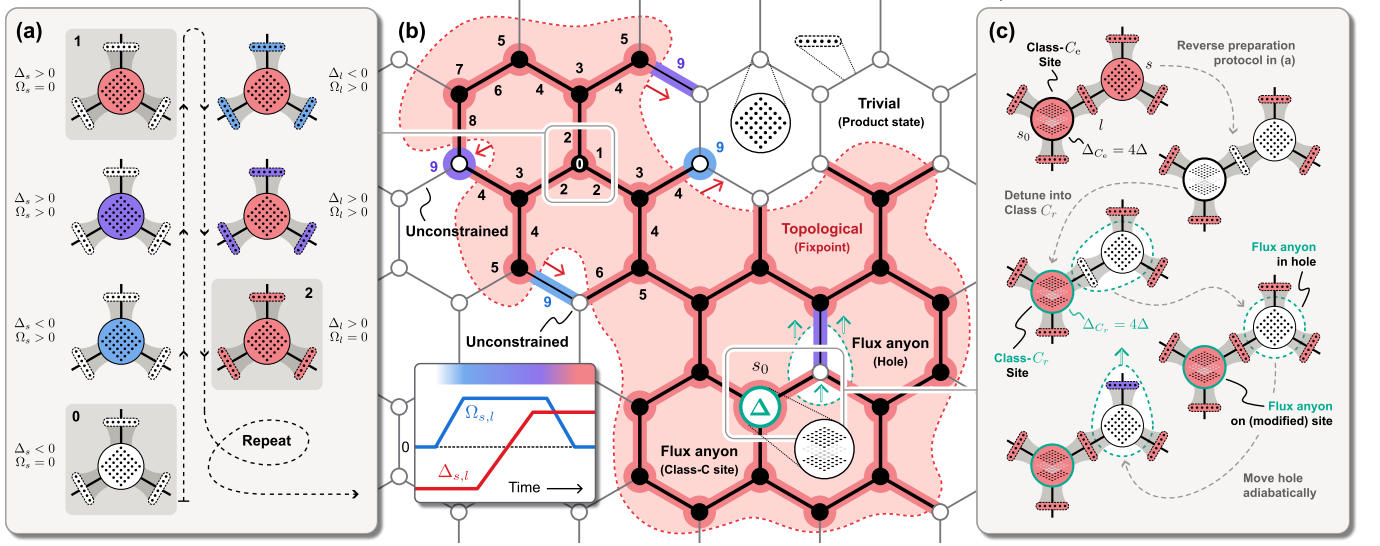


Figure 4. **Adiabatic preparation of ground states and flux anyons.** (a,b) The topological fixpoint ground state can be adiabatically “grown” starting from a completely de-excited array of two-level systems (i.e.,  $\Delta_s < 0$  and  $\Delta_l < 0$  for all sites and links, white filling). One then iterates the ramping procedure (white  $\rightarrow$  blue  $\rightarrow$  purple  $\rightarrow$  red) shown in the inset of panel (b) for sites and adjacent links repeatedly. Note that transverse fields  $\Omega_{s,l}$  and detunings  $\Delta_{s,l}$  are adiabatically modified uniformly for all two-level systems on a site or link, thereby respecting the local symmetries of the model at all times. A possible (non-optimal) initialization sequence is shown in (b) where numbers label time steps. Note that a site (link) can only be initialized in the ground state if there is at least one adjacent link (site) uninitialized (see four cases in time step 9). Since  $\Omega_s = 0 = \Omega_l$  after initialization (red area), the prepared ground state is the fixpoint wave function of the quantum double  $\hat{H}_G(0, \omega)$ , without admixtures from classical excited states in  $\mathcal{H}_G^e$ . (c) Once a patch is prepared in the topological ground state, one can use the generalized site graph  $\mathcal{G}_{s_0}[\Delta]$  to adiabatically inject flux anyons into the system [labelled  $\Delta$  in panel (b), see Section III for its construction]. The special site  $s_0$  is initialized with  $\Delta_{C_e} = -\Delta \nearrow 4\Delta$  (and all other  $\Delta_C = -\Delta = \text{const}$ ) to prepare the no-flux constraint  $g_1 g_2 g_3 = e$ . Then this site, together with an adjacent link  $l$  and site  $s$  are de-excited again [following the inverse protocol in panel (a)]. Subsequently, the special site is re-initialized with  $\Delta_{C_r} = -\Delta \nearrow 4\Delta$  (green boundary, red filling) so that it enforces the constraint  $g_1 g_2 g_3 \in C_r$  for some non-trivial conjugacy class  $C_r$ . This protocol prepares two flux anyons in the vacuum fusion channel:  $[C_r, E]$  localized on the “flux factory” site  $s_0$ , and the corresponding antiparticle  $[\bar{C}_r, E]$  in the hole of de-excited sites and links. The hole (carrying its anyon) can then be adiabatically moved by sequences of (de-/re-)initializations of links and sites (purple link).

In the next step, we proceed to all links connected to site  $s$  and repeat the adiabatic ramping procedure with  $\Omega_l \sim \Delta$  and final value  $\Delta_l = 2\Delta$ . Due to the blockade interactions between the vertices on the links and the excited vertex on the site, one vertex on each link is in blockade while the others can be efficiently adiabatically excited on the time scale  $\hbar/\Delta$ . At the end of this procedure, the new ground state is

$$|\psi_2\rangle = \mathcal{N} \left[ \bigotimes_{i \notin \{s,l\}} |0\rangle_i \right] \left[ \sum_{g_1, g_2 \in G} |g_1, g_2, g_3\rangle |w_s^{g_1 g_2}\rangle \right], \quad (19)$$

where the states  $|g_1, g_2, g_3\rangle$  on the three links  $l \equiv l_{1,2,3}$  obey the no-flux condition  $g_1 g_2 g_3 = e$  [Fig. 4 (a)].

The next step is to repeat the adiabatic ramping on all sites connected to the links  $l_1, l_2$ , and  $l_3$ , and then proceed with all links connected to these sites, etc. This iterative ramping protocol, alternating between links and sites, grows the topological phase from the inside of the patch towards its boundary, see Fig. 4 (b). In each step, the blockade interactions between links and sites constrains the excitation patterns to the ground state manifold  $\mathcal{H}_G^0$ .

While there is much freedom in the sequence of sites and links that are passed by the ramping procedure [Fig. 4 (b)], it is important that for each link only *one* connected site has already been excited, and for each site *at most two* connected links have already been excited. This guarantees that the constraints imposed by the blockade interaction can always be fulfilled. Note that on sites with only *one* connected link already excited, there is still a collective enhanced coupling  $\sqrt{|G|}\Omega_s$ , whereas on sites with two excited links there is no collective enhancement. But with proper local addressing, this can be compensated by the strength of the transverse field  $\Omega_s$ , such that each step can be implemented on a time scale  $\sim \hbar/\Delta$ .

This protocol prepares a unique state on an open patch of the honeycomb lattice and respects all local symmetries, i.e., the wave function  $|\psi_t\rangle$  during the adiabatic ramping always satisfies  $\Theta_p(\hbar)|\psi_t\rangle = |\psi_t\rangle$  and remains in the symmetric sector,  $|\psi_t\rangle \in \mathcal{H}_G^S$ . It is convenient to stop the preparation of a finite patch such that every initialized site has all three emanating links initialized as well, i.e., the patch has “rough” boundaries with dangling links. Then, the protocol prepares the exact and unique ground

state of  $\tilde{H}_G(0, \omega)$ , i.e., the equal-weight superposition of all configurations satisfying the zero-flux constraint on every initialized site. This state corresponds to the unique ground state of the quantum double model (3) for “rough” boundary conditions. Note that after this initialization, it is still possible to ramp up a homogeneous transverse field  $\Omega$  to prepare the true ground state  $|\Omega\rangle$  of the Hamiltonian  $H_G$  on a time scale  $\sim \hbar/\Delta$  due to the excitation gap in the symmetric sector.

In summary, the adiabatic preparation of the topological state  $|\Omega\rangle$  can be achieved on a time scale  $\tau \sim 2\sqrt{A}\hbar/\Delta$  with  $A$  the total number of sites in the patch of the honeycomb lattice. As required for the local unitary preparation of a state with topological order from a trivial product state, the time for the preparation scheme scales with the system size (but only with a  $\sqrt{A}$  scaling) [76]. Note that if the adiabatic ramping scheme *violates* the local symmetries, the ramping must be slower than the gap *between* different symmetry sectors to avoid the excitation of charge anyons. In particular, since the charge gap is now essential for the adiabatic preparation, the transverse fields  $\Omega_s$  and  $\Omega_l$  can no longer be switched off to prepare the fixpoint ground state. Fortunately, this does not alter the overall scaling of the preparation time with system size.

The protocol for adiabatic ground state preparation can be generalized to states with well-defined flux anyons (ground states of  $H_G$ ), and the subsequent adiabatic braiding of these anyons. Flux anyons can be either trapped inside holes, i.e., contiguous areas of sites and links with all vertices in state  $|0\rangle$ , or pinned to generalized site graphs  $\mathcal{G}_s[\Delta_s]$  (introduced in Section III), where the site-specific chemical potentials  $\Delta_s$  can be used to control the flux anyon type pinned at this site. To prepare well-defined flux anyons with the above method – which is based on the interplay of adiabatic ramping and blockade interactions – one needs at least one special site  $s_0$  with the generalized blockade graph  $\mathcal{G}_{s_0}[\Delta]$ , detuned by  $\Delta = \{\Delta_C\}$ . This site plays the role of a “flux factory” to adiabatically inject fluxes into the system, which subsequently can be trapped and moved inside holes (which does not require modified sites), see Fig. 4 (b). The preparation starts with the initialization of the topological ground state in the symmetric sector  $\mathcal{H}_G^S$ , with all sites in the zero-flux state. For the generalized site  $s_0$  this means  $\Delta_{C_e} = -\Delta \nearrow 4\Delta$  and  $\Delta_C = -\Delta = \text{const}$  for all  $C \neq C_e$ , Fig. 4 (c). To inject flux anyons into the system, one selects the special site  $s_0$ , an adjacent site  $s$ , and the link  $l$  connecting them, and applies the inverse adiabatic ramping procedure to bring all vertices on this link and the two sites into state  $|0\rangle$ . This creates a hole encompassing the two sites, with detunings  $\Delta_C = -\Delta$  for all conjugacy classes  $C$  on the modified vertex  $s_0$ . To create a flux anyon  $[C_r, E]$  and its antiparticle  $[\bar{C}_r, E]$  on the two sites, one adiabatically ramps the transverse field  $\Omega_{s_0}$  on all site vertices, and subsequently the detunings  $\Delta_{C_r} = -\Delta \nearrow 4\Delta$  of the site vertices that belong to class  $C_r$  (for  $C \neq C_r$  the detunings  $\Delta_C = -\Delta$  remain constant). Finally, one also performs

the ramping on the link to site  $s$ . This prepares a state on the three adjacent links that satisfies the generalized condition  $g_1 g_2 g_3 \in C_r$ . This step creates *two* flux anyons:  $[C_r, E]$  pinned at the special site  $s_0$  as the lowest energy state, and  $[\bar{C}_r, E]$  trapped inside the hole at the neighboring site  $s$ . Note that the hole necessarily carries the anti-flux anyon  $[\bar{C}_r, E]$  since the surrounding bulk state requires that these two anyons fuse into the vacuum. Furthermore, the procedure prepares a well-defined state in the fusion space of these two anyons, namely the unique topological state of two anyons  $[C_r, E]$  and  $[\bar{C}_r, E]$  in the vacuum fusion channel. After this initial creation of a flux pair, the hole can be adiabatically moved around by ramping down a connecting link and an adjacent site, and subsequently ramping up the original site and the connecting link again, Fig. 4 (b,c). In a similar fashion, anyons pinned at site  $s_0$  can first be immersed into a hole and subsequently moved away. Then the “flux factory”  $s_0$  can be reused for the creation of the next pair of flux anyons. Finally, the Wilson loop operators  $W^R(\gamma)$  [or  $W^C(\gamma)$ ] for loops  $\gamma$  around flux-carrying holes can be used to measure the enclosed total flux, which probes the fusion channel of the encircled holes.

In summary, we have developed a complete toolbox to explore the non-abelian character of flux anyons in quantum double models  $\mathcal{D}(G)$ : (i) adiabatic ground state preparation, (ii) deterministic and adiabatic creation of flux anyons in a well-defined fusion channel, (iii) adiabatic transport of these anyons (necessary for braiding and fusion), and finally, (iv) probing of fusion channels by measuring Wilson loop operators around flux anyons. In the remainder of this paper, we apply this toolbox to the simplest non-abelian quantum double  $\mathcal{D}(S_3)$ .

## V. EXAMPLES FOR $\mathcal{D}(S_3)$

For the abelian group  $G = \mathbb{Z}_2$ , the construction of the Hamiltonian  $H_G$  and its corresponding graph  $\mathcal{G}$  reproduces the blockade structure studied in Ref. [56], which leads to an *abelian* topological phase known as the toric code [5]. Therefore we focus in the following on the simplest *non-abelian* quantum double derived from the permutation group  $G = S_3 \equiv C_{3v}$  with six elements  $\{e, R, R^2, \sigma, \sigma R, \sigma R^2\}$  with  $R$  a three cycle and  $\sigma$  a two cycle ( $\sigma^2 = e$ ,  $R^3 = e$  and  $\sigma R = R^2 \sigma$ ). Thus we have  $|G| = N = 6$ , so that on each link there are six two-level systems and on each site there are 36 two-level systems; this setup is sketched in Fig. 1 (b). The quantum double  $\mathcal{D}(S_3)$  features eight anyon types, given by the irreducible representation of the Drinfeld double  $\mathcal{D}(S_3)$  [5, 69]. In particular, this implies an eight-fold ground state degeneracy on a torus. As discussed in Section III, the anyons can be labeled by a conjugacy class  $C$  of the group  $G$  and an irreducible representation of the centralizer of a representative of the conjugacy class. The group  $S_3$  has three conjugacy classes  $C_e$ ,  $C_\sigma$ , and  $C_R$ , and three irreducible representations: the trivial representation  $E$ , a

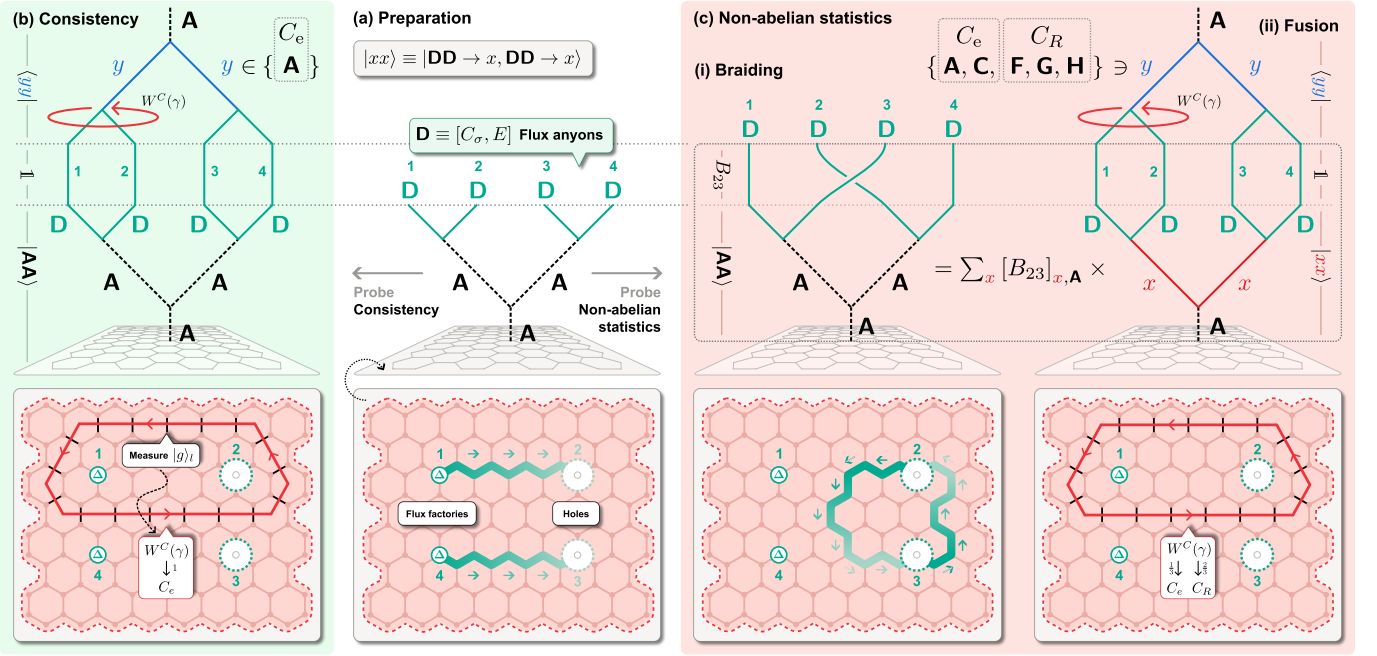


Figure 5. **Probing non-abelian statistics.** Protocol for the preparation, braiding and measurement (fusion) of anyons. The splitting/fusion diagrams (time evolution) are shown in the top row, the corresponding spatial configurations and manipulations in the bottom row. (a) As an initial step, two pairs (1, 2) and (3, 4) of  $\mathbf{D} \equiv [C_\sigma, E]$  flux anyons (solid green lines) are created and separated within a topological domain (red area) following the protocol described in Section IV and Fig. 4 (c). We denote splitting/fusion states of this form as  $|xx\rangle \equiv |\mathbf{D}\mathbf{D} \rightarrow x, \mathbf{D}\mathbf{D} \rightarrow x\rangle$ . With this nomenclature, the system is initialized in the state  $|\mathbf{A}\mathbf{A}\rangle$  where both pairs fuse into the vacuum  $\mathbf{A}$  (black dashed lines). (b) As a consistency check, the Wilson loop  $W^C(\gamma)$  can be computed from measuring the link states  $|g\rangle_l$  along the depicted dual loop  $\gamma$  (solid red line). Only for  $C = C_e$  the expectation value should be non-zero since the enclosed anyons are in the vacuum channel. (c) Alternatively, the two anyons 2 and 3 from different pairs can be exchanged with a half-braid (again using the protocol for adiabatically moving holes) to produce the new state  $B_{23} |\mathbf{A}\mathbf{A}\rangle$  shown in (c-i). Here,  $B_{23}$  denotes the unitary braiding matrix for exchanging flux 2 and 3. Using the  $F$ - and  $R$ -matrices of the unitary braided fusion category that describes the quantum double  $\mathcal{D}(S_3)$  (see Appendix F), this state can be expanded in the basis  $|xx\rangle$ , where the fusion rules allow  $x \in \{\mathbf{A}, \mathbf{C}, \mathbf{F}, \mathbf{G}, \mathbf{H}\}$ . Here,  $\{\mathbf{A}, \mathbf{C}\}$  carry no flux of type  $C_e$  and  $\{\mathbf{F}, \mathbf{G}, \mathbf{H}\}$  carry non-zero flux of type  $C_R$ . These fluxes can be measured again by the same Wilson loop  $W^C(\gamma)$ , where now the expectation value for  $C = C_R$  is finite. This demonstrates the non-abelian nature of  $\mathcal{D}(S_3)$  in that the two states depicted in the lower left and right corners are locally indistinguishable while being linearly independent.

one dimensional representation  $\Gamma_1$ , and a two-dimensional representation  $\Gamma_2$ . Taken together, these label the pure flux anyons and the pure charge anyons. Following the standard notation, these are denoted as  $\mathbf{A} \equiv [C_e, E]$  for the vacuum,  $\mathbf{D} \equiv [C_\sigma, E]$  and  $\mathbf{F} \equiv [C_R, E]$  for the flux anyons, and  $\mathbf{B} \equiv [C_e, \Gamma_1]$ , and  $\mathbf{C} \equiv [C_e, \Gamma_2]$  for the charge anyons. In addition, there are three dyons:  $\mathbf{E} \equiv [C_\sigma, \Gamma_\sigma]$  for the non-trivial irreducible representation of the centralizer of  $C_\sigma$ , and  $\mathbf{G} \equiv [C_R, \Gamma_{R_1}]$  and  $\mathbf{H} \equiv [C_R, \Gamma_{R_2}]$  for the two non-trivial irreducible representations of the centralizer of  $C_R$ . A full review of the anyon content of  $\mathcal{D}(S_3)$ , their fusion channels,  $F$ -matrices and  $R$ -matrices can be found in Ref. [66].

Drawing from the toolbox developed above, we now describe a simple braiding scheme for flux anyons to probe their non-abelian statistics, see Fig. 5. For this, we start by preparing a setup with four  $\mathbf{D} = [C_\sigma, E]$  anyons using (ideally) two “flux factories” as explained in Section IV and illustrated in Fig. 5 (a). As discussed previously, the initial state is therefore in the fusion channel where the

first and second pair of  $\mathbf{D}$  anyons each fuse into the vacuum. It is convenient to define a basis of the fusion space of four  $\mathbf{D}$  anyons  $\mathcal{H}_\mathbf{A}^{\mathbf{D}\mathbf{D}\mathbf{D}\mathbf{D}}$  that are in the global vacuum channel  $\mathbf{A}$ . We denote as  $|xx\rangle \equiv |\mathbf{D}\mathbf{D} \rightarrow x, \mathbf{D}\mathbf{D} \rightarrow x\rangle$  the fusion state where each pair fuses into anyon  $x$ ; note that both pairs must fuse into the same anyon since the fusion of all four anyons yields the vacuum  $\mathbf{A}$  and for  $\mathcal{D}(S_3)$  all anyons are their own antiparticle. The fusion rule [66]

$$\mathbf{D} \otimes \mathbf{D} = \mathbf{A} \oplus \mathbf{C} \oplus \mathbf{F} \oplus \mathbf{G} \oplus \mathbf{H} \quad (20)$$

then determines a basis of the five-dimensional fusion space, namely

$$\mathcal{H}_\mathbf{A}^{\mathbf{D}\mathbf{D}\mathbf{D}\mathbf{D}} = \text{span}\{|\mathbf{A}\mathbf{A}\rangle, |\mathbf{C}\mathbf{C}\rangle, |\mathbf{F}\mathbf{F}\rangle, |\mathbf{G}\mathbf{G}\rangle, |\mathbf{H}\mathbf{H}\rangle\}, \quad (21)$$

where our system is initialized in the state  $|\mathbf{A}\mathbf{A}\rangle$ .

Consequently, a measurement of the Wilson loop  $W^C(\gamma)$  [via post-selection, recall Eq. (17)] around the first (and second) pair of anyons must yield the flux  $C_e$  with probability 1, which can be used to probe the consistency

of the adiabatic preparation scheme, Fig. 5 (b). Now we can perform braiding using the adiabatic ramping protocol from Section IV, see Fig. 5 (c). In general, braiding anyons induces unitary transformations on the fusion space, here  $\mathcal{H}_A^{\text{DDDD}}$ . If we braid the first and second anyon around each other, the fusion state  $|\mathbf{AA}\rangle$  remains invariant – which can again be tested by measuring Wilson loop operators. By contrast, if we exchange (“half-braid”) the second and the third anyon, the initial state  $|\mathbf{AA}\rangle$  transforms into (see Appendix F and Ref. [66])

$$|\mathbf{AA}\rangle \mapsto \frac{1}{3} \left[ \overbrace{|\mathbf{AA}\rangle + \sqrt{2}|\mathbf{CC}\rangle}^{C_e} + \sqrt{2} \underbrace{(|\mathbf{FF}\rangle + e^{i\frac{2\pi}{3}}|\mathbf{GG}\rangle + e^{-i\frac{2\pi}{3}}|\mathbf{HH}\rangle)}_{C_R} \right]. \quad (22)$$

As before, this state can be probed by measuring the Wilson loop around the first two anyons. With probability  $1/3$  one measures again the trivial flux  $C_e$ , but with probability  $2/3$  one now finds the non-trivial flux  $C_R$ . Hence this simple braiding protocol already reveals the non-abelian character of the quantum double  $\mathcal{D}(S_3)$ : by adiabatically exchanging two identical anyons trapped in two holes one can change the fusion channel of the system without ever leaving the ground state manifold.

## VI. CONCLUSION AND OUTLOOK

We introduced and studied a family of two-dimensional models, constructed from two-level systems subject to local transverse fields and detunings, where excited states interact via a strong blockade interaction. These models are motivated by the Rydberg platform with neutral atoms in optical tweezers. On an abstract level, the Hamiltonians can be described by vertex-weighted blockade graphs  $\mathcal{G}$ , with vertices representing two-level systems and edges blockade interactions. We presented a construction for a family of blockade graphs, such that for every finite group  $G$ , the ground state of the blockade Hamiltonian with weak transverse fields is in the topologically ordered phase of the quantum double model  $\mathcal{D}(G)$ . This family of topological phases is characterized by anyonic flux and charge excitations which exhibit non-abelian statistics for non-abelian groups  $G$ . We proved the emergence of topological order in the many-body ground state analytically. In an upcoming paper, we show the existence of a finite excitation gap for the special case  $G = \mathbb{Z}_2$  [62]. The core idea of our construction is to enforce the no-flux constraint in the ground state by tailored blockade interactions such that the blockade graph exhibits local graph automorphisms. These automorphisms translate to local symmetries of the Hamiltonian, and the symmetric sector corresponds to the zero-charge sector of the corresponding quantum double model. In this framework, we developed a complete toolbox to explore the non-abelian character of flux anyons. This includes (i) efficient protocols for the

adiabatic preparation of ground states, (ii) deterministic and adiabatic preparation schemes of flux anyons in a well-defined fusion channel, (iii) a protocol for the adiabatic motion of these anyons (needed for braiding and fusion), and finally, (iv) a procedure to probe the fusion channel of anyons by measuring Wilson loops around them. Combined, these tools pave the way towards probing non-abelian topological phases in artificial matter based on realistic two-body interactions.

In this paper, both the construction of the blockade graph  $\mathcal{G}$  and the development of the toolbox were illustrated on the trivalent honeycomb lattice as this is the simplest setting to discuss quantum doubles. Note that this is not necessary, and the construction can be straightforwardly generalized to arbitrary lattices and even irregular planar graphs, in accordance with Kitaev’s original formulation of quantum doubles [5].

Another generalization concerns the choice of detunings. In our construction of  $\mathcal{G}$ , the detunings on sites and links were chosen such that  $\Delta_s = 2\Delta_l$ , combined with a sufficiently large blockade interaction  $U_0 > \Delta_s$ . These choices are not unique. For example, it is easy to see that the classical ground state manifold remains unchanged for  $\Delta_s > 2\Delta_l$  since larger  $\Delta_s$  only stabilize the no-flux constraint. An interesting open question is how the phase diagram is affected by variations of these parameters.

While our framework is motivated by the Rydberg platform, we stress that our abstract analysis omits the influence of microscopic van der Waals interactions. To study their effects, a concrete *embedding* of the blockade graphs in two or three dimensions would be necessary. For the special case  $G = \mathbb{Z}_2$  (toric code topological order), an explicit embedding of the corresponding blockade graph  $\mathcal{G}$  was provided in Ref. [56]. It is an interesting open question whether the proposed blockade graphs for general groups  $G$  can be embedded as well, and if so, how to achieve this most efficiently.

Alternatively, the proposed models could be realized on other platforms. Especially cold polar molecules in optical tweezers have recently seen significant progress, with the potential advantage of much longer lifetimes of excited states [63] and a high tunability of interaction potentials [31]. On the other hand, superconducting qubits that are connected by microwave cavities – which act as a bus to mediated blockade interactions [64] – have the potential to realize blockade graphs with far less restrictions on geometry. Such ideas can naturally be extended to Rydberg atoms in optical cavities that are connected by wave guides. On these platforms, the realization of the blockade graph directly translates to a wave guide structure, and therefore becomes a straightforward engineering task.

We close with a comment on an intriguing though abstract problem. Our construction leads to graphs with local automorphisms that, under certain circumstances, generate a single orbit on the set of maximum-weight independent sets. While there are trivial graphs which satisfy this condition, the maximum-weight independent

sets of our models have an intricate structure due to the local constraints; in particular, they cannot be “factorized” (the corresponding low-energy Hilbert space has no local tensor product structure). This raises the question how graphs with these properties can be classified and/or systematically constructed. This could be useful as each such graph might give rise to an interesting quantum many-body phase. For example, it would be interesting to explore whether there are graphs that stabilize the topological order of Fibonacci anyons, the simplest anyon model universal for topological quantum computation.

If this turns out to be *impossible*, it would be helpful to understand *why* to sharpen our understanding of the limitations of blockade structures.

## ACKNOWLEDGMENTS

We thank Jean-Noël Fuchs for his introduction to quantum double models and Spyridon Michalakis for providing clarifications about the gap stability theorem.

- 
- [1] A. Kitaev and J. Preskill, *Topological Entanglement Entropy*, Physical Review Letters **96**, 110404 (2006), doi:[10.1103/physrevlett.96.110404](https://doi.org/10.1103/physrevlett.96.110404).
- [2] M. Levin and X.-G. Wen, *Detecting Topological Order in a Ground State Wave Function*, Physical Review Letters **96**, 110405 (2006), doi:[10.1103/physrevlett.96.110405](https://doi.org/10.1103/physrevlett.96.110405).
- [3] X.-G. Wen, *Topological Order: From Long-Range Entangled Quantum Matter to a Unified Origin of Light and Electrons*, International Scholarly Research Notices **2013**(1), 198710 (2013), doi:<https://doi.org/10.1155/2013/198710>.
- [4] X.-G. Wen, *Colloquium : Zoo of quantum-topological phases of matter*, Reviews of Modern Physics **89**(4), 041004 (2017), doi:[10.1103/revmodphys.89.041004](https://doi.org/10.1103/revmodphys.89.041004).
- [5] A. Kitaev, *Fault-tolerant quantum computation by anyons*, Annals of Physics **303**(1), 2 (2003), doi:[10.1016/s0003-4916\(02\)00018-0](https://doi.org/10.1016/s0003-4916(02)00018-0).
- [6] H. Bombin and M. A. Martin-Delgado, *Topological Quantum Distillation*, Phys. Rev. Lett. **97**, 180501 (2006), doi:[10.1103/PhysRevLett.97.180501](https://doi.org/10.1103/PhysRevLett.97.180501).
- [7] B. M. Terhal, *Quantum error correction for quantum memories*, Rev. Mod. Phys. **87**, 307 (2015), doi:[10.1103/RevModPhys.87.307](https://doi.org/10.1103/RevModPhys.87.307).
- [8] M. H. Freedman, A. Kitaev, M. J. Larsen and Z. Wang, *Topological quantum computation*, Bulletin of the American Mathematical Society **40**(1), 31 (2002), doi:[10.1090/s0273-0979-02-00964-3](https://doi.org/10.1090/s0273-0979-02-00964-3).
- [9] C. Nayak, S. H. Simon, A. Stern, M. Freedman and S. Das Sarma, *Non-Abelian anyons and topological quantum computation*, Reviews of Modern Physics **80**, 1083 (2008), doi:[10.1103/revmodphys.80.1083](https://doi.org/10.1103/revmodphys.80.1083).
- [10] Z. Wang, *Topological Quantum Computation*, No. 112 in Regional Conference Series in Mathematics / Conference Board of the Mathematical Sciences. American Mathematical Society, Providence, Rhode Island, ISBN 9780821849309 (2010).
- [11] H. Bartolomei, M. Kumar, R. Bisognin, A. Marguerite, J.-M. Berroir, E. Bocquillon, B. Plaças, A. Cavanna, Q. Dong, U. Gennser, Y. Jin and G. Fève, *Fractional statistics in anyon collisions*, Science **368**(6487), 173 (2020), doi:[10.1126/science.aaz5601](https://doi.org/10.1126/science.aaz5601).
- [12] J. Nakamura, S. Liang, G. C. Gardner and M. J. Manfra, *Direct observation of anyonic braiding statistics*, Nature Physics **16**(9), 931 (2020), doi:<https://doi.org/10.1038/s41567-020-1019-1>.
- [13] K. Pakrouski, M. R. Peterson, T. Jolicœur, V. W. Scarola, C. Nayak and M. Troyer, *Phase Diagram of the  $\nu = 5/2$  Fractional Quantum Hall Effect: Effects of Landau-Level Mixing and Nonzero Width*, Phys. Rev. X **5**, 021004 (2015), doi:[10.1103/PhysRevX.5.021004](https://doi.org/10.1103/PhysRevX.5.021004).
- [14] A. Stern, *Non-Abelian states of matter*, Nature **464**(7286), 187 (2010), doi:<https://doi.org/10.1038/nature08915>.
- [15] S. C. Zhang, T. H. Hansson and S. Kivelson, *Effective-Field-Theory Model for the Fractional Quantum Hall Effect*, Phys. Rev. Lett. **62**, 82 (1989), doi:[10.1103/PhysRevLett.62.82](https://doi.org/10.1103/PhysRevLett.62.82).
- [16] A. Lopez and E. Fradkin, *Fractional quantum Hall effect and Chern-Simons gauge theories*, Phys. Rev. B **44**, 5246 (1991), doi:[10.1103/PhysRevB.44.5246](https://doi.org/10.1103/PhysRevB.44.5246).
- [17] B. I. Halperin, P. A. Lee and N. Read, *Theory of the half-filled Landau level*, Phys. Rev. B **47**, 7312 (1993), doi:[10.1103/PhysRevB.47.7312](https://doi.org/10.1103/PhysRevB.47.7312).
- [18] M. A. Levin and X.-G. Wen, *String-net condensation: A physical mechanism for topological phases*, Physical Review B **71**, 045110 (2005), doi:[10.1103/physrevb.71.045110](https://doi.org/10.1103/physrevb.71.045110).
- [19] L. Fidkowski, M. Freedman, C. Nayak, K. Walker and Z. Wang, *From String Nets to Nonabelions*, Communications in Mathematical Physics **287**(3), 805 (2009), doi:[10.1007/s00220-009-0757-9](https://doi.org/10.1007/s00220-009-0757-9).
- [20] A. Kitaev, *Anyons in an exactly solved model and beyond*, Annals of Physics **321**(1), 2 (2006), doi:[10.1016/j.aop.2005.10.005](https://doi.org/10.1016/j.aop.2005.10.005).
- [21] N. Lang and H. P. Büchler, *Topological states in a microscopic model of interacting fermions*, Phys. Rev. B **92**, 041118 (2015), doi:[10.1103/PhysRevB.92.041118](https://doi.org/10.1103/PhysRevB.92.041118).
- [22] R. M. Lutchyn, J. D. Sau and S. Das Sarma, *Majorana Fermions and a Topological Phase Transition in Semiconductor-Superconductor Heterostructures*, Phys. Rev. Lett. **105**, 077001 (2010), doi:[10.1103/PhysRevLett.105.077001](https://doi.org/10.1103/PhysRevLett.105.077001).
- [23] L. Fidkowski, R. M. Lutchyn, C. Nayak and M. P. A. Fisher, *Majorana zero modes in one-dimensional quantum wires without long-ranged superconducting order*, Phys. Rev. B **84**, 195436 (2011), doi:[10.1103/PhysRevB.84.195436](https://doi.org/10.1103/PhysRevB.84.195436).
- [24] N. Read and D. Green, *Paired states of fermions in two dimensions with breaking of parity and time-reversal symmetries and the fractional quantum Hall effect*, Phys. Rev. B **61**, 10267 (2000), doi:[10.1103/PhysRevB.61.10267](https://doi.org/10.1103/PhysRevB.61.10267).
- [25] D. A. Ivanov, *Non-Abelian Statistics of Half-Quantum Vortices in  $p$ -Wave Superconductors*, Phys. Rev. Lett. **86**, 268 (2001), doi:[10.1103/PhysRevLett.86.268](https://doi.org/10.1103/PhysRevLett.86.268).

- [26] N. Regnault and B. A. Bernevig, *Fractional Chern Insulator*, Phys. Rev. X **1**, 021014 (2011), doi:[10.1103/PhysRevX.1.021014](https://doi.org/10.1103/PhysRevX.1.021014).
- [27] K. Sun, Z. Gu, H. Katsura and S. Das Sarma, *Nearly Flatbands with Nontrivial Topology*, Phys. Rev. Lett. **106**, 236803 (2011), doi:[10.1103/PhysRevLett.106.236803](https://doi.org/10.1103/PhysRevLett.106.236803).
- [28] E. Tang, J.-W. Mei and X.-G. Wen, *High-Temperature Fractional Quantum Hall States*, Phys. Rev. Lett. **106**, 236802 (2011), doi:[10.1103/PhysRevLett.106.236802](https://doi.org/10.1103/PhysRevLett.106.236802).
- [29] Y. Jia, J. Yu, J. Liu, J. Herzog-Arbeitman, Z. Qi, H. Pi, N. Regnault, H. Weng, B. A. Bernevig and Q. Wu, *Moiré fractional Chern insulators. I. First-principles calculations and continuum models of twisted bilayer MoTe<sub>2</sub>*, Phys. Rev. B **109**, 205121 (2024), doi:[10.1103/PhysRevB.109.205121](https://doi.org/10.1103/PhysRevB.109.205121).
- [30] L.-M. Duan, E. Demler and M. D. Lukin, *Controlling Spin Exchange Interactions of Ultracold Atoms in Optical Lattices*, Phys. Rev. Lett. **91**, 090402 (2003), doi:[10.1103/PhysRevLett.91.090402](https://doi.org/10.1103/PhysRevLett.91.090402).
- [31] A. Micheli, G. K. Brennen and P. Zoller, *A toolbox for lattice-spin models with polar molecules*, Nature Physics **2**(5), 341 (2006), doi:[10.1038/nphys287](https://doi.org/10.1038/nphys287).
- [32] N. C. and, *Rapidly rotating atomic gases*, Advances in Physics **57**(6), 539 (2008), doi:[10.1080/00018730802564122](https://doi.org/10.1080/00018730802564122).
- [33] C. V. Kraus, M. Dalmonte, M. A. Baranov, A. M. Läuchli and P. Zoller, *Majorana Edge States in Atomic Wires Coupled by Pair Hopping*, Phys. Rev. Lett. **111**, 173004 (2013), doi:[10.1103/PhysRevLett.111.173004](https://doi.org/10.1103/PhysRevLett.111.173004).
- [34] A. Bühler, N. Lang, C. V. Kraus, G. Möller, S. D. Huber and H. P. Büchler, *Majorana modes and p-wave superfluids for fermionic atoms in optical lattices*, Nature Communications **5**(1), 4504 (2014), doi:[10.1038/ncomms5504](https://doi.org/10.1038/ncomms5504).
- [35] N. Y. Yao, A. V. Gorshkov, C. R. Laumann, A. M. Läuchli, J. Ye and M. D. Lukin, *Realizing Fractional Chern Insulators in Dipolar Spin Systems*, Phys. Rev. Lett. **110**, 185302 (2013), doi:[10.1103/PhysRevLett.110.185302](https://doi.org/10.1103/PhysRevLett.110.185302).
- [36] S. Weber, R. Bai, N. Makki, J. Mögerle, T. Lahaye, A. Browaeys, M. Daghofer, N. Lang and H. P. Büchler, *Experimentally Accessible Scheme for a Fractional Chern Insulator in Rydberg Atoms*, PRX Quantum **3**, 030302 (2022), doi:[10.1103/PRXQuantum.3.030302](https://doi.org/10.1103/PRXQuantum.3.030302).
- [37] S. de Léséleuc, V. Lienhard, P. Scholl, D. Barredo, S. Weber, N. Lang, H. P. Büchler, T. Lahaye and A. Browaeys, *Observation of a symmetry-protected topological phase of interacting bosons with Rydberg atoms*, Science **365**(6455), 775 (2019), doi:[10.1126/science.aav9105](https://doi.org/10.1126/science.aav9105).
- [38] R. Verresen, M. D. Lukin and A. Vishwanath, *Prediction of Toric Code Topological Order from Rydberg Blockade*, Physical Review X **11**(3), 031005 (2021), doi:[10.1103/physrevx.11.031005](https://doi.org/10.1103/physrevx.11.031005).
- [39] G. Semeghini, H. Levine, A. Keesling, S. Ebadi, T. T. Wang, D. Bluvstein, R. Verresen, H. Pichler, M. Kalinowski, R. Samajdar, A. Omran, S. Sachdev *et al.*, *Probing topological spin liquids on a programmable quantum simulator*, Science **374**(6572), 1242 (2021), doi:[10.1126/science.abi8794](https://doi.org/10.1126/science.abi8794).
- [40] R. Sahay, A. Vishwanath and R. Verresen, *Quantum Spin Puddles and Lakes: NISQ-Era Spin Liquids from Non-Equilibrium Dynamics*, arXiv (2022), doi:[10.48550/arxiv.2211.01381](https://doi.org/10.48550/arxiv.2211.01381).
- [41] G. Giudici, M. D. Lukin and H. Pichler, *Dynamical Preparation of Quantum Spin Liquids in Rydberg Atom Arrays*, Physical Review Letters **129**(9), 090401 (2022), doi:[10.1103/physrevlett.129.090401](https://doi.org/10.1103/physrevlett.129.090401).
- [42] F. Nogrette, H. Labuhn, S. Ravets, D. Barredo, L. Béguin, A. Vernier, T. Lahaye and A. Browaeys, *Single-Atom Trapping in Holographic 2D Arrays of Microtraps with Arbitrary Geometries*, Physical Review X **4**(2), 021034 (2014), doi:[10.1103/physrevx.4.021034](https://doi.org/10.1103/physrevx.4.021034).
- [43] D. Barredo, S. de Léséleuc, V. Lienhard, T. Lahaye and A. Browaeys, *An atom-by-atom assembler of defect-free arbitrary two-dimensional atomic arrays*, Science **354**(6315), 1021 (2016), doi:[10.1126/science.aah3778](https://doi.org/10.1126/science.aah3778).
- [44] H. Bernien, S. Schwartz, A. Keesling, H. Levine, A. Omran, H. Pichler, S. Choi, A. S. Zibrov, M. Endres, M. Greiner, V. Vuletić and M. D. Lukin, *Probing many-body dynamics on a 51-atom quantum simulator*, Nature **551**(7682), 579 (2017), doi:[10.1038/nature24622](https://doi.org/10.1038/nature24622).
- [45] D. Barredo, V. Lienhard, S. de Léséleuc, T. Lahaye and A. Browaeys, *Synthetic three-dimensional atomic structures assembled atom by atom*, Nature **561**(7721), 79 (2018), doi:[10.1038/s41586-018-0450-2](https://doi.org/10.1038/s41586-018-0450-2).
- [46] D. Jaksch, J. I. Cirac, P. Zoller, S. L. Rolston, R. Côté and M. D. Lukin, *Fast Quantum Gates for Neutral Atoms*, Physical Review Letters **85**(10), 2208 (2000), doi:[10.1103/physrevlett.85.2208](https://doi.org/10.1103/physrevlett.85.2208).
- [47] M. Saffman, T. G. Walker and K. Mølmer, *Quantum information with Rydberg atoms*, Reviews of Modern Physics **82**(3), 2313 (2010), doi:[10.1103/RevModPhys.82.2313](https://doi.org/10.1103/RevModPhys.82.2313).
- [48] D. Barredo, H. Labuhn, S. Ravets, T. Lahaye, A. Browaeys and C. S. Adams, *Coherent Excitation Transfer in a Spin Chain of Three Rydberg Atoms*, Phys. Rev. Lett. **114**, 113002 (2015), doi:[10.1103/PhysRevLett.114.113002](https://doi.org/10.1103/PhysRevLett.114.113002).
- [49] H. Pichler, S.-T. Wang, L. Zhou, S. Choi and M. D. Lukin, *Computational complexity of the Rydberg blockade in two dimensions*, arXiv (2018), doi:[10.48550/arxiv.1809.04954](https://doi.org/10.48550/arxiv.1809.04954).
- [50] C. J. Turner, A. A. Michailidis, D. A. Abanin, M. Serbyn and Z. Papić, *Weak ergodicity breaking from quantum many-body scars*, Nature Physics **14**(7), 745 (2018), doi:[10.1038/s41567-018-0137-5](https://doi.org/10.1038/s41567-018-0137-5).
- [51] C.-J. Lin and O. I. Motrunich, *Exact Quantum Many-Body Scar States in the Rydberg-Blockaded Atom Chain*, Phys. Rev. Lett. **122**, 173401 (2019), doi:[10.1103/PhysRevLett.122.173401](https://doi.org/10.1103/PhysRevLett.122.173401).
- [52] D. Bluvstein, A. Omran, H. Levine, A. Keesling, G. Semeghini, S. Ebadi, T. T. Wang, A. A. Michailidis, N. Maskara, W. W. Ho, S. Choi, M. Serbyn *et al.*, *Controlling quantum many-body dynamics in driven Rydberg atom arrays*, Science **371**(6536), 1355 (2021), doi:[10.1126/science.abg2530](https://doi.org/10.1126/science.abg2530).
- [53] S. Ebadi, A. Keesling, M. Cain, T. T. Wang, H. Levine, D. Bluvstein, G. Semeghini, A. Omran, J.-G. Liu, R. Samajdar, X.-Z. Luo, B. Nash *et al.*, *Quantum optimization of maximum independent set using Rydberg atom arrays*, Science **376**(6598), 1209 (2022), doi:[10.1126/science.abo6587](https://doi.org/10.1126/science.abo6587).
- [54] M.-T. Nguyen, J.-G. Liu, J. Wurtz, M. D. Lukin, S.-T. Wang and H. Pichler, *Quantum Optimization with Arbitrary Connectivity Using Rydberg Atom Arrays*, PRX Quantum **4**, 010316 (2023), doi:[10.1103/PRXQuantum.4.010316](https://doi.org/10.1103/PRXQuantum.4.010316).
- [55] S. Stastny, H. P. Büchler and N. Lang, *Functional completeness of planar Rydberg blockade structures*, Physical Review B **108**(8), 085138 (2023), doi:[10.1103/physrevb.108.085138](https://doi.org/10.1103/physrevb.108.085138).

- [56] T. F. Maier, H. P. Büchler and N. Lang, *Topological Order in Symmetric Blockade Structures*, PRX Quantum **6**(3) (2025), doi:[10.1103/dtlf-2q82](https://doi.org/10.1103/dtlf-2q82).
- [57] C. Chamon, D. Green and Z.-C. Yang, *Constructing quantum spin liquids using combinatorial gauge symmetry*, Physical Review Letters **125**(6) (2020), doi:[10.1103/physrevlett.125.067203](https://doi.org/10.1103/physrevlett.125.067203).
- [58] Z.-C. Yang, D. Green, H. Yu and C. Chamon,  *$\mathbb{Z}_3$  Quantum Double in a Superconducting Wire Array*, PRX Quantum **2**, 030327 (2021), doi:[10.1103/PRXQuantum.2.030327](https://doi.org/10.1103/PRXQuantum.2.030327).
- [59] D. Green and C. Chamon, *Constructing non-abelian quantum spin liquids using combinatorial gauge symmetry*, SciPost Physics **15**(2) (2023), doi:[10.21468/scipostphys.15.2.067](https://doi.org/10.21468/scipostphys.15.2.067).
- [60] H. Yu, D. Green, A. E. Ruckenstein and C. Chamon, *Abelian combinatorial gauge symmetry*, SciPost Physics Core **7**(1) (2024), doi:[10.21468/scipostphyscore.7.1.014](https://doi.org/10.21468/scipostphyscore.7.1.014).
- [61] H. Yu, D. Green and C. Chamon, *Non-Abelian combinatorial gauge theory*, Phys. Rev. B **111**, 235115 (2025), doi:[10.1103/PhysRevB.111.235115](https://doi.org/10.1103/PhysRevB.111.235115).
- [62] S. Fell, T. F. Maier, H. P. Büchler and N. Lang, to be published (2025).
- [63] D. K. Ruttley, T. R. Hepworth, A. Guttridge and S. L. Cornish, *Long-lived entanglement of molecules in magic-wavelength optical tweezers*, Nature **637**(8047), 827 (2025), doi:[10.1038/s41586-024-08365-1](https://doi.org/10.1038/s41586-024-08365-1).
- [64] A. Blais, A. L. Grimsmo, S. M. Girvin and A. Wallraff, *Circuit quantum electrodynamics*, Rev. Mod. Phys. **93**, 025005 (2021), doi:[10.1103/RevModPhys.93.025005](https://doi.org/10.1103/RevModPhys.93.025005).
- [65] H. Bombin and M. A. Martin-Delgado, *Family of non-Abelian Kitaev models on a lattice: Topological condensation and confinement*, Phys. Rev. B **78**, 115421 (2008), doi:[10.1103/PhysRevB.78.115421](https://doi.org/10.1103/PhysRevB.78.115421).
- [66] S. X. Cui, S.-M. Hong and Z. Wang, *Universal quantum computation with weakly integral anyons*, Quantum Information Processing **14**(8), 2687 (2015), doi:[10.1007/s11128-015-1016-y](https://doi.org/10.1007/s11128-015-1016-y).
- [67] A. Kómar and O. Landon-Cardinal, *Anyons are not energy eigenspaces of quantum double Hamiltonians*, Phys. Rev. B **96**, 195150 (2017), doi:[10.1103/PhysRevB.96.195150](https://doi.org/10.1103/PhysRevB.96.195150).
- [68] S. X. Cui, D. Ding, X. Han, G. Penington, D. Ranard, B. C. Rayhaun and Z. Shangnan, *Kitaev's quantum double model as an error correcting code*, Quantum **4**, 331 (2020), doi:[10.22331/q-2020-09-24-331](https://doi.org/10.22331/q-2020-09-24-331).
- [69] S. H. Simon, *Topological Quantum*, Oxford University Press, Oxford, ISBN 978-0-19-888672-3 (2023).
- [70] R. Dijkgraaf, V. Pasquier and P. Roche, *Quasi hopf algebras, group cohomology and orbifold models*, Nuclear Physics B - Proceedings Supplements **18**(2), 60 (1991), doi:[https://doi.org/10.1016/0920-5632\(91\)90123-V](https://doi.org/10.1016/0920-5632(91)90123-V).
- [71] S. Majid, *Quantum Double for Quasi-Hopf Algebras*, Letters in Mathematical Physics **45**(1), 1 (1998), doi:[10.1023/A:1007450123281](https://doi.org/10.1023/A:1007450123281).
- [72] On a torus, not all ground state configurations  $|\mathbf{g}\rangle \in \mathcal{H}_G^0$  (satisfying the no-flux constraint on every site) can be generated by applying plaquette (or loop) automorphisms on the state  $|e\rangle$  with all  $g_i = e$ . This partitions  $\mathcal{H}_G^0$  into *topological sectors* – and the amplitudes in the (unique) ground state between these sectors are not necessarily fixed by symmetries.
- [73] S. Bravyi, M. B. Hastings and S. Michalakis, *Topological quantum order: Stability under local perturbations*, Journal of Mathematical Physics **51**(9) (2010), doi:[10.1063/1.3490195](https://doi.org/10.1063/1.3490195).
- [74] S. Michalakis and J. P. Zwolak, *Stability of Frustration-Free Hamiltonians*, Communications in Mathematical Physics **322**(2), 277 (2013), doi:[10.1007/s00220-013-1762-6](https://doi.org/10.1007/s00220-013-1762-6).
- [75] S. Bravyi and M. B. Hastings, *A Short Proof of Stability of Topological Order under Local Perturbations*, Communications in Mathematical Physics **307**(3), 609 (2011), doi:[10.1007/s00220-011-1346-2](https://doi.org/10.1007/s00220-011-1346-2).
- [76] X. Chen, Z.-C. Gu and X.-G. Wen, *Local unitary transformation, long-range quantum entanglement, wave function renormalization, and topological order*, Physical Review B **82**(15), 155138 (2010), doi:[10.1103/physrevb.82.155138](https://doi.org/10.1103/physrevb.82.155138).
- [77] S. Bravyi, D. P. DiVincenzo and D. Loss, *Schrieffer-Wolff transformation for quantum many-body systems*, Annals of Physics **326**(10), 2793 (2011), doi:[10.1016/j.aop.2011.06.004](https://doi.org/10.1016/j.aop.2011.06.004).
- [78] V. G. Drinfel'd, *Quantum groups*, Journal of Soviet Mathematics **41**(2), 898 (1988), doi:[10.1007/bf01247086](https://doi.org/10.1007/bf01247086).
- [79] K. G. Wilson, *Confinement of quarks*, Phys. Rev. D **10**, 2445 (1974), doi:[10.1103/PhysRevD.10.2445](https://doi.org/10.1103/PhysRevD.10.2445).
- [80] K. Fredenhagen and M. Marcu, *Charged states in  $\mathbb{Z}_2$  gauge theories*, Communications in Mathematical Physics **92**(1), 81 (1983), doi:[10.1007/BF01206315](https://doi.org/10.1007/BF01206315).
- [81] K. Gregor, D. A. Huse, R. Moessner and S. L. Sondhi, *Diagnosing deconfinement and topological order*, New Journal of Physics **13**(2), 025009 (2011), doi:[10.1088/1367-2630/13/2/025009](https://doi.org/10.1088/1367-2630/13/2/025009).



**Important:** The technical nature of these appendices demands for a streamlined notation which does not always match the notation of the main text. We emphasize these differences when necessary.

## Appendix A: The graph for one site

In this appendix, we rigorously construct and discuss a generalized graph  $\mathcal{G}_C$  for a “class- $C$  site” with three emanating links. This site graph enforces the flux condition  $g_1 g_2 g_3 \in C$  for a conjugacy class  $C$  of the group  $G$ .  $\mathcal{G}_C$  corresponds to one part of the generalized site graph  $\mathcal{G}_s[\Delta]$  introduced in Section III and used in Fig. 4 (c), where  $\Delta_C = 4\Delta$  for one fixed class and all other site vertices that do not belong to this class are omitted. At the end, we consider the special case  $C = \{1\}$  where we recover the graph  $\mathcal{G}_{\{1\}}$  (labeled  $\mathcal{G}_s$  in the main text) from Fig. 1 (b) for a site with the zero-flux condition  $g_1 g_2 g_3 = 1$ . Note that throughout this appendix, we refer to the neutral element of a group as 1 (in the main text we use  $e$  instead).

In Appendix A1 we construct the graph  $\mathcal{G}_C$  and lay out the notation. Subsequently, in Appendix A2, we discuss its (local) graph automorphisms and the structure of its automorphism group. Specifically for  $C = \{1\}$ , we show that  $\text{Aut}_{\text{loc}}(\mathcal{G}_{\{1\}}) \cong G^2 \times \text{Aut}(G)$  for local graph automorphisms, as claimed in Section I. Then we discuss its maximum-weight independent sets in Appendix A3 and show that the graph is fully-symmetric in Appendix A4. Finally, in Appendix A5, we construct and discuss the “multi-class graph”  $\mathcal{G}_C$  from Section III for a site that incorporates all conjugacy classes (labeled  $\mathcal{G}_s[\Delta]$  in the main text).

### 1. Definition of the graph $\mathcal{G}_C$

We consider a generic group  $G$  of order  $N = |G|$  and a conjugacy class  $C \subseteq G$  of size  $M = |C|$ . In this subsection, we construct the vertex-weighted graph  $\mathcal{G}_C = (V_C, E_C, \Delta_C)$  for a class  $C$ -site  $s$  with three emanating links  $l \in \mathbb{Z}_3 := \{1, 2, 3\}$ . The labels  $l$  fix an ordering for the links. [In the tessellated structure in Appendix B, this ordering alternates between adjacent sites of the two sublattices. For just one site in this section, without any embedding in a larger graph these are just labels used for the construction.] Note the difference in notation compared to the main text, where we used the variables  $\{l_1, l_2, l_3\}$ . An exemplary construction with  $N = 6$  and  $M = 3$  is shown in Fig. 6.

We start with a fully-connected (= complete) graph  $K_{N^2 M} = (V_s^C, E_s^C, \Delta_s^C)$  with vertices  $V_s^C = G^2 \times C$  on the site. In this notation, each site-vertex is identified with a triple of group elements. As  $K_{N^2 M}$  is fully-connected, the edges  $E_s^C = \{\{v_s, w_s\} \mid v_s \neq w_s \in V_s^C\}$  on the site include each unordered pair of vertices. This is illustrated

by the thick green circle in Fig. 6. We choose a uniform weight  $\Delta_v = 4\Delta$  for the vertices  $v \in V_s^C$ .

Next, we construct the full graph  $\mathcal{G}_C$  as a graph extension of  $K_{N^2 M}$ . The full set of vertices  $V_C = V_s^C \cup \bigcup_{l \in \mathbb{Z}_3} V_l^C$  consists of the vertices on the site and additionally includes the vertices  $V_l^C = \{l\} \times G$  for each link. That is, the full graph consists of  $N^2 M + 3N$  vertices. In this notation, each link-vertex is identified with the label of its link and a group element from  $G$ . For the vertices  $v \in \mathbb{Z}_3 \times G$  on the links, we choose again uniform weights  $\Delta_v = 1\Delta$ . These vertices are fully-disconnected, meaning no two vertices on the links are connected. This is illustrated by the dashed black boxes in Fig. 6.

Finally, we define the edges between the vertices on the links and the site. To this end, we introduce the compact notation

$$\begin{aligned} g_3 &\equiv (g_1 g_2)^{-1} c \quad \text{for } w \equiv (g_1, g_2, c) \in V_s^C, \\ v_l &\equiv (l, h_l) \in V_l^C. \end{aligned} \quad (\text{A1})$$

Using this notation, we can write

$$E_l^C = \{\{w, v_l\} \mid w \in V_s^C, v_l \in V_l^C, g_l = h_l\} \quad (\text{A2})$$

for the set of edges between site-vertices and vertices of link  $l$ . These edges are drawn as the thin black lines in Fig. 6. The full set of edges of  $\mathcal{G}_C$  is then given by

$$E_C = E_s^C \cup \bigcup_{l \in \mathbb{Z}_3} E_l^C. \quad (\text{A3})$$

This fully defines the graph  $\mathcal{G}_C$ .

We conclude our construction with some remarks. Firstly, note that each vertex  $(g_1, g_2, c) \in V_s^C$  on the site is connected to the three vertices  $(l, g_l) \in V_l^C$  on the links, such that their group elements fulfill the *site constraint*

$$g_1 g_2 g_3 \in C. \quad (\text{A4})$$

Thus the site constraint writes the group structure of  $G$  into the edges of the graph  $\mathcal{G}_C$ . This makes the constraint Eq. (A4) central to the construction.

Secondly, note that for  $C = \{1\}$ , the above construction corresponds exactly to the graph defined in Fig. 1 (b). In the main text, we denoted the vertices on site  $s$  as  $w_s^{g_1 g_2 c}$  and the vertices on the link  $l \in \mathbb{Z}_3$  as  $v_l^{h_l}$  with group elements  $g_1, g_2, h_l \in G$  and  $c \in C$ . This notation can be interpreted as bijective maps

$$w_s : G^2 \times C \rightarrow V_s^C : (g_1, g_2, c) \mapsto w_s^{g_1 g_2 c}, \quad (\text{A5a})$$

$$v_l : \{l\} \times G \rightarrow V_l^C : (l, h_l) \mapsto v_l^{h_l}. \quad (\text{A5b})$$

In the above construction, we used these bijections to identify the vertex sets  $V_s^C \hat{=} G^2 \times C$  and  $V_l^C \hat{=} \{l\} \times G$ . This allows in the following for a more concise notation.

Finally, we note that this construction is not limited to the case of  $|\mathbb{Z}_3| = 3$  links on the honeycomb lattice. For  $n > 3$  links this construction remains well-defined for then  $N^{n-1} M$  vertices on the site.

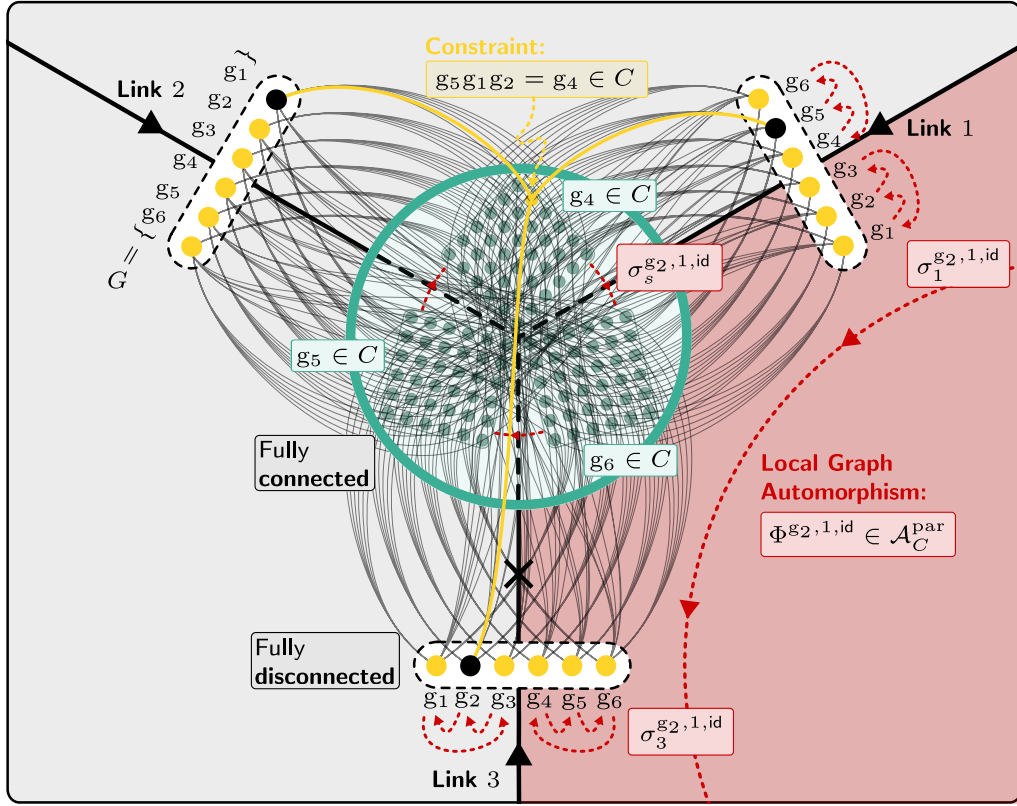


Figure 6. **Construction and automorphisms of  $\mathcal{G}_C$ .** Construction of a generalized site graph  $\mathcal{G}_C$  with three emanating links  $l \in \{1, 2, 3\}$  for an arbitrary conjugacy class  $C$  of the group  $G$ . This construction extends the condition for the group multiplication on this site to  $g_1 g_2 g_3 \in C$ , where  $g_l$  is the group element on link  $l$ . Italic symbols  $g_l$  label dummy variables and roman symbols  $g_l$  label specific group elements. Illustrated is an example for the group  $G = S_3$  with  $N = |G| = 6$  and elements  $(g_1, g_2, g_3, g_4, g_5, g_6) = (1, R, R^2, \sigma, R\sigma, R^2\sigma)$ . As conjugacy class, we consider  $C = \{\sigma, R\sigma, R^2\sigma\}$  with  $M = |C| = 3$ . The  $N^2 M$  vertices on the site (green points and one yellow) are fully connected (blockades not shown). On each link there are  $N$  vertices (black and yellow points) that are fully disconnected. Each vertex on the site is connected via an edge (thin black lines) to one vertex on each link. Each link is assigned an inward-pointing orientation (black arrow). We mark the link  $l = 2$  (black X) to fix the group multiplication order  $g_1 g_2 g_3$  of the group elements  $g_l$  on the links, as well as the labeling  $(g_1, g_2, c) \in G^2 \times C$  of vertices on the site. (It is important to stress that the constructed graph is still rotation symmetric.) The exemplary group multiplication  $g_5 g_1 g_2 = g_4$ , which satisfies the constraint for this site, is highlighted by yellow edges. The yellow vertices on the site and on the links are the corresponding maximum-weight independent set (MWIS)  $M_w$  with  $w = (g_5, g_1, g_4)$ . Note that this MWIS includes all but one vertex on each link, which associates the group element to the link. Also shown is a specific local graph automorphism  $\Phi^{g_2, 1, \text{id}} \in \mathcal{A}_C$  that corresponds to a plaquette automorphism  $\Theta_p(g_2)$  on the lower-right plaquette (dashed red lines). It splits into the group permutations (short dashed red arrows)  $\sigma_0^{g_2, 1, \text{id}}$ ,  $\sigma_2^{g_2, 1, \text{id}}$  and  $\sigma_3^{g_2, 1, \text{id}}$  on link 0, link 2, and site  $s$ , respectively. This specific automorphisms leaves the vertices of link 1 invariant.

## 2. Graph automorphisms of $\mathcal{G}_C$

A *graph automorphism* of a vertex-weighted graph  $\mathcal{G} = (V, E, W)$  is a bijection  $\Phi \in \text{Sym}(V)$  on the vertices that preserves ...

1. the connectivity,

$$\{v, w\} \in E \Leftrightarrow \{\Phi(v), \Phi(w)\} \in E, \quad (\text{A6})$$

2. and the vertex weights,

$$\forall v \in V : \Delta_{\Phi(v)} = \Delta_v. \quad (\text{A7})$$

Here,  $\text{Sym}(X)$  denotes the group of permutations on the set  $X$ . The graph automorphisms of  $\mathcal{G}$  form a group  $\text{Aut}(\mathcal{G})$  via concatenation.

In the following, we consider the vertex-weighted graph  $\mathcal{G}_C$  constructed in Appendix A1. We use the shorthand notation (A1) and denote as  $\mathcal{A}_C \equiv \text{Aut}(\mathcal{G}_C)$  its group of graph automorphisms. Note that the graph  $\mathcal{G}_C$  consists of vertices  $V_s^C$  and  $V_l^C$  with different weights. Hence a graph automorphism  $\Phi \in \mathcal{A}_C$  only satisfies the condition (A7) if it has the form

$$\Phi = \phi_s \circ \varphi_l, \quad (\text{A8})$$

with  $\phi_s \in \text{Sym}(V_s^C)$  and  $\varphi_l \in \text{Sym}(\bigcup_{l \in \mathbb{Z}_3} V_l^C)$ .

As a starting point, notice that  $\mathcal{G}_C$  features the graph automorphism

$$\begin{aligned} \Phi_R : V_l^C &\rightarrow V_{l+1}^C : (l, h_l) &\mapsto (l+1, h_l) \\ V_s^C &\rightarrow V_s^C : (g_1, g_2, c) &\mapsto (g_3, g_1, g_3 c g_3^{-1}), \end{aligned} \quad (\text{A9})$$

with  $g_3 \equiv (g_1 g_2)^{-1} c$  as defined above; here addition of link labels is meant modulo-3. This automorphism reflects the rotation symmetry of the site since it permutes the link vertices by increasing their indices  $l \mapsto l+1 \pmod{3}$ . Note that in the current notation, it is not obvious that this is a graph automorphism. To see this, we extend the shorthand notation (A1) by

$$\begin{aligned} g'_3 &\equiv (g'_1 g'_2)^{-1} c' \quad \text{for } w' \equiv (g'_1, g'_2, c') \equiv \Phi(w), \\ v'_{l'} &\equiv (l', h'_{l'}) \equiv \Phi(v_l). \end{aligned} \quad (\text{A10})$$

First, note that  $g_3 c g_3^{-1} \in C$  so that the map (A9) is well-defined. With  $\Phi_R^2(w) = (g_2, g_3, [g_2 g_3] c [g_2 g_3]^{-1})$ , it is easy to see that  $\Phi_R^3 = \text{id}$ ; therefore the map is bijective. Second,  $\Phi_R$  acts bijectively on  $E_C$  [recall Eq. (A6)] since

$$g'_1 = g_3 = h_3 = h'_1, \quad (\text{A11a})$$

$$g'_2 = g_1 = h_1 = h'_2, \quad (\text{A11b})$$

$$g'_3 = (g_3 g_1)^{-1} g_3 c g_3^{-1} = g_2 = h_2 = h'_3. \quad (\text{A11c})$$

Since  $\Phi_R$  does not mix  $V_l^C$  and  $V_s^C$ , Eq. (A7) is trivially satisfied. This shows that  $\Phi_R \in \mathcal{A}_C$  is indeed a graph automorphism of  $\mathcal{G}_C$ . This is also apparent in the rotational symmetry of Fig. 6.

At this point the question arises whether  $\mathcal{G}_C$  also features a mirror symmetry of the form

$$\begin{aligned} \Phi_M : V_1^C &\rightarrow V_2^C : (1, h_1) &\mapsto (2, h_1) \\ V_2^C &\rightarrow V_1^C : (2, h_2) &\mapsto (1, h_2) \\ V_s^C &\rightarrow V_s^C : (g_1, g_2, c) &\mapsto (g_2, g_1, c), \end{aligned} \quad (\text{A12})$$

that exchanges only the vertices  $V_1^C$  and  $V_2^C$  leaving  $V_3^C$  invariant. This map is bijective as  $\Phi_M^2 = \text{id}$ , and  $\Phi_M$  satisfies Eq. (A7) as it does not mix  $V_l^C$  and  $V_s^C$ . Nevertheless, the map (A12) is *no* graph automorphism for a non-abelian group  $G$  as  $\Phi_M$  does not act bijectively on  $E_C$  [recall Eq. (A6)]:

$$g'_3 = (g_2 g_1)^{-1} c \neq (g_1 g_2)^{-1} c = g_3 = h_3 = h'_3; \quad (\text{A13})$$

the site constraint (A4) that characterizes the edges  $E_C$  inherently depends on the ordering of the links (up to cyclic permutations). In fact, the (non-abelian) example constructed in Fig. 6 is actually not mirror symmetric. Only for abelian groups the multiplication  $g_1 g_2 = g_2 g_1$  is commutative for every group element  $g_1, g_2 \in G$ ; in this case Eq. (A12) defines a valid graph automorphism.

Although the rotation symmetry of  $\mathcal{G}_C$  is conceptually important, it is not relevant for the following discussion. Henceforth we are interested in *local graph automorphisms* of the more restrictive form [cf. Eq. (A8)]

$$\Phi = \phi_s \circ \varphi_1 \circ \varphi_2 \circ \varphi_3, \quad (\text{A14})$$

where  $\phi_s \in \text{Sym}(V_s^C)$  and  $\varphi_l \in \text{Sym}(V_l^C)$ . This means that local graph automorphisms only permute vertices *within links*, but not between links. The local graph automorphisms span a subgroup of the full automorphism group, we denote this subgroup as  $\mathcal{A}_C^{\text{loc}}$ .

Consider a local graph automorphism  $\Phi \in \mathcal{A}_C^{\text{loc}}$  of the form (A14). Using the shorthand notation of Eqs. (A1) and (A10), this implies  $l' = l$ . Then we can define  $\sigma_l \in \text{Sym}(G)$  and  $\varsigma_s : V_s^C \rightarrow C$  by  $\sigma_l(h_l) = h'_l$  and  $\varsigma_s(w) = c'$ , respectively. As a graph automorphism,  $\Phi$  must fulfill the connectivity condition (A6), that means  $g'_l = h'_l$  if and only if  $g_l = h_l$ . With the newly defined  $\sigma_l$  and  $\varsigma_s$ , this implies

$$\varphi_l(v_l) = (l, \sigma_l(h_l)), \quad (\text{A15a})$$

$$\phi_s(w) = (\sigma_1(g_1), \sigma_2(g_2), \varsigma_s(w)), \quad (\text{A15b})$$

$$\varsigma_s(w) = \sigma_1(g_1) \sigma_2(g_2) \sigma_3(g_3), \quad (\text{A15c})$$

for all  $g_1, g_2 \in G$  and  $c \in C$ . Eq. (A15c) poses a constraint on the allowed choices for  $\sigma_l$  and  $\varsigma_s$ ; if it is satisfied, then Eq. (A15a) and Eq. (A15b) define  $\varphi_l$  and  $\phi_s$  which, in turn, fully determine  $\Phi \in \mathcal{A}_C^{\text{loc}}$  via Eq. (A14).

Note that  $\varsigma_s(w)$  with  $w \equiv (g_1, g_2, c)$  generally depends on all three variables  $g_1, g_2 \in G$  and  $c \in C$ . For a general group  $G$ , we are not aware of a way to classify *all possible* functions  $\sigma_l$  and  $\varsigma_s$  that satisfy Eq. (A15c). However, this is not necessary for our purposes anyway. To solve Eq. (A15c), we make the ansatz  $\varsigma_s(w) = \sigma_s(c)$  which does not depend on the specific group elements  $g_1, g_2 \in G$ , such that  $\sigma \in \text{Sym}(C)$  is well-defined. This leads to the simpler constraint

$$\sigma_s(c) = \sigma_1(g_1) \sigma_2(g_2) \sigma_3(g_3) \quad (\text{A16})$$

with  $g_3 \equiv (g_1 g_2)^{-1} c$  for every  $(g_1, g_2, c) \in V_s^C$ . Pictorially in Fig. 6, this restricts the local graph automorphisms to collective permutations of the patches of vertices with equal  $c$  on the site. Crucially, for the case  $C = \{1\}$ , there is only one patch and the function  $\sigma_s$  can only be constant and equal to 1. Thus, for this special case, the following characterization yields the *full* local automorphism group.

In the next step, we derive a set of equivalent relations from Eq. (A16). For  $c \in C$  and  $g, h \in G$ , consider the three vertices  $(gh, 1, c)$ ,  $(g, h, c)$ , and  $(1, gh, c) \in V_s^C$  for which  $g_3 = (gh)^{-1} c$ . Plugging this in Eq. (A16) and equating for  $\sigma_s(c) [\sigma_3(g_3)]^{-1}$ , we obtain

$$\sigma_1(gh) \sigma_2(1) = \sigma_1(g) \sigma_2(h) = \sigma_1(1) \sigma_2(gh). \quad (\text{A17})$$

Specifically for  $h = 1$ , we can evaluate the right-hand side of Eq. (A17) as

$$\sigma_2(g) = [\sigma_1(1)]^{-1} \sigma_1(g) \sigma_2(1), \quad (\text{A18})$$

and plugging this in the left-hand side of Eq. (A17) yields

$$\sigma_1(gh) = \sigma_1(g) [\sigma_1(1)]^{-1} \sigma_1(h). \quad (\text{A19})$$

Finally, for  $c \in C$  and  $g \in G$  consider  $(c g^{-1}, 1, c) \in V_s^C$  with  $g_3 = g$ . Then Eq. (A16) yields

$$\sigma_3(g) = [\sigma_1(c g^{-1}) \sigma_2(1)]^{-1} \sigma_s(c). \quad (\text{A20})$$

Eqs. (A18) to (A20) must be valid for all  $g, h \in G$  and  $c \in C$ .

We now use Eq. (A19) to translate  $\sigma_1$  into known algebraic objects. To this end, we define the left ( $\lambda$ ) and right ( $\rho$ ) translation and the conjugation ( $\chi$ ) on the group as follows:

$$\lambda: G \rightarrow \text{Sym}(G) : g \mapsto (\lambda_g : h \mapsto gh), \quad (\text{A21a})$$

$$\rho: G \rightarrow \text{Sym}(G) : g \mapsto (\rho_g : h \mapsto hg^{-1}), \quad (\text{A21b})$$

$$\chi: G \rightarrow \text{Sym}(G) : g \mapsto \chi_g = \lambda_g \circ \rho_g. \quad (\text{A21c})$$

Setting  $\tau := \lambda_{[\sigma_1(1)]^{-1}} \circ \sigma_1 \in \text{Sym}(G)$ , condition (A19) becomes  $\tau(gh) = \tau(g)\tau(h)$  for all  $g, h \in G$ ; this means that  $\tau \in \text{Aut}(G)$  must be a *group automorphism*. If we select a group element  $p_1 := \sigma_1(1) \in G$  and a group automorphism  $\tau \in \text{Aut}(G)$ , this already fully defines  $\sigma_1 = \lambda_{p_1} \circ \tau$ . In addition, we can choose a group element  $p_2 := [\sigma_2(1)]^{-1} \in G$ . Then Eq. (A18) already fully determines  $\sigma_2 = \rho_{p_2} \circ \tau$ .

Finally, we determine  $\sigma_3$  and  $\sigma_s$ . To this end, we define  $p_3 := p_1^{-1}[\sigma_3(1)]^{-1}p_2$ . Then for  $g = 1$ , Eq. (A20) determines  $\sigma_s = \chi_{p_3} \circ (\rho_{p_3} \circ \tau)$ . But  $\sigma_s$  can only take values in  $C$ , thus  $\rho_{p_3} \circ \tau$  must map to  $C$ . We are not aware of a general criterion on  $\tau$  and  $p_3$  such that this is satisfied; but again, this is not necessary for our purposes. In the following, we restrict ourselves to the subgroup of  $\mathcal{A}_C^{\text{loc}}$  where  $p_3 = 1$  and  $\tau \in \text{Aut}_C(G)$ . Here,  $\text{Aut}_C(G)$  denotes the subgroup of  $\text{Aut}(G)$  that preserves the conjugacy class  $C$ . This includes at least the conjugations (= *inner automorphisms*)  $\chi_G$ . Then we obtain  $\sigma_s = \chi_{p_1} \circ \tau$ , and Eq. (A20) fully defines  $\sigma_3 = \lambda_{p_2} \circ \rho_{p_1} \circ \tau$ . Crucially, for  $C = \{1\}$ , the full automorphism group  $\text{Aut}(G) = \text{Aut}_{\{1\}}(G)$  is  $C$ -preserving, such that  $p_3 = 1$  is the only  $C$ -preserving choice. Thus, for this case, this characterization yields the full local automorphism group.

In summary, we parametrize the group permutations

$$\sigma_s^{p_1, p_2, \tau}(c) = p_1 \tau(c) p_1^{-1} \quad (\text{A22a})$$

$$\sigma_1^{p_1, p_2, \tau}(g) = p_1 \tau(g), \quad (\text{A22b})$$

$$\sigma_2^{p_1, p_2, \tau}(g) = \tau(g) p_2^{-1}, \quad (\text{A22c})$$

$$\sigma_3^{p_1, p_2, \tau}(g) = p_2 \tau(g) p_1^{-1} \quad (\text{A22d})$$

on  $g \in G$  and  $c \in C$  by parameters  $p_1, p_2 \in G$ , and  $\tau \in \text{Aut}_C(G)$ . It is now easy to see that the group permutations (A22) fulfill Eq. (A16) for any choice of parameters, and it is  $\sigma_s(c) \in C$  as required.

Now we derive the underlying structure of the parametrizing group. Consider  $p_1, p_2, p'_1, p'_2 \in G$  and  $\tau, \tau' \in \text{Aut}_C(G)$ , then concatenation yields

$$\sigma_x^{p_1, p_2, \tau} \circ \sigma_x^{p'_1, p'_2, \tau'} = \sigma_x^{p_1 \tau(p'_1), p_2 \tau(p'_2), \tau \circ \tau'} \quad (\text{A23})$$

for  $x \in \mathbb{Z}_3$  or  $x = s$ . Hence the parametrizing group is given by the semidirect product  $G^2 \rtimes \text{Aut}_C(G)$  with group product

$$(p_1, p_2, \tau) \cdot (p'_1, p'_2, \tau') = (p_1 \tau(p'_1), p_2 \tau(p'_2), \tau \circ \tau') \quad (\text{A24})$$

for  $(p_1, p_2, \tau), (p'_1, p'_2, \tau') \in G^2 \rtimes \text{Aut}_C(G)$ .

For each element  $(p_1, p_2, \tau) \in G^2 \rtimes \text{Aut}_C(G)$ , the parametrization (A22), together with Eqs. (A15a) and (A15b), determines a distinct local graph automorphism  $\Phi^{p_1, p_2, \tau} \in \mathcal{A}_C^{\text{loc}}$  of the form Eq. (A14). These local graph automorphisms span a subgroup  $\mathcal{A}_C^{\text{par}}$  of the full group of local graph automorphisms:

$$G^2 \rtimes \text{Aut}_C(G) \cong \mathcal{A}_C^{\text{par}} \leq \mathcal{A}_C^{\text{loc}}. \quad (\text{A25})$$

Crucially, for the case  $C = \{1\}$ , all our choices were dictated by the constraint (A15c). Hence, for this case, we have shown:

**Proposition 1.** *For  $C = \{1\}$ , the group of local graph automorphisms on  $\mathcal{G}_{\{1\}}$  ( $\mathcal{G}_s$  in the main text) is isomorphic to  $G^2 \rtimes \text{Aut}(G)$ .*

More generally, consider  $C = \{c\}$  with only one element  $c \in Z_G$  in the center of  $G$ . Note that this is the general case if  $G$  is Abelian. In this case,  $\varsigma_s(w) = c = \sigma_s(c)$  must be constant, hence condition (A16) is equivalent to condition (A15c). Furthermore, the condition  $\rho_{p_3} \circ \tau \in C$  is uniquely solved by  $p_3 \equiv c^{-1} \tau(c)$  for any  $\tau \in \text{Aut}(G)$ . This yields  $\sigma_s(c) = c$  and  $\sigma_3(g) = p_2 \tau(g) p_3^{-1} p_1^{-1}$  for  $g \in G$ . Together with Eqs. (A22b) and (A22c), it is easy to see that Eq. (A16) is fulfilled for any  $p_1, p_2 \in G$  and  $\tau \in \text{Aut}(G)$ . Note that  $p_3, p_3^{-1} \in Z_G$  are in the center since  $c^{-1}, \tau(c) \in Z_G$  for  $c \in Z_G$ . Then it is easy to check that Eq. (A23) remains satisfied for  $\sigma_s$  and  $\sigma_3$ . Therefore, the parametrizing group is still given by the semidirect product  $G^2 \rtimes \text{Aut}(G)$  with group product (A24). This construction therefore also yields the full group of local graph automorphisms:

**Proposition 2.** *For an Abelian group  $G$ , the group of local graph automorphisms on  $\mathcal{G}_C$  is isomorphic to  $G^2 \rtimes \text{Aut}(G)$ .*

By contrast, for a non-Abelian group  $G$  with  $C \not\subseteq Z_G$  not in the center, the above parametrization only yields a subgroup  $\mathcal{A}_C^{\text{par}}$  of  $\mathcal{A}_C^{\text{loc}}$ . For example, consider  $G = S_3$  and  $C = \{\sigma, \sigma R, \sigma R^2\}$  with the notation used in Section V. Note that  $\rho_{p_3} \circ \tau$  maps to  $C$  for  $\tau = \text{id}$  and  $p_3 = R$ . This makes

$$\begin{aligned} \Phi: V_3 &\rightarrow V_3 : (3, h_3) \mapsto (3, h_3 R^{-1}), \\ V_s^C &\rightarrow V_s^C : (g_1, g_2, c) \mapsto (g_1, g_2, c R^{-1}) \end{aligned} \quad (\text{A26})$$

with  $p_1, p_2 = 1$  a local graph automorphism on  $\mathcal{G}_C$  – which we did not capture with the above parametrization.

We conclude this section with some remarks on the rotation symmetry  $\Phi_R$  given by Eq. (A9). The subgroup  $\mathcal{A}_C^{\text{par}}$  determined by Eq. (A22) is not manifestly rotationally symmetric. This is due to our asymmetric choice of parametrization. For the concatenation with  $\Phi_R$  we obtain

$$\Phi^{p_1, p_2, \tau} \circ \Phi_R = \Phi_R \circ \Phi^{p_2^{-1}, p_1 p_2^{-1}, \chi_{p_2} \circ \tau}. \quad (\text{A27})$$

That is,  $\Phi_R$  permutes elements within  $\mathcal{A}_C^{\text{par}}$  such that  $\tau \mapsto \chi_{p_2} \circ \tau$  is modified by an additional conjugation. However, the full group  $\mathcal{A}_C^{\text{par}}$  is rotationally symmetric:

$$\mathcal{A}_C^{\text{par}} \circ \Phi_R = \Phi_R \circ \mathcal{A}_C^{\text{par}}. \quad (\text{A28})$$

### 3. Maximum-weight independent sets of $\mathcal{G}_C$

Since the subgraph  $K_{N^2M} = (V_s^C, E_s^C, \Delta_s^C)$  of  $\mathcal{G}_C$  on the site is fully connected, any independent set (IS) of  $\mathcal{G}_C$  can contain at most one vertex from  $V_s^C$ .

Consider a maximal IS (MIS)  $M_0$  of  $\mathcal{G}_C$  which includes no vertex from  $V_s^C$ . As the vertices  $V_l^C$  of link  $l$  are only connected to vertices of  $V_s^C$ , for  $M_0$  to be maximal, it must be  $V_l^C \subseteq M_0$ . Therefore, the MIS  $M_0 = \bigcup_{l \in \mathbb{Z}_3} V_l^C$  consists of all  $3N$  vertices on the links. Each such link-vertex has weight  $1\Delta$ , therefore  $M_0$  possesses the total weight  $3N\Delta$ .

Now we consider a MIS  $M_w$  of  $\mathcal{G}_C$  which includes one vertex  $w \equiv (g_1, g_2, c) \in V_s^C$  on the site. The vertex  $w$  is connected to three link-vertices  $(1, g_1)$ ,  $(2, g_2)$  and  $(3, g_3)$ , where we use the shorthand notation  $g_3 \equiv (g_1 g_2)^{-1} c$  from Eq. (A1). Thus, for  $M_w$  to be maximal, it must include all but these three link-vertices:

$$M_w = \{w\} \cup \bigcup_{l \in \mathbb{Z}_3} [V_l^C \setminus (l, g_l)]. \quad (\text{A29})$$

Each such  $M_w$  for  $w \in V_s^C$  includes  $|M_w| = 3N - 2$  elements. The vertex  $w$  has weight  $4\Delta$ , hence  $M_w$  possesses the total weight  $(3N + 1)\Delta$ .

This makes the MISs  $M_w$  for each vertex  $w \in V_s^C$  the maximum-weight independent sets (MWISs) of  $\mathcal{G}_C$ . Thus, there are in total  $N^2M$  MWISs. We denote their set by  $\mathcal{M}_C$ .

Each MWIS  $M_w$  is associated to a unique vertex  $w$  on the site. The three link-vertices  $(1, g_1)$ ,  $(2, g_2)$  and  $(3, g_3)$  that are not part of  $M_w$  satisfy the class- $C$  site constraint from Eq. (A4). Conversely, for each such triple which satisfies the site constraint, there exists the vertex  $w = (g_1, g_2, g_1 g_2 g_3) \in V_s^C$  with corresponding MWIS  $M_w \in \mathcal{M}_C$ . That is, the MWISs of  $\mathcal{G}_C$  precisely encode all possible configurations that satisfy the site constraint.

### 4. Full symmetry of $\mathcal{G}_C$

A graph automorphism is a permutation on the vertex set, that conserves connectivity [recall Eq. (A6)] and the vertex weights [recall Eq. (A7)]. That is, an MWIS must always be mapped to another MWIS under element-wise application of a graph automorphism. For the blockade graph  $\mathcal{G}_C$ , from Appendix A3 we know that the MWISs are given by  $\mathcal{M}_C$ . Therefore, for a given graph automorphism  $\Phi \in \mathcal{A}_C$ , the MWIS  $M_w$  which includes the vertex  $w \in V_s^C$  must be mapped to the MWIS  $\Phi(M_w) = M_{\Phi(w)}$  which includes vertex  $\Phi(w) \in V_s^C$ . This induced mapping

$\Phi : \mathcal{M}_C \rightarrow \mathcal{M}_C$  on the MWISs is bijective, as  $\Phi$  acts bijectively on the vertex set.

For an MWIS  $M_w \in \mathcal{M}_C$ , we can define the set

$$\mathcal{A}_C \cdot M_w := \{\Phi(M_w) \mid \Phi \in \mathcal{A}_C\} \quad (\text{A30})$$

via element-wise application of all graph automorphisms. The graph  $\mathcal{G}_C$  is *fully symmetric* (in the sense of Ref. [56]) if  $\mathcal{A}_C \cdot M_w = \mathcal{M}_C$  for some  $M_w \in \mathcal{M}_C$ , that is if  $\mathcal{M}_C$  is an orbit under the action of  $\mathcal{A}_C$ .

In the following, we use the shorthand notation  $w \equiv (g_1, g_2, c)$  with  $g_3 \equiv (g_1 g_2)^{-1} c$  and  $w' \equiv (g'_1, g'_2, c')$  with  $g'_3 \equiv (g'_1 g'_2)^{-1} c'$  from Eq. (A1) and Eq. (A10), respectively. For two elements  $c, c' \in C$  in the same conjugacy class, by definition, there exists an element  $r_{c \rightarrow c'} \in G$  such that  $\chi_{r_{c \rightarrow c'}}(c) = c'$ . If the centralizer  $Z_G(c) \neq \{e\}$  is non-trivial, this element is not unique, and we can choose some representative in the set  $r_{c \rightarrow c'} Z_G(c)$  [defined by elementwise multiplication]. For any  $w, w' \in V_s^C$  and  $\tau' \in \text{Aut}_C(G)$ , we can now define the graph automorphism  $\Phi_{w \rightarrow w'} := \Phi^{p_1, p_2, \tau'}$  via the parameters

$$p_1 := g'_1 [\chi_q \circ \tau'] (g_1^{-1}), \quad (\text{A31a})$$

$$p_2 := g'_2 [\chi_q \circ \tau'] (g_2), \quad (\text{A31b})$$

$$\tau := [\chi_q \circ \tau'] \quad (\text{A31c})$$

with  $q := g_1^{-1} r \tau' (g_1)$  and  $r := r_{\tau'(c) \rightarrow c'}$ . Plugging in  $q$ , Eq. (A31a) and Eq. (A31b) can be rewritten as

$$p_1 = r q^{-1}, \quad (\text{A32a})$$

$$p_2 = g'_3 c'^{-1} r \tau' (c g_3^{-1}) q^{-1} = g'_3 r \tau' (g_3^{-1}) q^{-1}, \quad (\text{A32b})$$

respectively. Then, by construction, the group permutations (A22) become

$$\sigma_1(g_1) = p_1 \tau(g_1) = g'_1, \quad (\text{A33a})$$

$$\sigma_2(g_2) = \tau(g_2) p_2^{-1} = g'_2, \quad (\text{A33b})$$

$$\sigma_3(g_3) = p_2 \tau(g_3) p_1^{-1} = g'_3, \quad (\text{A33c})$$

$$\sigma_s(c) = \chi_{p_1}(\tau(c)) = \chi_r(\tau'(c)) = c'. \quad (\text{A33d})$$

This is what is required such that Eqs. (A15a) and (A15b) yield  $\Phi_{w \rightarrow w'}(w) = w'$  for  $\Phi_{w \rightarrow w'}$  of the form (A14).

It obviously is  $\Phi_{w \rightarrow w'} \in \mathcal{A}_C$  because  $(p_1, p_2, \tau) \in G^2 \times \text{Aut}_C(G)$ . For a given  $M_{w'} \in \mathcal{M}_C$ , we can now choose  $\Phi = \Phi_{w \rightarrow w'}$  for some  $\tau' \in \text{Aut}_C(G)$  such that  $M_w \in \mathcal{M}_C$  is mapped to  $\Phi(M_w) = M_{\Phi(w)} = M_{w'}$ . There always exists a  $\tau' \in \text{Aut}_C(G)$  since conjugations (= inner automorphisms)  $\chi_G$  are always part of  $\text{Aut}_C(G)$ . In general, there is some freedom in the choice of  $\tau'$  so that the choice of  $\Phi$  is not unique. We conclude:

**Proposition 3.** *The generalized graph  $\mathcal{G}_C$  for a class- $C$  site is fully symmetric.*

As a concluding remark, we specialize to  $C = \{1\}$ . In this case,  $c, c' = 1$  is fixed, and  $\tau' \in \text{Aut}(G)$  can be any group automorphism. Without loss of generality, we can choose  $r_{1 \rightarrow 1} = g'_1 \tau'(g_1)^{-1}$  as representative, such that  $q = 1$  and  $\chi_q = \text{id}$  become trivial. This simplifies the parameters to  $p_1 = g'_1 \tau'(g_1)^{-1}$ ,  $p_2 = g'_3 g'_1 \tau'(g_3 g_1)^{-1}$ , and  $\tau = \tau'$ .

## 5. The graph $\mathcal{G}_{C_1}$ for all conjugacy classes

The construction from Appendix A 1 of the graph  $\mathcal{G}_C$  for a class  $C$ -site can readily be generalized to incorporate all conjugacy classes  $C \in \text{Cl}(G)$  of the group  $G$ . This results in the graph  $\mathcal{G}_{C_1}$  of the multi-class site discussed in Section III (and denoted there by  $\mathcal{G}_s[\Delta]$ ). In this section, we rigorously construct this graph, discuss its automorphisms and MWISs, and show that it is fully symmetric.

In the following, we denote the graph of a class- $C$  site as  $\mathcal{G}_C = (V_C, E_C, \Delta_C)$ , and the graph of the multi-class site as  $\mathcal{G}_{C_1} = (V_{C_1}, E_{C_1}, \Delta_{C_1})$ . The construction of  $\mathcal{G}_{C_1}$  from the  $\mathcal{G}_C$  works as follows. For each conjugacy class  $C \in \text{Cl}(G)$ , consider the graph  $\mathcal{G}_C$  and increase the weight of the vertices  $w \in V_s^C$  on the site uniformly to  $\Delta_C^w = \Delta_C$ . We assume  $\Delta_C > 3\Delta$  for each conjugacy class. The maximal weight is denoted  $\Delta_{\max} := \max_{C \in \text{Cl}(G)} \Delta_C$ . Crucially, we assume that the maximal weight is unique for a conjugacy class  $C_{\max}$ , i.e.,

$$\Delta_C = \Delta_{C'} = \Delta_{\max} \Leftrightarrow C = C' = C_{\max} \quad (\text{A34})$$

for  $C, C' \in \text{Cl}(G)$ . As the weights are uniform on the site, they change neither the graph automorphisms  $\text{Aut}(\mathcal{G}_C)$  nor the MWISs  $\mathcal{M}_C$  of the graphs  $\mathcal{G}_C$ .

For each conjugacy class  $C \in \text{Cl}(G)$ , we can now “stack” the graphs  $\mathcal{G}_C$  on top of each other by identifying their vertices  $V_l^{C_1} = V_l^C = \{l\} \times G$  on the links. Then we fully connect any pair of vertices from different conjugacy classes on the site via an additional edge in  $E_{C_1}$ . Hence we end up with a fully-connected (= complete) subgraph  $K_{N^3} = (V_s^{C_1}, E_s^{C_1}, \Delta_s^{C_1})$  with vertices

$$V_s^{C_1} = \bigcup_{C \in \text{Cl}(G)} V_s^C = G^3 \quad (\text{A35})$$

on the site. Each vertex  $w \equiv (g_1, g_2, c) \in V_s^{C_1}$  is still connected to three link-vertices  $(1, g_1)$ ,  $(2, g_2)$  and  $(3, g_3)$ , where we use the shorthand notation  $g_3 \equiv (g_1 g_2)^{-1} c$  from Eq. (A1). The total vertex set is then  $V_{C_1} = V_s^{C_1} \cup \bigcup_{l \in \mathbb{Z}_3} V_l^{C_1}$ , and the total set of edges is  $E_{C_1} = E_s^{C_1} \cup \bigcup_{l \in \mathbb{Z}_3} E_l^{C_1}$  with edges

$$E_l^{C_1} = \{ \{w, v_l\} \mid w \in V_s^{C_1}, v_l \in V_l^{C_1}, g_l = h_l \} \quad (\text{A36})$$

between the site vertices and vertices of link  $l$ .

We now discuss the parametrization of local graph automorphisms.  $\varsigma_s : V_s^{C_1} \rightarrow G$  must fulfill the condition

$$\varsigma_s(w) = \sigma_1(g_1)\sigma_2(g_2)\sigma_3(g_3) \quad (\text{A37})$$

for all  $g_1, g_2, c \in G$  with the shorthand notation Eq. (A1), in analogy to Eq. (A15c). In the generic case, the weights  $\Delta_C$  are different, thus we must require that  $\varsigma_s(w) \in C_c \equiv \text{Cl}(c)$  preserves the conjugacy class. This makes the classification problem of local graph automorphisms similar to the one solved in Appendix A 2. The condition  $\varsigma_s(w) \in C_c$  is now slightly stricter, as it requires

that  $\tau \in \text{Aut}_{\text{Cl}(G)}(G)$  is  $C$ -preserving for *every* conjugacy class  $C \in \text{Cl}(G)$ . Hence we obtain the parametrized group  $\mathcal{A}_C^{\text{par}} \cong G^2 \rtimes \text{Aut}_{\text{Cl}(G)}(G)$  as subgroup of  $\mathcal{A}_C^{\text{loc}}$ .

The subgraph  $K_{N^3}$  on the site is again fully-connected. This excludes ISs with multiple vertices on the site. By the same reasoning as in Appendix A 3, we can argue that the MISs are given by  $M_0$  and  $M_w$  for each  $w \in V_s^{C_1}$ . Again,  $M_0$  possesses the weight  $3N\Delta$ , and the  $\mathcal{M}_C$  possess the weights  $(3N - 3 + \Delta_C)\Delta$ . Assuming condition (A34) for our weights, the MWISs are given by  $\mathcal{M}_{C_{\max}}$  with weight  $(3N - 3 + \Delta_{\max})\Delta$ .

Finally, we show full symmetry of  $\mathcal{G}_{C_1}$  in the sense of Ref. [56], that is,  $\mathcal{A}_C \cdot M_w = \mathcal{M}_{C_{\max}}$  for some  $M_w \in \mathcal{M}_{C_{\max}}$ . Fortunately, we can simply construct  $\Phi_{w \rightarrow w'} = \Phi^{p_1, p_2, \tau}$  via the parametrization (A31) for some  $\tau \in \text{Aut}_{\text{Cl}(G)}(G)$ , similar to the previous Appendix A 4. This is possible since we guaranteed that  $w, w' \in V_s^{C_{\max}}$  correspond to the same conjugacy class  $C_{\max}$  by assumption (A34). We can conclude that:

**Proposition 4.** *The generalized graph  $\mathcal{G}_{C_1}$  for a multi-class site is fully symmetric.*

## Appendix B: The tessellated blockade structure $\mathcal{G}$ on the torus

In this appendix we discuss the automorphism group of the tessellated graph  $\mathcal{G}$  on the honeycomb lattice with periodic boundaries. Note that without modifications, the honeycomb lattice can only be embedded on a torus or, as a finite patch with appropriate boundary conditions, in the plane. Here we discuss the situation on the torus. In Appendix C we discuss how boundary conditions affect our model.

### 1. Construction and maximum-weight independent sets

To characterize the maximum-weight independent sets (MWISs) of the tessellation, it is convenient to phrase the construction differently than in the main text. We can view the tessellated complex as an *amalgamation* (see Ref. [55]) of the building blocks introduced in Appendix A, see Fig. 7. Let  $\Lambda_{\circ} = (S_{\circ}, L_{\circ}, P_{\circ})$  denote the honeycomb lattice, where  $S_{\circ}$  denotes the sites,  $L_{\circ}$  the set of links and  $P_{\circ}$  the set of plaquettes. As the honeycomb lattice is bipartite, we can partition it into two subsets  $S_{\circ} = A \cup B$  such that sites from  $A$  are only connected to sites from  $B$  and vice versa. We place the graph  $\mathcal{G}_C$ , as constructed in Appendix A, on the sites in  $A$ , and a mirrored version of this graph on every site in  $B$ . We denote these graphs associated to specific sites as  $\mathcal{G}_{C_s}^s$  for  $s \in S_{\circ}$ .

On each link  $l \in L_{\circ}$ , there are now two sets of  $|G|$  vertices (from the two graphs placed on the endpoints of  $l$ ). The vertices in both sets are in one-to-one correspondence with group elements from  $G$ . To amalgamate the graphs

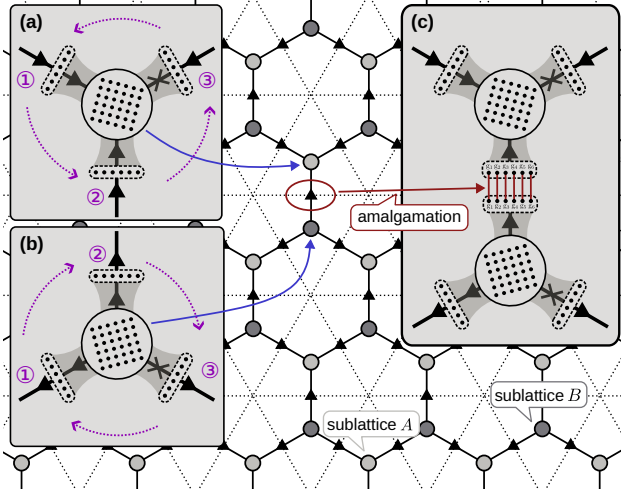


Figure 7. **Construction of the tessellated graph  $\mathcal{G}$ .** The honeycomb lattice is bipartite and can be partitioned into two sublattices  $A$  and  $B$ , indicated by light and dark gray circles. (a) On every site in sublattice  $A$ , we place the graph constructed in Appendix A, such that the links numbered 1, 2 and 3 are ordered *counterclockwise* around the site. (b) On every site in sublattice  $B$ , we place the graph constructed in Appendix A, such that the links numbered 1, 2 and 3 are ordered *clockwise* around the site. (c) We amalgamate these graphs by identifying (on every link of the honeycomb lattice) the vertices that correspond to the same group element.

$\mathcal{G}_{C_s}^s$ , we first identify the vertices on the same link which are associated to the same group element, and then add up their detunings. Hence we obtain the detuning  $2\Delta$  for the vertices on the links. In the following, we label the vertices on links by  $(l, g)$  for  $l \in L_{\mathcal{O}}$ ,  $g \in G$ , and the vertices on the sites as  $(s, g_1, g_2, r)$  for  $s \in S_{\mathcal{O}}$  and  $g_1, g_2, r \in G$ . If  $\mathcal{G}_{C_s}^s$  is the graph for the conjugacy class  $C_s = \{1\}$ , then we omit the last argument and write  $(s, g_1, g_2)$ . This construction is shown in Fig. 7.

Next, we characterize the MWISs of the tessellated graph  $\mathcal{G}$ . It is straightforward to see that if there exists an *independent set*  $M$  of  $\mathcal{G}$ , such that its restriction on  $\mathcal{G}_{C_s}^s$  is a MWIS of  $\mathcal{G}_{C_s}^s$  for all  $s \in S_{\mathcal{O}}$ , then  $M$  is a MWIS of  $\mathcal{G}$ . We refer to an independent set with this property as a *globally consistent independent set*. It is then easy to check that *if* a globally consistent IS exists, then *all* MWIS of  $\mathcal{G}$  have the property that their restriction on  $\mathcal{G}_{C_s}^s$  is a MWIS of  $\mathcal{G}_{C_s}^s$  for every  $s \in S_{\mathcal{O}}$ . Note that these observations are true for arbitrary weighted graphs. The existence of a globally consistent independent set is equivalent to the condition given in Ref. [55, Section V.B] (namely that the “ $\gamma$ -intersection” of the languages associated to the structures  $\mathcal{G}_{C_s}^s$  is nonempty).

Whether a globally consistent IS exists must be checked for each choice of conjugacy classes  $\{C_s\}$ . For the important case  $C_s \equiv \{1\}$  on all sites  $s \in S_{\mathcal{O}}$  (flux-free vacuum),

the set

$$M := \{(l, g) \mid l \in L_{\mathcal{O}}, g \in G \setminus \{1\}\} \cup \{(s, 1, 1) \mid s \in S_{\mathcal{O}}\} \quad (\text{B1})$$

is independent since  $(s, 1, 1)$  is adjacent to  $(l, 1)$  on the links  $l$  emanating from  $s$ , and to  $(s, g_1, g_2)$  for all  $(g_1, g_2) \in G^2 \setminus \{(1, 1)\}$ . Furthermore, the restriction of  $M$  on each  $\mathcal{G}_s \equiv \mathcal{G}_{\{1\}}^s$  is a MWIS (see Appendix A 3). This makes  $M$  globally consistent. So in this case, the restriction of every MWIS  $M$  of  $\mathcal{G}$  on  $\mathcal{G}_s$  is a MWIS of  $\mathcal{G}_s$  for all  $s \in S_{\mathcal{O}}$ . Therefore all MWIS of  $\mathcal{G}$  are uniquely characterized by group elements  $g_l \in G$  for each link  $l \in L_{\mathcal{O}}$  which satisfy the zero-flux condition. This means that for the emanating links  $l_1, l_2, l_3$  of  $s$ , listed in counterclockwise order, the group elements satisfy

$$g_{l_1} g_{l_2} g_{l_3} = 1 \quad (\text{B2a})$$

if the links at  $s$  are pointing inwards, and

$$g_{l_3} g_{l_2} g_{l_1} = 1 \quad (\text{B2b})$$

if the links at  $s$  are pointing outwards. The form of condition (B2b) stems from the fact that the graph on these sites is mirrored.

In conclusion, the MWIS of  $\mathcal{G}$  are in one-to-one correspondence with the (product) ground states of Kitaev’s quantum double model  $H_G$  for  $J_p = 0$  and group  $G$ . In the following, we define  $\mathcal{L}_G$  as the *subset* of  $G^{|L_{\mathcal{O}}|}$  that contains configurations  $\mathbf{g} = (g_l)_{l \in L_{\mathcal{O}}} \in G^{|L_{\mathcal{O}}|}$  which satisfy Eqs. (B2a) and (B2b). Note that for non-abelian  $G$ ,  $\mathcal{L}_G$  is not a group as it is not closed under (link-wise) multiplication.

## 2. Definitions and preliminaries

The goal of the following sections is to characterize the automorphism group of  $\mathcal{G}$ . In particular, we are interested in the question if (and if so, which) automorphisms exist besides products of plaquette automorphisms. Since we lack an exhaustive characterization of the automorphism group of the single-vertex graph  $\mathcal{G}_C$  for arbitrary conjugacy classes  $C$ , we focus here on the flux-free case  $C_s \equiv \{1\}$ . We comment on the general case in Appendix B 6. We start in this section with definitions used throughout this appendix.

We denote the set of vertices associated to link  $l \in L_{\mathcal{O}}$  as  $V_l$ , and the set of vertices associated to site  $s \in S_{\mathcal{O}}$  as  $V_s$ . We are primarily interested in a subgroup of the full automorphism group  $\text{Aut}(\mathcal{G}) \equiv \mathcal{A}_{\mathcal{G}}$ , consisting of automorphisms that map the sets  $V_l$  to themselves. This immediately implies that the same must be true for the vertex sets  $V_s$ . We denote this subgroup of the automorphism group as  $\mathcal{A}_{\mathcal{G}}^{\text{loc}}$ . It is easy to see that every automorphism in  $\text{Aut}(\mathcal{G})$  can be expressed as an automorphism in  $\mathcal{A}_{\mathcal{G}}^{\text{loc}}$  followed by a symmetry of the underlying decorated Honeycomb lattice.

Every automorphism in  $\mathcal{A}_G^{\text{loc}}$  can be written in the form

$$\Phi = \prod_{l \in L_O} \varphi_l \circ \prod_{s \in S_O} \phi_s, \quad (\text{B3})$$

where  $\varphi_l \in \text{Sym}(V_l)$  and  $\phi_s \in \text{Sym}(V_s)$ . So in particular the restriction  $\Phi_s : \mathcal{G}_s \rightarrow \mathcal{G}_s$  of  $\Phi$  onto  $\mathcal{G}_s$  is well-defined and an automorphism of  $\mathcal{G}_s$ . Conversely, if  $\Phi$  is a permutation of  $V_G$  such that its restriction  $\Phi_s$  onto  $\mathcal{G}_s$  is an automorphism of  $\mathcal{G}_s$  for every  $s \in S_O$ , then  $\Phi$  is an automorphism of  $\mathcal{G}$ . This is so, because the amalgamation does not introduce additional edges. Thus, to characterize the automorphisms  $\Phi \in \mathcal{A}_G^{\text{loc}}$ , we can apply our results from Appendix A2 to the restrictions  $\Phi_s$  for every  $s \in S_O$ .

This implies that the permutations  $\varphi_s$  are uniquely determined by the permutations  $\varphi_l$ . By identifying the vertices with group elements (see Appendix B1), the permutations  $\varphi_l$  are uniquely represented by functions  $\sigma_l \in \text{Sym}(G)$ . For every site  $s$  with emanating links  $l_1, l_2, l_3$ , listed in counterclockwise order, condition (A16) for  $C = \{1\}$  leads to the constraints

$$\sigma_{l_3}((gh)^{-1}) = (\sigma_{l_1}(g)\sigma_{l_2}(h))^{-1} \quad \forall g, h \in G \quad (\text{B4a})$$

if the edges are directed inwards at  $s$ , and

$$\sigma_{l_3}((gh)^{-1}) = (\sigma_{l_2}(g)\sigma_{l_1}(h))^{-1} \quad \forall g, h \in G \quad (\text{B4b})$$

if the edges are directed outwards at  $s$  (recall Fig. 7).

We denote the subgroup of  $\text{Sym}(G)^{|L_O|}$ , consisting of elements that satisfy Eq. (B4a) and Eq. (B4b) at every site  $s$ , as  $\mathcal{L}_{\text{Sym}(G)}$ . Moreover, every  $\sigma \in \mathcal{L}_{\text{Sym}(G)}$  can be translated back to a set of permutations  $\varphi_l$ . For these, there exist unique permutations  $\phi_s$ , such that their composition is an automorphism in  $\mathcal{A}_G^{\text{loc}}$ . Overall, this shows that there is a bijection

$$\Lambda : \mathcal{L}_{\text{Sym}(G)} \rightarrow \mathcal{A}_G^{\text{loc}}. \quad (\text{B5})$$

For convenience, we still refer to the elements of  $\mathcal{L}_{\text{Sym}(G)}$  as *automorphisms*. In the following, we characterize the group  $\mathcal{L}_{\text{Sym}(G)}$ .

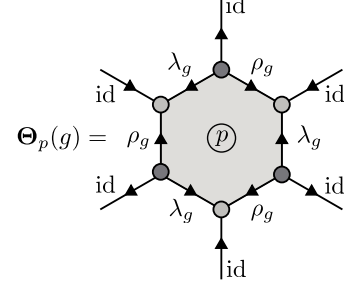
The classification in Appendix A2 shows that for every element  $(\sigma_l)_{l \in L_O} \in \mathcal{L}_{\text{Sym}(G)}$ , the functions  $\sigma_l$  have the form

$$\sigma_l = \lambda_{g_l} \circ \rho_{h_l} \circ \tau_l \quad (\text{B6})$$

on every link  $l \in L_O$ , for some  $g_l, h_l \in G$  and  $\tau_l \in \text{Aut}(G)$ . This expression does not use the full strength of our result in Appendix A2. However, the form (B6) has the advantage that there is no distinguished link. Later, we factor out global group automorphisms such that only left- and right-multiplications remain. This step anyway breaks the form of our classification in Appendix A2, as the group automorphism  $\tau_l$  can “leave behind” a conjugation, so that keeping track of the explicit forms from Appendix A2 would only complicate the proof without much benefit.

Note that in the case  $\tau_l = \text{id}$ , the permutation  $\sigma_l = \lambda_{g_l} \circ \rho_{h_l}$  exactly corresponds to the permutation  $\varphi_l(g_l, h_l)$  defined in the main text.

In Sections I and II we constructed the plaquette automorphisms  $\Theta_p(g) \in \mathcal{A}_G^{\text{loc}}$ . Via the bijection  $\Lambda$ , these can be translated to elements of  $\mathcal{L}_{\text{Sym}(G)}$ . We refer to these maps as  $\Theta_p(g) := \Lambda^{-1}(\Theta_p(g))$ . Pictorially they are represented as follows:



It is straightforward to verify that the maps  $\Theta_p(g)$  satisfy Eq. (B4a) and Eq. (B4b). We denote the subgroup of  $\mathcal{L}_{\text{Sym}(G)}$  that is generated by plaquette automorphisms as  $\mathcal{P}_G$ .

Lastly, we define the natural group action of  $\mathcal{L}_{\text{Sym}(G)}$  on  $\mathcal{L}_G$  by

$$\begin{aligned} \mathcal{L}_{\text{Sym}(G)} \times \mathcal{L}_G &\rightarrow \mathcal{L}_G, \\ \sigma \cdot (g_l)_{l \in L_O} &\mapsto (\sigma_l(g_l))_{l \in L_O}. \end{aligned} \quad (\text{B7})$$

In the following, we omit the dot and write the group action just as juxtaposition. Every subgroup of  $\mathcal{L}_{\text{Sym}(G)}$  then also induces a natural group action on  $\mathcal{L}_G$  by Eq. (B7).

### 3. Orbits of $\mathcal{L}_G$ under plaquette automorphisms

In this section, we review a result by Cui *et al.* [68, Theorem 2.4] concerning the number of orbits in  $\mathcal{L}_G$  under the group action of plaquette automorphisms  $\mathcal{P}_G$ .

To characterize the orbits, it is useful to introduce another group action

$$\begin{aligned} G \times \text{Hom}(\pi_1(\mathbb{T}, p_0), G) &\rightarrow \text{Hom}(\pi_1(\mathbb{T}, p_0), G), \\ g \cdot \psi &\mapsto (\gamma \mapsto g\psi(\gamma)g^{-1}). \end{aligned} \quad (\text{B8})$$

Here,  $\pi_1(\mathbb{T}, p_0)$  denotes the first homotopy group of the torus with base point  $p_0$ , i.e.,  $\pi_1(\mathbb{T}, p_0) \simeq \mathbb{Z}^2$ . We use a plaquette  $p_0$  as base point, since we consider paths on the dual lattice  $\tilde{\Lambda}_O = (\tilde{S}_O, \tilde{L}_O, \tilde{P}_O)$  with  $\tilde{S}_O = P_O$ ,  $\tilde{P}_O = V_O$  and  $\tilde{L}_O = \{\{p, p'\} \mid p, p' \in \tilde{S}_O\} \simeq L_O$ . That is, the base point  $p_0$  is a plaquette of the original lattice  $\Lambda_O$ . For two groups  $G, H$ ,  $\text{Hom}(G, H)$  denotes the set of group homomorphisms from  $G$  to  $H$ . We denote the set of orbits under this group action by  $\text{Hom}(\pi_1(\mathbb{T}, p_0), G)/G$ . In the following,  $X = \{\psi_1, \dots, \psi_m\}$  denotes a set of representatives of these orbits.

As introduced in Section III, we endow the dual lattice with an orientation in the following way. Let  $\gamma = (\dots, p_1, p_2, \dots)$  be an oriented path on the dual lattice. This path contains the dual edge  $\{p_1, p_2\}$ , which corresponds uniquely to an edge  $l$  of the original lattice. We



say that  $\gamma$  crosses the edge  $l$ . We set  $\text{sign}(\{p_1, p_2\}, \gamma) = 1$  if the crossed edge  $l$  points to the left of  $\gamma$ , and we set  $\text{sign}(\{p_1, p_2\}, \gamma) = -1$  if the crossed edge  $l$  points to the right of  $\gamma$ . [So  $\text{sign}(\{p_1, p_2\}, \gamma) = \sigma_{\{p_1, p_2\}}$  in the notation of the main text, recall Fig. 3.]

For every path  $\gamma$  on the dual lattice, we define the *directed product* as  $g_\gamma := \prod_{l \in \gamma} g_l^{\text{sign}(l, \gamma)}$ . Let  $s \in \tilde{P}_\circ = S_\circ$  be a dual plaquette (= a site of the honeycomb lattice). Let  $\gamma_s$  be a path that traverses the boundary of this dual plaquette in counterclockwise direction; we denote the crossed links as  $l_1, l_2, l_3 \in L_\circ$ . If the links are directed inwards at  $s$ , then  $g_{\gamma_s} = g_{l_1} g_{l_2} g_{l_3}$ . If the links are directed outwards at  $s$ , then  $g_{\gamma_s} = g_{l_1}^{-1} g_{l_2}^{-1} g_{l_3}^{-1}$ . In both cases, and for configurations in  $\mathcal{L}_G$ , Eqs. (B2a) and (B2b) imply that  $g_{\gamma_s} = 1$ . It is easy to see that this implies  $g_\gamma = 1$  for every contractible loop  $\gamma$ . This observation is crucial for the proof by Cui *et al.* [68].

Let  $T$  be a spanning tree of the dual lattice (i.e., a subgraph without cycles that connects to every site), and  $p_1, p_2 \in P_\circ$  some plaquettes such that  $l := \{p_1, p_2\} \notin T$ . Then there exist unique paths  $\gamma_1, \gamma_2 \subseteq T$  that connect  $p_0$  to  $p_1$  and  $p_2$  and do not contain duplicate edges. For each  $\psi \in X$ , we define the group elements

$$g_{\{p_1, p_2\}}^\psi := [\psi(\gamma_1 \circ (p_1, p_2) \circ \gamma_2^{-1})]^{-\text{sign}(\{p_1, p_2\}, (p_1, p_2))}. \quad (\text{B9})$$

In this equation,  $(p_1, p_2)$  is interpreted as the path on the dual lattice that starts at  $p_1$  and ends at  $p_2$ ; “ $\circ$ ” denotes the concatenation of paths on the dual lattice. With these group elements, we define a configuration  $(g_l^\psi)_{l \in L_\circ} \in \mathcal{L}_G$  by

$$g_l^\psi := \begin{cases} 1, & l \in T, \\ g_{\{p_1, p_2\}}^\psi, & l = \{p_1, p_2\} \notin T. \end{cases} \quad (\text{B10})$$

This definition ensures that for every closed path  $\gamma$  on the dual lattice which contains  $p_0$ , the directed product satisfies

$$\psi(\gamma) = \prod_{l \in \gamma} (g_l^\psi)^{\text{sign}(l, \gamma)}. \quad (\text{B11})$$

Finally, we can formulate the theorem from Ref. [68]:

**Theorem 1** (Cui *et al.* [68]). *The elements  $(g_l^\psi)_{l \in L_\circ} \in \mathcal{L}_G$  for  $\psi \in X$  form a set of representatives of the orbits  $\mathcal{L}_G/\mathcal{P}_G$ . A given element  $\mathbf{h} := (h_l)_{l \in L_\circ} \in \mathcal{L}_G$  is in the same orbit as  $(g_l^\psi)_{l \in L_\circ}$  if and only if the map*

$$\Psi_{\mathbf{h}} : \pi_1(\mathbb{T}, p_0) \rightarrow G, \quad \gamma \mapsto \prod_{l \in \gamma} h_l^{\text{sign}(l, \gamma)} \quad (\text{B12})$$

*lies in the same orbit as  $\psi$  in  $\text{Hom}(\pi_1(\mathbb{T}, p_0), G)$ .*

We later use this theorem to obtain a characterization of the automorphisms that have the form  $\sigma_l = \lambda_{z_l}$  for  $z_l \in Z(G)$  (see Appendix B4).

#### 4. Global automorphisms and loop automorphisms

In this section, we introduce global automorphisms and general loop automorphisms. Together with plaquette automorphisms, these form the building blocks of the automorphism group  $\mathcal{L}_{\text{Sym}(G)}$  (recall Eq. (B5)).

Let  $\tau \in \text{Aut}(G)$  be a group automorphism, then we define the *global automorphism*  $\tau \in \mathcal{L}_{\text{Sym}(G)}$  by

$$\tau := (\tau)_{l \in L_\circ}, \quad (\text{B13})$$

i.e., the map  $\tau$  is associated to every link. Conditions (B4a) and (B4b) follow directly from  $\tau$  being a group automorphism.

To define general *loop automorphisms*, consider  $(z_l)_{l \in L_\circ} \in \mathcal{L}_{Z(G)}$ , i.e., a configuration of elements from the center  $Z(G)$  of  $G$ , such that for every site with links  $l_1, l_2, l_3$  (listed in counterclockwise order) the constraint

$$z_{l_1} z_{l_2} z_{l_3} = 1 \quad (\text{B14})$$

is satisfied. Note that as  $Z(G)$  is abelian no case distinction is needed. Also note that in contrast to  $\mathcal{L}_G$ ,  $\mathcal{L}_{Z(G)}$  forms a group under component-wise multiplication because  $Z(G)$  is abelian. Such a configuration defines an element in  $\mathcal{L}_{\text{Sym}(G)}$  by left multiplication with  $z_l$  on every link  $l \in L_\circ$ . Hence, we have an injective group homomorphism

$$\Gamma : \mathcal{L}_{Z(G)} \rightarrow \mathcal{L}_{\text{Sym}(G)}, \quad (z_l)_{l \in L_\circ} \mapsto (\lambda_{z_l})_{l \in L_\circ}. \quad (\text{B15})$$

The map  $\lambda_g$  for  $g \in G$  is defined in Eq. (A21a). The fact that  $\Gamma(\mathbf{z}) \in \mathcal{L}_{\text{Sym}(G)}$  for  $\mathbf{z} \in \mathcal{L}_{Z(G)}$  follows from Eq. (B14) and because elements of the center commute with all group elements.  $\Gamma$  is a group homomorphism since for all  $x \in G$

$$\lambda_{zz'}(x) = zz'x = z\lambda_{z'}(x) = (\lambda_z \circ \lambda_{z'})(x). \quad (\text{B16})$$

Finally, if  $\Gamma(\mathbf{z}) = (\text{id})_{l \in L_\circ}$ , then it follows that for all  $x \in G$  it is  $x = \lambda_{z_l}(x) = z_l x$  and thus  $z_l = 1$ . Hence  $\ker(\Gamma) = \mathbf{1}$ , which shows injectivity.

The definition of  $\Gamma$  immediately shows that for  $\mathbf{y}, \mathbf{z} \in \mathcal{L}_{Z(G)}$  it holds that  $\Gamma(\mathbf{y})\mathbf{z} = \mathbf{y}\mathbf{z}$ . Here, the right-hand side is to be understood as component-wise multiplication in  $\mathcal{L}_{Z(G)}$ . This allows us to define a subgroup of  $\mathcal{L}_{\text{Sym}(G)}$  as  $\mathcal{Z}_{\text{Sym}(G)} := \Gamma(\mathcal{L}_{Z(G)})$ . The previous comment and the homomorphism property show that for  $\mathbf{z} \in \mathcal{L}_{Z(G)}$  and  $\sigma \in \mathcal{Z}_{\text{Sym}(G)}$ , it holds that  $\Gamma(\sigma\mathbf{z}) = \sigma\Gamma(\mathbf{z})$ . Hence, we find that  $\Gamma(\sigma\mathbf{1}) = \sigma$ .

A special class of automorphisms in  $\mathcal{Z}_{\text{Sym}(G)}$  are *loop automorphisms*. Let  $\ell = (l_1, l_2, \dots)$  be an arbitrary directed, closed loop on the lattice  $\Lambda_\circ$ . For  $l \in \ell$  we write  $\ell \uparrow \uparrow l$  if the direction of  $\ell$  matches the direction of the link  $l$  and otherwise we write  $\ell \uparrow \downarrow l$ . Then we define  $\Theta_\ell(z) \in \mathcal{Z}_{\text{Sym}(G)}$  by

$$[\Theta_\ell(z)]_l := \begin{cases} \lambda_z & \text{for } \ell \uparrow \uparrow l, \\ \lambda_{z^{-1}} & \text{for } \ell \uparrow \downarrow l, \\ \text{id} & \text{for } l \notin \ell, \end{cases} \quad (\text{B17})$$

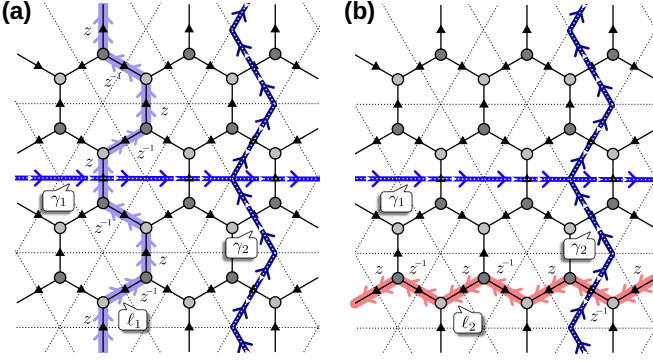


Figure 8. **Generators of  $\pi_1(\mathbb{T}, p_0)$**  (a) The dual paths  $\gamma_1$  and  $\gamma_2$  generate the group  $\pi_1(\mathbb{T}, p_0)$ . Applying the loop automorphism  $\Theta_{\ell_1}(z)$  on an arbitrary configuration in  $\mathcal{L}_{Z(G)}$  multiplies every edge along  $\ell_1$  with  $z$  ( $z^{-1}$ ) if the edge points in the same (opposite) direction as  $\ell_1$ . The directed product of group elements along  $\gamma_2$  remains unchanged, whereas the directed product along  $\gamma_1$  is multiplied by  $z$ . (b) Applying  $\Theta_{\ell_2}(z)$  on any configuration in  $\mathcal{L}_{Z(G)}$  leaves the directed product along  $\gamma_1$  unchanged, the directed product along  $\gamma_2$  is multiplied by  $z$ .

for every  $z \in Z(G)$ . It is easy to check, that  $\Theta_{\ell}(z)$  satisfies Eqs. (B4a) and (B4b) and thus defines an automorphism in  $\mathcal{L}_{\text{Sym}(G)}$ . Note that if  $\ell$  is the boundary of a plaquette, we recover the plaquette automorphisms, in this case the definition (B17) defines an automorphism for every  $z \in G$ . However, in the general case, Eq. (B17) only defines an automorphism if  $z \in Z(G)$ . This is consistent with Ref. [56] where some of us found loop automorphisms for every closed loop when working with the abelian group  $\mathbb{Z}_2$ .

We now show that  $\mathcal{Z}_{\text{Sym}(G)}$  is generated by plaquette automorphisms and loop automorphisms along non-contractible loops.

To achieve this we use the one-to-one correspondence of configurations  $\mathcal{L}_{Z(G)}$  and automorphisms in  $\mathcal{Z}_{\text{Sym}(G)}$ , i.e., we must classify configurations in  $\mathcal{L}_{Z(G)}$ ; to this end, we invoke Theorem 1. As  $Z(G)$  is abelian, the group action of  $Z(G)$  by conjugation [see Eq. (B8)] is trivial and therefore  $X = \text{Hom}(\pi_1(\mathbb{T}, p_0), Z(G))$ . Now choose two loops  $\gamma_1$  and  $\gamma_2$  on the dual lattice that generate the group  $\pi_1(\mathbb{T}, p_0)$ , and two loops  $\ell_1$  and  $\ell_2$  on the lattice that are non-contractible and not homotopic, as shown in Fig. 8. Consider the configurations

$$\mathbf{g}^{z_1, z_2} := \Theta_{\ell_1}(z_1) \Theta_{\ell_2}(z_2) \mathbf{1}, \quad (\text{B18})$$

for arbitrary  $z_1, z_2 \in Z(G)$ . These configurations satisfy

$$\Psi_{\mathbf{g}^{z_1, z_2}}(\gamma_1) = \prod_{l \in \ell_1} (g_l^{z_1, z_2})^{\text{sign}(l, \gamma_1)} = z_1, \quad (\text{B19a})$$

$$\Psi_{\mathbf{g}^{z_1, z_2}}(\gamma_2) = \prod_{l \in \ell_2} (g_l^{z_1, z_2})^{\text{sign}(l, \gamma_2)} = z_2. \quad (\text{B19b})$$

This shows that all configurations  $\mathbf{g}^{z_1, z_2}$  belong to mutually distinct orbits. Furthermore, every orbit is reached

by this construction because every homomorphism in  $\text{Hom}(\pi_1(\mathbb{T}, p_0), Z(G))$  is uniquely defined by the image of the generators  $\gamma_1$  and  $\gamma_2$ . Thus we have shown that every element  $\mathbf{h} \in \mathcal{L}_{Z(G)}$  can be written as

$$\mathbf{h} = \left( \Theta_{\ell_1}(z_1) \circ \Theta_{\ell_2}(z_2) \circ \prod_{p \in P_{\mathcal{O}}} \Theta_p(z_p) \right) \mathbf{1}, \quad (\text{B20})$$

for suitable  $z_1, z_2 \in Z(G)$  and  $z_p \in Z(G)$  for  $p \in P_{\mathcal{O}}$ . The characterization of  $\mathcal{Z}_{\text{Sym}(G)}$  follows almost trivially:

**Proposition 5.** *Every element  $\sigma \in \mathcal{Z}_{\text{Sym}(G)}$  has the form*

$$\sigma = \Theta_{\ell_1}(z_1) \circ \Theta_{\ell_2}(z_2) \circ \prod_{p \in P_{\mathcal{O}}} \Theta_p(z_p) \quad (\text{B21})$$

for some  $z_1, z_2 \in Z(G)$  and  $z_p \in Z(G)$  for  $p \in P_{\mathcal{O}}$ .

*Proof.* By definition, every element  $\sigma \in \mathcal{Z}_{\text{Sym}(G)}$  is generated by a configuration  $\mathbf{h} = (h_l)_{l \in L_{\mathcal{O}}} \in \mathcal{L}_{Z(G)}$ , i.e.,  $\sigma = \Gamma(\mathbf{h})$ . As shown,  $\mathbf{h}$  has the form Eq. (B20), thus we obtain

$$\Gamma(\mathbf{h}) = \Theta_{\ell_1}(z_1) \circ \Theta_{\ell_2}(z_2) \circ \prod_{p \in P_{\mathcal{O}}} \Theta_p(z_p) \circ \Gamma(\mathbf{1}) \quad (\text{B22a})$$

$$= \Theta_{\ell_1}(z_1) \circ \Theta_{\ell_2}(z_2) \circ \prod_{p \in P_{\mathcal{O}}} \Theta_p(z_p) \quad (\text{B22b})$$

which concludes the proof.  $\blacksquare$

## 5. Characterization of $\mathcal{L}_{\text{Sym}(G)}$

We are now equipped to characterize the automorphism group  $\mathcal{L}_{\text{Sym}(G)}$ . As a first step, we show that the group automorphism in Eq. (B6) can be removed by pre-composing a suitable group automorphism on each link.

**Lemma 1.** *Let  $\sigma \in \mathcal{L}_{\text{Sym}(G)}$ , then there exists  $\tau \in \text{Aut}(G)$  such that for each link  $l \in L_{\mathcal{O}}$ ,  $\sigma_l \circ \tau = \lambda_{g_l} \circ \rho_{h_l}$  for some  $g_l, h_l \in G$ .*

*Proof.* Let  $l \in L_{\mathcal{O}}$  be an arbitrary link; by Eq. (B6) we have  $\sigma_l = \lambda_{\tilde{g}_l} \circ \rho_{\tilde{h}_l} \circ \tau$  with  $\tau \in \text{Aut}(G)$  and some  $\tilde{g}_l, \tilde{h}_l \in G$ . Then

$$\sigma_l \circ \tau^{-1} = \lambda_{\tilde{g}_l} \circ \rho_{\tilde{h}_l}. \quad (\text{B23})$$

Suppose that  $l, l_2, l_3$  are the emanating links of site  $s$  and all links are directed inwards. Then Eq. (B4a) implies that for all  $x \in G$

$$\sigma_{l_3}(x) = \sigma_{l_2}(1)^{-1} \sigma_l(x^{-1})^{-1} \quad (\text{B24a})$$

$$= \sigma_{l_2}(1)^{-1} [\tilde{g}_l \tau(x^{-1}) \tilde{h}_l^{-1}]^{-1} \quad (\text{B24b})$$

$$= [\sigma_{l_2}(1)^{-1} \tilde{h}_l] \tau(x) \tilde{g}_l^{-1}, \quad (\text{B24c})$$

and therefore

$$\sigma_{l_3} \circ \tau = \lambda_{\sigma_{l_2}(1)^{-1} \tilde{h}_l} \circ \rho_{\tilde{g}_l}. \quad (\text{B25})$$

This argument also holds for  $l_2$  and for sites with outward directed links. As the honeycomb lattice is a connected graph, every link  $l' \in L_\circ$  can be connected to  $l$  by a sequence of links and sites. For every site in this sequence, the argument above applies. This concludes the proof. ■

Lemma 1 shows that we only have to characterize the graph automorphisms that arise from pure multiplications. This motivates the definition of the subgroup

$$\mathcal{L}_{\text{Sym}(G)}^{\text{red}} := \{\sigma \in \mathcal{L}_{\text{Sym}(G)} \mid \forall l \in L_\circ : \sigma_l = \lambda_{g_l} \circ \rho_{h_l} \text{ for } g_l, h_l \in G\}. \quad (\text{B26})$$

Before we proceed to the main part of the characterization of  $\mathcal{L}_{\text{Sym}(G)}^{\text{red}}$ , we prove a technical lemma:

**Lemma 2.** *Let  $g, h \in G$ . If for all  $x \in G$  it holds  $x = gxh$ , then  $g = h^{-1}$  and  $g, h \in Z(G)$ .*

*Proof.* For  $x = 1$  we obtain  $1 = gh$ , which implies  $g = h^{-1}$ . Then it follows that for all  $x \in G$ :

$$x = gxh = gxg^{-1} \Rightarrow g \in Z(G). \quad (\text{B27})$$

■

Lemma 2 allows us to prove the first part of the characterization of  $\mathcal{L}_{\text{Sym}(G)}^{\text{red}}$ :

**Lemma 3.** *Let  $\sigma = (\sigma_l)_{l \in L_\circ} \in \mathcal{L}_{\text{Sym}(G)}^{\text{red}}$ . Then for every site  $s \in S_\circ$  with inwards pointing links and  $l_1, l_2, l_3 \in L_\circ$  its emanating links listed in counterclockwise order, the permutations  $\sigma_{l_i}$  for  $i \in \{1, 2, 3\}$  have the form*

$$(\sigma_{l_1}, \sigma_{l_2}, \sigma_{l_3}) = (\lambda_{g_1} \circ \rho_{g_2}, \lambda_{g_2} \circ \rho_{g_3}, \lambda_{g_3} \circ \rho_{g_1}). \quad (\text{B28})$$

for some  $g_1, g_2, g_3 \in G$ .

*Proof.* Let  $s \in S_\circ$  be a site with inwards pointing links and  $l_1, l_2, l_3$  its emanating links listed in counterclockwise order. By definition,  $\sigma$  satisfies Eq. (B4a), hence the group elements  $g_l, h_l \in G$  [see Eq. (B26)] satisfy

$$h_{l_3} g_l h_{l_3}^{-1} = g_{l_1} g_{h_{l_1}^{-1} g_{l_2} h_{l_2}^{-1}} \quad (\text{B29})$$

for all  $g, h \in G$ . Setting  $h = 1$  and invoking Lemma 2, we obtain

$$h_{l_3}^{-1} g_{l_1} = (h_{l_1}^{-1} g_{l_2} h_{l_2}^{-1} g_{l_3})^{-1} \in Z(G). \quad (\text{B30})$$

Analogously, for  $g = 1$  we obtain

$$h_{l_3}^{-1} g_{l_1} h_{l_1}^{-1} g_{l_2} = (h_{l_2}^{-1} g_{l_3})^{-1} \in Z(G). \quad (\text{B31})$$

This shows that  $z_{12} := h_{l_1}^{-1} g_{l_2} \in Z(G)$ ,  $z_{13} := h_{l_3}^{-1} g_{l_1} \in Z(G)$  and  $z_{23} := h_{l_2}^{-1} g_{l_3} \in Z(G)$ . Furthermore, from Eq. (B30) it follows that these group elements satisfy  $z_{13} = (z_{12} z_{23})^{-1}$ . Thus, we find that

$$\begin{aligned} \sigma_{l_2} &= \lambda_{g_{l_2}} \circ \rho_{h_{l_2}} = \lambda_{g_{l_2} z_{12}^{-1}} \circ \rho_{h_{l_2} z_{12}^{-1}} \\ &= \lambda_{h_{l_1}} \circ \rho_{h_{l_2} z_{12}^{-1}} \end{aligned} \quad (\text{B32})$$

and

$$\begin{aligned} \sigma_{l_3} &= \lambda_{g_{l_3}} \circ \rho_{h_{l_3}} = \lambda_{g_{l_3} z_{23}^{-1} z_{12}^{-1}} \circ \rho_{h_{l_3} z_{23}^{-1} z_{12}^{-1}} \\ &= \lambda_{h_{l_2} z_{12}} \circ \rho_{h_{l_3} z_{13}} = \lambda_{h_{l_2} z_{12}} \circ \rho_{g_{l_1}}. \end{aligned} \quad (\text{B33})$$

In conclusion we have shown that

$$(\sigma_{l_1}, \sigma_{l_2}, \sigma_{l_3}) = (\lambda_{g_{l_1}} \circ \rho_{h_{l_1}}, \lambda_{h_{l_1}} \circ \rho_{h_{l_2} z_{12}^{-1}}, \lambda_{h_{l_2} z_{12}} \circ \rho_{g_{l_1}}), \quad (\text{B34})$$

as desired. ■

Now we can prove the main result:

**Proposition 6.** *Every automorphism  $\sigma \in \mathcal{L}_{\text{Sym}(G)}^{\text{red}}$  has the form*

$$\sigma = \Theta_{\ell_1}(z_1) \circ \Theta_{\ell_2}(z_2) \circ \prod_{p \in P_\circ} \Theta_p(g_p), \quad (\text{B35})$$

for some group elements  $g_p \in G$  and elements from the center  $z_1, z_2 \in Z(G)$ .

*Proof.* Let  $S_\circ^i$  be the set of all sites with links directed inwards. The links of the honeycomb lattice (disregarding their direction) are parallel to one of three possible directions, we denote them  $\hat{e}_1, \hat{e}_2, \hat{e}_3$ . The three links emanating from one site are in one-to-one correspondence with the three directions. We now imagine deleting all links parallel to  $\hat{e}_1$ . We denote the resulting set of links as  $L'_\circ$ . Then, for each site  $s \in S_\circ^i$ , we define  $p_s$  to be the unique plaquette that contains the two links in  $L'_\circ$  that emanate from  $s$ .

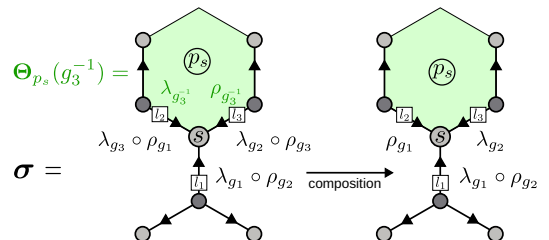
Now consider an arbitrary element  $\sigma \in \mathcal{L}_{\text{Sym}(G)}^{\text{red}}$  and some site  $s \in S_\circ^i$ . Let  $l_1, l_2, l_3$  denote the links emanating from  $s$  (listed in counterclockwise order) such that  $l_1 \notin L'_\circ$ . By Lemma 3 we know that

$$(\sigma_{l_1}, \sigma_{l_2}, \sigma_{l_3}) = (\lambda_{g_1} \circ \rho_{g_2}, \lambda_{g_2} \circ \rho_{g_3}, \lambda_{g_3} \circ \rho_{g_1}). \quad (\text{B36})$$

Now we post-compose  $\sigma$  with the plaquette automorphism  $\Theta_{p_s}(g_3^{-1})$ , i.e., we define the new automorphism  $\sigma' := \Theta_{p_s}(g_3^{-1}) \circ \sigma$ . Then the maps associated to  $l_1, l_2$  and  $l_3$  are given by

$$(\sigma'_{l_1}, \sigma'_{l_2}, \sigma'_{l_3}) = (\lambda_{g_1} \circ \rho_{g_2}, \lambda_{g_2}, \rho_{g_1}). \quad (\text{B37})$$

This construction can be illustrated as follows:

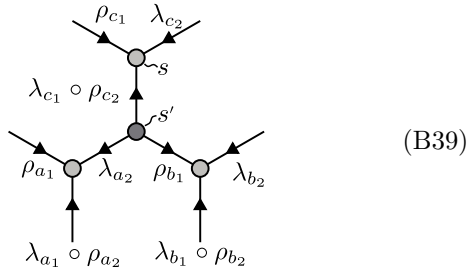


Note that pre-composing another plaquette automorphism on some of the neighboring plaquettes changes only the group elements  $g_1$  and  $g_2$  in Eq. (B37) (but not the overall structure) so that this procedure can be repeated for all sites  $s \in S_{\mathcal{O}}^i$ . Thus we have shown that every  $\sigma \in \mathcal{L}_{\text{Sym}(G)}^{\text{red}}$  has the form

$$\sigma = \left( \prod_{p \in P_{\mathcal{O}}} \Theta_p(g_p) \right) \circ \sigma' \quad (\text{B38})$$

for suitable  $g_p \in G$  and  $\sigma' \in \mathcal{L}_{\text{Sym}(G)}^{\text{red}}$  which satisfies Eq. (B37) for every site with inward pointing links. It remains to characterize the latter.

Consider a site  $s' \notin S_{\mathcal{O}}^i$ ; it has three neighboring sites in  $S_{\mathcal{O}}^i$ . On the links connected to these neighboring sites, the associated maps satisfy Eq. (B37). This can be illustrated as follows:



Note that here the vertical links are the ones that are parallel to  $\hat{e}_1$ . For the three links emanating from  $s'$ , Eq. (B4b) must be satisfied and we find for all  $x, y \in G$

$$\lambda_{a_2}((xy)^{-1}) = (\lambda_{c_1} \circ \rho_{c_2}(x) \rho_{b_1}(y))^{-1} \quad (\text{B40a})$$

$$\Rightarrow a_2(xy)^{-1} = (c_1 x c_2^{-1} y b_1^{-1})^{-1} \quad (\text{B40b})$$

$$= b_1 y^{-1} c_2 x^{-1} c_1^{-1}. \quad (\text{B40c})$$

For  $x = 1$  and  $y = 1$ , this implies

$$a_2 y^{-1} = b_1 y^{-1} c_2 c_1^{-1} \quad (\text{B41a})$$

$$\text{and } a_2 x^{-1} = b_1 c_2 x^{-1} c_1^{-1}. \quad (\text{B41b})$$

Hence, by Lemma 2 it follows

$$c_2 c_1^{-1} \in Z(G) \quad \text{and} \quad c_1^{-1} \in Z(G) \quad (\text{B42})$$

and therefore  $c_1, c_2 \in Z(G)$ . This argument applies to every site  $s \in S_{\mathcal{O}}^i$ , as we can always consider the site  $s' \notin S_{\mathcal{O}}^i$  that is adjacent to  $s$  such that the link connecting  $s$  and  $s'$  points is parallel to  $\hat{e}_1$ . Then, for site  $s'$  we recover the situation in Fig. (B39), with  $s$  the site on the top. This shows that  $\sigma'$  only contains multiplications by elements in the center. Therefore all these multiplications can be reordered to be left-multiplications, i.e.,  $\sigma' = (\lambda_{z_l})_{l \in L_{\mathcal{O}}}$  for some  $z_l \in Z(G)$ . As  $\sigma'$  satisfies Eqs. (B4a) and (B4b), it directly follows that  $(z_l)_{l \in L_{\mathcal{O}}}$  must satisfy Eq. (B14), which shows that  $\sigma' \in \mathcal{Z}_{\text{Sym}(G)}$ . Now we invoke Proposition 5 and conclude that  $\sigma'$  has the form

$$\sigma' = \Theta_{\ell_1}(z_1) \circ \Theta_{\ell_2}(z_2) \circ \prod_{p \in P_{\mathcal{O}}} \Theta_p(z_p) \quad (\text{B43})$$

for suitable  $z_1, z_2, z_p \in Z(G)$ . Together with Eq. (B38), we conclude that

$$\sigma = \Theta_{\ell_1}(z_1) \circ \Theta_{\ell_2}(z_2) \circ \prod_{p \in P_{\mathcal{O}}} \Theta_p(g_p) \quad (\text{B44})$$

for some  $z_1, z_2 \in Z(G)$  and  $g_p \in G$ , as desired.  $\blacksquare$

Combining Eq. (B44) with Lemma 1 we obtain the surjective group homomorphism

$$\begin{aligned} \iota : (G^{|P_{\mathcal{O}}|} \times Z(G)^2) \rtimes \text{Aut}(G) &\rightarrow \mathcal{L}_{\text{Sym}(G)}, \\ ((g_p)_{p \in P_{\mathcal{O}}}, z_1, z_2, \tau) &\mapsto \\ &\Theta_{\ell_1}(z_1) \circ \Theta_{\ell_2}(z_2) \circ \prod_{p \in P_{\mathcal{O}}} \Theta_p(g_p) \circ \tau. \end{aligned} \quad (\text{B45})$$

The group structure on the domain of  $\iota$  is defined as

$$\begin{aligned} ((g_p)_{p \in P_{\mathcal{O}}}, z_1, z_2, \tau) \cdot ((g'_p)_{p \in P_{\mathcal{O}}}, z'_1, z'_2, \tau') \\ = ((g_p \tau(g'_p))_{p \in P_{\mathcal{O}}}, z_1 \tau(z'_1), z_2 \tau(z'_2), \tau \tau'). \end{aligned} \quad (\text{B46})$$

Unfortunately, this group homomorphism is not injective (i.e., not an isomorphism), e.g., for every  $z \in Z(G)$

$$\begin{aligned} \iota((z)_{p \in P_{\mathcal{O}}}, 1, 1, \text{id}) &= (\text{id})_{l \in L_{\mathcal{O}}} \\ &= \iota((1)_{p \in P_{\mathcal{O}}}, 1, 1, \text{id}), \end{aligned} \quad (\text{B47})$$

as each link is multiplied from the left with  $z$  and from the right with  $z^{-1}$ . However, this characterization is sufficient, e.g., to determine which topological sectors are connected by graph automorphisms.

## 6. Automorphisms of $\tilde{\mathcal{G}}$ with generalized site graphs

In this section we comment on the automorphism group of  $\tilde{\mathcal{G}}$  if the latter contains site graphs  $\mathcal{G}_C^s$  for arbitrary conjugacy classes  $C$  or universal site graphs  $\mathcal{G}_{C_1}^s$ . In particular, we show that the automorphisms  $\Theta_p(h)$  and  $\Theta_\ell(z)$  defined in Appendix B5 carry over to  $\tilde{\mathcal{G}}$ .

Recall [Eq. (A16)] that a set of maps  $\sigma_1, \sigma_2, \sigma_3$  and  $\sigma_c$  that satisfy the condition

$$\sigma_s(c) = \sigma_1(g_1) \sigma_2(g_2) \sigma_3((g_1 g_2)^{-1} c), \quad (\text{B48})$$

for all  $g_1, g_2 \in G$  and  $c \in C$ , describes an automorphism of the site graph  $\mathcal{G}_C^s$ . Thus to define an automorphism of  $\tilde{\mathcal{G}}$  we must not only specify the group permutations on the links  $(\sigma_1, \sigma_2, \sigma_3)$  but also permutations of conjugacy classes on the sites  $(\sigma_s)$ . We say that an automorphism  $\tilde{\sigma} = ((\tilde{\sigma}_l)_{l \in L_{\mathcal{O}}}, (\tilde{\sigma}_s)_{s \in S_{\mathcal{O}}})$  of  $\tilde{\mathcal{G}}$  extends the automorphism  $\sigma = (\sigma_l)_{l \in L_{\mathcal{O}}} \in \mathcal{L}_{\text{Sym}(G)}$ , if  $\tilde{\sigma}_l = \sigma_l$  for all  $l \in L_{\mathcal{O}}$ .

We first construct an extension of  $\Theta_p(h)$  to  $\tilde{\mathcal{G}}$ . Let  $s \in S_{\mathcal{O}}$  be an arbitrary site such that  $\Theta_p(h)$  acts nontrivially on  $\mathcal{G}_C^s$ . Then there are three possibilities:

$$\sigma_1 = \rho_g, \quad \sigma_2 = \lambda_g, \quad \sigma_3 = \text{id}, \quad (\text{B49a})$$

$$\text{or } \sigma_1 = \text{id}, \quad \sigma_2 = \rho_g, \quad \sigma_3 = \lambda_g, \quad (\text{B49b})$$

$$\text{or } \sigma_1 = \lambda_g, \quad \sigma_2 = \text{id}, \quad \sigma_3 = \rho_g. \quad (\text{B49c})$$

For all of these there exists a suitable permutation  $\sigma_s \in \text{Sym}(C)$ , such that Eq. (B48) is satisfied. For Eqs. (B49a) and (B49b) we can choose  $\sigma_s = \text{id}$ , for Eq. (B49c) we can choose  $\sigma_s = \chi_{g^{-1}}$  (which obviously preserves the conjugacy class  $C$ ). This shows that the plaquette automorphisms  $\Theta_p(h)$  can be extended to an automorphism of  $\tilde{G}$ . The argument is analogous for  $\tilde{\mathcal{G}}$  that contain site graphs  $\mathcal{G}_{C_1}^s$ .

The situation for loop automorphisms  $\Theta_\ell(z)$  for  $z \in Z(G)$  is even simpler. In this case, one of the maps on the right-hand side of Eq. (B48) is  $\lambda_z$ , one is  $\rho_z$ , and the remaining one is  $\text{id}$ . As  $z$  commutes with all group elements, the left-multiplication by  $z$  cancels with the right-multiplication by  $z^{-1}$ , so that we can satisfy Eq. (B48) with  $\sigma_s = \text{id}$ . This shows that  $\Theta_\ell(z)$  can be extended to an automorphism of  $\tilde{G}$ .

For global automorphisms that arise from group automorphisms [recall Eq. (B13)] the situation is more complicated. Consider a graph  $\tilde{\mathcal{G}}$  that contains exactly one site graph  $\mathcal{G}_C^s$  with  $C \neq \{1\}$ . Eq. (B48) then shows that the global permutation  $\tau$  for  $\tau \in \text{Aut}(G)$  can be extended to an automorphism of  $\tilde{G}$  if and only if  $\tau$  preserves the conjugacy class  $C$ . For graphs  $\tilde{\mathcal{G}}$  with more than one class- $C$  site,  $\tau$  must preserve all present conjugacy classes.

## 7. Notes on loop automorphisms

In Section II of the main text, we mentioned the loop permutations  $\Theta_\ell(h)$  for  $h \in G$  and a generic loop  $\ell$  on the honeycomb lattice. In this appendix, we define these permutations and show that they are graph automorphisms if  $h \in Z(G)$ .

We first define  $\Theta_\ell(h)$  on the links of the lattice, in analogy with plaquette automorphisms. For the directed links of the honeycomb lattice  $\Lambda_\circ$ , we write  $l \uparrow \ell$  if the direction of  $\ell$  coincides with the direction of  $l$  and  $l \downarrow \ell$  otherwise. On the former links,  $\Theta_\ell(h)$  acts by left-multiplication with  $h$ , which corresponds to the permutation  $\varphi_l(h, 1)$  as defined in Eq. (5). On the latter links,  $\Theta_\ell(h)$  acts by right-multiplication with  $h^{-1}$ , which corresponds to the permutation  $\varphi_l(1, h)$ . On all links that are not part of the path  $\ell$ , the permutation  $\Theta_\ell(h)$  acts as the identity.

Next, we define  $\Theta_\ell(h)$  on the sites of the lattice. To this end, we partition the sites into two subsets  $S_1(\ell)$  and  $S_2(\ell)$ : Let  $s \in S_\circ$  be a site and  $l_1, l_2, l_3 \in L_\circ$  its emanating links such that two of these links are part of  $\ell$ . Without loss of generality, we define  $l_3$  as the link that is *not* part of  $\ell$ . The links are ordered clockwise if the links are outward directed at  $s$  and anticlockwise otherwise. Then we define  $s \in S_1(\ell)$  if  $l_1 \uparrow \ell$  and  $s \in S_2(\ell)$  if  $l_1 \downarrow \ell$ . This allows us to define

$$\begin{aligned} \Theta_\ell(h) &= \prod_{l \uparrow \ell} \varphi_l(h, 1) \prod_{l \downarrow \ell} \varphi_l(1, h) \\ &\times \prod_{s \in S_1(\ell)} \phi_s(1, h, 1) \prod_{s \in S_2(\ell)} \phi_s(h, 1, h). \end{aligned} \quad (\text{B50})$$

Note that if  $\ell$  is the counterclockwise oriented boundary of a plaquette, then  $S_2(\ell)$  is empty and we recover Eq. (8).

If  $z \in Z(G)$ , then for every link  $l \in L_\circ$  it holds that  $\varphi_l(z, z) = \varphi_l(1, 1) = \text{id}$ . In this case,  $\Theta_\ell(z)$  has the form (7) when restricted to a site  $s \in S_\circ$  and its emanating links  $l_1, l_2, l_3$ . This shows that  $\Theta_\ell(z)$  is an automorphism of  $\mathcal{G}$ . As  $z$  is in the center of  $G$ ,  $\Theta_\ell(z)$  can be viewed as acting by left-multiplication on every link. Hence we find

$$\Theta_\ell(z) = \Lambda(\Theta_\ell(z)), \quad (\text{B51})$$

where  $\Theta_\ell(z)$  is the loop automorphism defined in Appendix B 4.

Conversely, one can show that an automorphism that acts on the links like  $\Theta_\ell(h)$  does not exist if  $h \notin Z(G)$ .

## Appendix C: The tessellated blockade structure $\mathcal{G}$ with open boundaries

In Appendix B we discussed the graph  $\mathcal{G}$  with periodic boundary conditions (= on the torus). Another important – and experimentally more realistic – setup are open boundary conditions. In this section, we discuss modifications of our results for periodic boundaries when  $\mathcal{G}$  is defined on a finite, open patch with *rough* boundary conditions.

“Rough” means that we consider a finite patch of the honeycomb lattice  $\Lambda_\circ$  such that each vertex remains trivalent. That is, the graph has “dangling” edges on the boundaries. This implies that there are “incomplete” plaquettes on the boundary. For these incomplete plaquettes, we can still define *reduced plaquette automorphisms* via Eq. (8), by restricting the products to sites and links that are part of the lattice.

It is easy to see that these are still graph automorphism in  $\mathcal{A}_\mathcal{G}^{\text{loc}}$ : In Appendix B 2 we established that permutations  $\Phi$  of  $V_\mathcal{G}$  (which map the vertex sets  $V_l$  and  $V_s$  to themselves) are automorphisms of  $\mathcal{G}$  if and only if their restriction  $\Phi_s$  to  $\mathcal{G}_s$  is an automorphism of  $\mathcal{G}_s$  for all sites  $s \in S_\circ$ . Since this statement is independent of boundary conditions, it still applies here. The action of a reduced plaquette automorphism on  $\mathcal{G}_s$  for some  $s \in S_\circ$  is identical to the action of a full plaquette automorphism. This shows that the reduced plaquette automorphisms are part of  $\mathcal{A}_\mathcal{G}^{\text{loc}}$ . Loop automorphisms and global automorphisms (derived from group automorphisms) can be adapted analogously.

The first homotopy group of a finite patch of the plane without holes is trivial. Thus, in view of our classification in Appendix B, we expect that for rough boundary conditions, all automorphisms in  $\mathcal{A}_\mathcal{G}^{\text{loc}}$  can be written as a product of plaquette automorphisms, followed by the global application of a group automorphism. However, we did not rigorously prove this. (Note that Theorem 1 does not consider manifolds with boundary, however for rough boundary conditions the proof of Cui *et al.* goes through unchanged.)

Lastly, we consider the maximum-weight independent sets of  $\mathcal{G}$ . The set defined by restricting Eq. (B1) to the finite lattice is a globally consistent independent set of  $\mathcal{G}$ . Hence the MWISs of  $\mathcal{G}$  are described by configurations of group elements  $(g_l)_{l \in L_O} \in \mathcal{L}_G$  which satisfy Eqs. (B2a) and (B2b) for each site that is part of the lattice. As  $\mathcal{G}$  can be embedded on a surface with trivial first homotopy group, invoking Theorem 2.4 from Ref. [68] (adapted for rough boundary conditions) shows that  $\mathcal{L}_G$  is a single orbit under the action of plaquette automorphisms. Thus the blockade structure  $\mathcal{G}$  is fully-symmetric as defined in Ref. [56].

## Appendix D: Proof of topological order

In this appendix, we give the detailed proof that the ground state of  $H_G$  is topologically ordered for finite  $\Omega \neq 0$  (see Section II of the main text).

For technical reasons (Appendix D2) we work with periodic boundary conditions. Throughout this appendix, we use the following notation. Excitation patterns of two-level-systems are described by  $\mathbf{n} \in \mathbb{Z}_2^n$  with  $n$  the number of two-level-systems in  $\mathcal{G}$ . An excitation pattern corresponds to a state  $|\mathbf{n}\rangle \in \mathcal{H}_G$ , these states form a basis of  $\mathcal{H}_G$ . The Hamiltonian  $H_G^0$  is diagonal in this basis. We denote the set of excitation patterns that correspond to ground states of  $H_G^0$  as  $\mathcal{L}_G$ . The ground state manifold is then given by  $\mathcal{H}_G^0 = \text{span}\{|\mathbf{n}\rangle \mid \mathbf{n} \in \mathcal{L}_G\}$ .

### 1. Overview

As discussed in Section II, the graph  $\mathcal{G}$  on a torus is not fully symmetric, i.e., the set of ground state configurations  $\mathcal{L}_G$  splits into multiple orbits  $Q_1, \dots, Q_O$ . Thus, as shown in Ref. [56], the unique ground state for  $\Omega \neq 0$  has the form

$$|\Omega\rangle = \sum_{k=1}^O \lambda_k(\Omega) \sum_{\mathbf{n} \in Q_k} |\mathbf{n}\rangle + \sum_{\mathbf{n} \notin \mathcal{L}_G} \eta_{\mathbf{n}}(\Omega) |\mathbf{n}\rangle. \quad (\text{D1})$$

Note that we have no control over the coefficients  $\lambda_k(\Omega)$ .

Despite the lack of full symmetry (and the resulting uncontrolled superposition of topological sectors) we can nevertheless establish that the ground state of  $H_G$  is topologically ordered. To this end, we generalize the technique introduced in Ref. [56]. In this section, we summarize the main argument; technical details for some of the steps are provided in subsequent sections.

As already stated in Section II, we introduce the auxiliary Hamiltonian (11)

$$\begin{aligned} \tilde{H}_G(\Omega, \omega) &:= H_G(\Omega) \\ &+ \omega \sum_p \left( \mathbb{1} - \underbrace{\frac{1}{|G|} \sum_h \Theta_p(h)}_{=: \Theta_p} \right). \end{aligned} \quad (\text{D2})$$

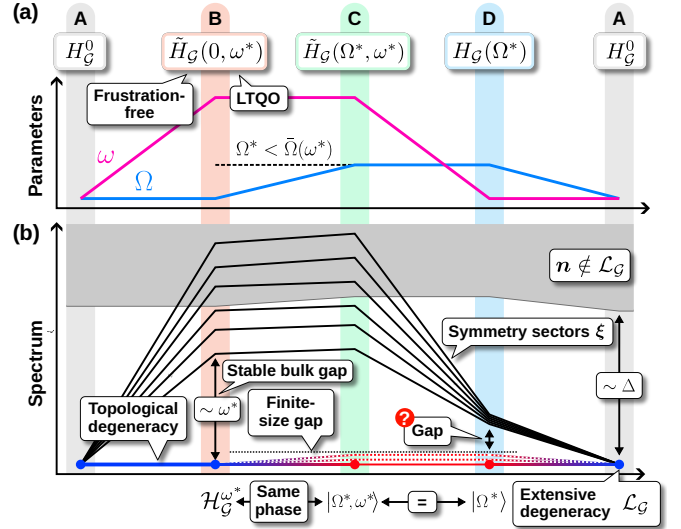


Figure 9. **Proof of topological order.** (a) Path that parameterizes the family of Hamiltonians  $\tilde{H}_G(\Omega, \omega)$ . Ultimately, we are interested in the quantum phase of the ground state in **D**. Following the path from **A** to **D** allows us to rigorously characterize the quantum phase of the ground state of  $H_G(\Omega)$ . (b) Schematic spectrum of  $\tilde{H}_G(\Omega, \omega)$  along the parametric path shown in (a). For  $\Omega = \omega = 0$  (**A**), the Hamiltonian  $H_G(0) = \tilde{H}_G(0, 0)$  is classical with an exponentially large, degenerate ground state manifold  $\mathcal{H}_G^0$  spanned by configurations in  $\mathcal{L}_G$ . (**B**) For  $\Omega = 0 < \omega^*$ , the Hamiltonian  $\tilde{H}_G(0, \omega^*)$  is frustration-free and satisfies a condition called *local topological quantum order* (local-TQO). Moreover, its ground state manifold is separated by a gap of order  $\omega^*$  from the rest of the spectrum. This ground state manifold  $\mathcal{H}_G^0$  can be mapped to the ground state manifold of Kitaev's quantum double model by a generalized local unitary transformation; in particular these states are topologically ordered. Because of frustration-freeness and local-TQO, the bulk gap of the Hamiltonian  $\tilde{H}_G(0, \omega^*)$  is stable against weak, local perturbations. Thus, for  $\Omega^* < \bar{\Omega}(\omega^*)$ , the Hamiltonian  $\tilde{H}_G(\Omega^*, \omega^*)$  (**C**) remains gapped. Here  $\bar{\Omega}(\omega^*)$  denotes an upper bound on the perturbation strength that guarantees gap stability. As the gap remains open when ramping up  $\Omega$ , the new (unique) ground state  $|\Omega^*, \omega^*\rangle$  remains topologically ordered. Lastly, switching off  $\omega \searrow 0$  leads to the target Hamiltonian  $H_G(\Omega^*) = \tilde{H}_G(\Omega^*, 0)$ , the ground state  $|\Omega^*\rangle$  of which we want to characterize. Due to the local symmetries it is  $|\Omega^*\rangle = |\Omega^*, \omega^*\rangle$ . Note that this construction does not prove the existence of a gap for  $H_G(\Omega^*)$ .

We say that the term proportional to  $\omega$  introduces *artificial plaquette fluctuations*. This term is chosen to resemble the plaquette term of the quantum double Hamiltonian (3).

We establish topological order in three steps (Fig. 9):

#### • Step 1: **A** $\rightarrow$ **B**

At **A** we have  $\Omega = \omega = 0$ . Thus the ground state manifold is extensively degenerate and spanned by the classical ground state configurations  $\mathcal{L}_G$ . The ground state manifold  $\mathcal{H}_G^0$  is separated by a gap of size  $\min_i(\Delta_i)$  from the rest of the spectrum.

To reach **B**, we ramp up the artificial plaquette fluctuations to some value  $0 < \omega^* < \Delta$ , keeping  $\Omega = 0$ . As

$$[\tilde{H}_G(0, \omega^*), \Theta_p] = 0 \quad (\text{D3a})$$

and

$$[\Theta_p, \Theta_{p'}] = 0 \quad (\text{D3b})$$

for all plaquettes  $p, p'$ , the spectrum of  $\tilde{H}_G(0, \omega^*)$  decomposes into sectors labeled by eigenvalues of  $\Theta_p$  (= symmetry sectors). Since  $\Theta_p$  is a projector, it has eigenvalues 0 and 1. States with eigenvalue 0 are energetically punished by the Hamiltonian (D2) with energy  $\omega^*$ . Thus the ground states of  $\tilde{H}_G(0, \omega^*)$  are in the sector characterized by  $\Theta_p = 1$  for all plaquettes  $p$ . The ground state manifold  $\mathcal{H}_G^{\omega^*}$  of  $\tilde{H}_G(0, \omega^*)$  consists of topologically degenerate ground states that are separated by a gap  $\omega^*$  from the rest of the spectrum. Moreover, it can be shown (see Appendix D 2 a) that the ground state manifold can be mapped to the degenerate ground state manifold  $\mathcal{H}_G^{J_p}$  of the quantum double model (3) for  $J_p > 0$  by a generalized local unitary transformation. Thus the Hamiltonians  $H_G$  and  $\tilde{H}_G(0, \omega^*)$  describe the same quantum phase, in particular the states in  $\mathcal{H}_G^{\omega^*}$  are topologically ordered.

• **Step 2: B  $\rightarrow$  C**

To reach **C**, we switch on quantum fluctuations with some finite value  $\Omega^* \neq 0$ . Note that the term  $\Omega^* \sum_i \sigma_i^x$  in  $H_G(\Omega^*)$  couples sectors with different excitation numbers. As a consequence, the Hamiltonian  $\tilde{H}_G(\Omega^*, \omega^*)$  can no longer be diagonalized exactly; in particular the ground state changes in an unknown way.

However, as long as the excitation gap above the ground state manifold does not close when  $\Omega$  is ramped up, the Hamiltonian  $\tilde{H}_G(\Omega^*, \omega^*)$  describes the same quantum phase as  $\tilde{H}_G(0, \omega^*)$  and consequently also the same quantum phase as  $H_G$ . In particular it follows that the new (now unique) ground state  $|\Omega^*, \omega^*\rangle \in \mathcal{H}_G^{\omega^*, \Omega^*}$  is topologically ordered.

Hence the remaining problem is to establish gap stability. We remark that this is a priori not obvious, as in general, arbitrarily weak perturbations can close spectral gaps in the thermodynamic limit [73]. Fortunately, the Hamiltonian  $\tilde{H}_G(0, \omega^*)$  is *frustration-free, locally gapped*, and satisfies a condition called *local topological quantum order* (local-TQO). Under these assumptions, it can be shown rigorously that the gap is stable under sufficiently weak, local perturbations [74].

Thus we can conclude that  $|\Omega^*, \omega^*\rangle$  is topologically ordered, as long as  $\Omega^* < \tilde{\Omega}(\omega^*)$ , where  $\tilde{\Omega}(\omega^*)$  denotes an upper bound on the perturbation strength

that guarantees gap stability. For a detailed proof of the gap stability, see Appendix D 2 b. Note that the uniqueness of the ground state  $|\Omega^*, \omega^*\rangle$  does not contradict the stability of the phase, since ground state degeneracies can be lifted by finite-size effects. In particular, Ref. [74] shows that such splittings of the ground state degeneracy are exponentially suppressed with system size.

• **Step 3: C  $\rightarrow$  D**

In the last step, we switch off the artificial plaquette fluctuations to reach **D** with the desired Hamiltonian  $\tilde{H}_G(\Omega^*, 0) = H_G(\Omega^*)$ . In contrast to step 2 above, this change of the Hamiltonian cannot be treated as a small perturbation since  $\omega^* \gg \Omega^*$ . In addition,  $\tilde{H}_G(\Omega^*, \omega^*)$  is *not* frustration-free, so the result of Ref. [74] is not applicable. (We are not aware of any gap stability results for frustrated Hamiltonians.)

Now we utilize the local symmetry projectors  $\Theta_p$ . By construction, these commute with the full Hamiltonian, i.e.,  $[\tilde{H}(\Omega, \omega), \Theta_p] = 0$ . Thus there exists a basis of eigenstates of both  $\tilde{H}_G(\Omega, \omega)$  and  $\Theta_p$  for all plaquettes  $p$  and arbitrary  $\Omega$  and  $\omega$ . By Eq. (D2), these states are also eigenstates of  $H_G(\Omega)$ . Thus we can label these eigenstates as  $|E_\Omega^\xi, \xi\rangle$  with

$$H_G(\Omega) |E_\Omega^\xi, \xi\rangle = E_\Omega^\xi |E_\Omega^\xi, \xi\rangle \quad (\text{D4a})$$

$$\Theta_p |E_\Omega^\xi, \xi\rangle = \xi_p |E_\Omega^\xi, \xi\rangle, \quad (\text{D4b})$$

and  $\xi_p \in \{0, 1\}$ . Eq. (D4a) and Eq. (D4b) yield an expression for the energy of the states  $|E_\Omega^\xi, \xi\rangle$ :

$$\begin{aligned} & \tilde{H}_G(\Omega, \omega) |E_\Omega^\xi, \xi\rangle \\ &= \left[ E_\Omega^\xi + \omega \sum_p (1 - \xi_p) \right] |E_\Omega^\xi, \xi\rangle. \end{aligned} \quad (\text{D5})$$

Consider the ground state  $|\Omega^*\rangle$  of  $\tilde{H}_G(\Omega^*, 0) = H_G(\Omega^*)$ . We cannot directly apply Proposition 1 from Ref. [56] to this Hamiltonian since  $\mathcal{G}$  is not necessarily fully-symmetric. However, the proof of this proposition shows that  $|\Omega^*\rangle$  nevertheless satisfies  $\Theta_p(h) |\Omega^*\rangle = |\Omega^*\rangle$  for all  $h \in G$  and all plaquettes  $p$ . This shows that  $\Theta_p |\Omega^*\rangle = |\Omega^*\rangle$  for all plaquettes  $p$ , i.e.,  $|\Omega^*\rangle$  is labeled by  $\xi = \mathbf{1}$ . Moreover,  $|\Omega^*\rangle$  is defined as eigenvector with smallest eigenvalue of  $H_G(\Omega^*)$ . Hence Eq. (D5) shows that  $|\Omega^*\rangle$  is a ground state of  $\tilde{H}_G(\Omega^*, \omega)$  for all  $\omega$ .

Let  $|E_\Omega^\xi, \xi\rangle$  be a ground state of  $\tilde{H}_G(\Omega^*, \omega)$ . As  $|\Omega^*\rangle$  minimizes both terms in Eq. (D5) simultaneously, the same must be true for  $|E_\Omega^\xi, \xi\rangle$ . This implies in particular that  $|E_\Omega^\xi, \xi\rangle$  is a ground state of  $H_G(\Omega^*)$ . Since the ground state of  $H_G(\Omega^*)$  is unique, it follows that  $|E_\Omega^\xi, \xi\rangle \propto |\Omega^*\rangle$ . Hence  $|\Omega^*\rangle$  is the unique ground state of  $\tilde{H}_G(\Omega^*, \omega)$  for all  $0 \leq \omega \leq \omega^*$ . This

implies in particular that  $|\Omega^*, \omega^*\rangle = |\Omega^*\rangle$ , hence  $|\Omega^*\rangle$  is topologically ordered.

## 2. Technical details

### a. Ground state manifold of $\tilde{H}_G(0, \omega)$

In this section, we discuss the degenerate ground state manifold of

$$\tilde{H}_G(0, \omega) = H_G^0 + \omega \sum_p (\mathbb{1} - \Theta_p), \quad (\text{D6})$$

defined on a torus. In particular, we show that the ground state manifold  $\mathcal{H}_G^0$  of the Hamiltonian (D6) can be mapped to the ground state manifold  $\mathcal{H}_G^{J_p}$  of the quantum double model for  $J_p > 0$  by a generalized local unitary (LU) transformation. This shows that both Hamiltonians represent the same quantum phase [76]. Since the models are defined on different Hilbert spaces, we first must embed them in a common Hilbert space.

Let  $\Lambda_\circ = (S_\circ, L_\circ, P_\circ)$  denote a honeycomb lattice with sites  $S_\circ$ , links  $L_\circ$  and plaquettes  $P_\circ$ . Both the quantum double model and our blockade structure realization are defined on this lattice.

The Hilbert space of the quantum double model has the natural basis  $|\mathbf{g}\rangle = |(g_l)_{l \in L_\circ}\rangle \in \mathcal{H}_G$  for  $g_l \in G$ . The quantum double Hamiltonian (3) for  $J_p = 0$  is diagonal in this basis. Thus we can define the set of ground state configurations as

$$\mathcal{L}_G := \{(g_l)_{l \in L_\circ} \in G^{L_\circ} \mid |\mathbf{g}\rangle \in \mathcal{H}_G^0\}, \quad (\text{D7})$$

such that the ground state manifold is given by  $\mathcal{H}_G^0 = \text{span}\{|\mathbf{g}\rangle \mid \mathbf{g} \in \mathcal{L}_G\}$ . In this basis, the plaquette operators  $A_p(h)$  act as permutations, thus they define a group action of  $G$  on  $\mathcal{L}_G$  in the natural way. By abuse of notation, we denote this group action as  $A_p(h) \cdot \mathbf{g}$ .

By Ref. [68, Theorem 2.4], the ground state manifold  $\mathcal{H}_G^{J_p}$  of  $H_G$  for  $J_p > 0$  is degenerate and its dimension is given by  $|\text{Hom}(\pi_1(\mathbb{T}, p_0), G)/G| = |\text{Hom}(\mathbb{Z}^2, G)/G|$ . Here / denotes the set of orbits under the group action of  $G$  on  $\text{Hom}(\pi_1(\mathbb{T}, p_0))$  by  $g \cdot \pi \mapsto g^{-1}\pi(\cdot)g$  and  $\mathbb{T}$  refers to the torus on which the lattice is embedded.  $p_0$  denotes an arbitrary plaquette that is used as the base point for the homotopy group. The ground states  $|\psi\rangle \in \mathcal{H}_G^{J_p}$  are characterized by

$$A_p |\psi\rangle = B_s |\psi\rangle = |\psi\rangle \quad (\text{D8})$$

for all sites  $s \in S_\circ$  and plaquettes  $p \in P_\circ$ . To give an explicit form of the ground states, we define an equivalence relation  $\sim$  on  $\mathcal{L}_G$  by  $\mathbf{g} \sim \mathbf{g}'$  if and only if  $\mathbf{g}$  can be transformed by plaquette operators  $A_p(h)$  into  $\mathbf{g}'$ . Then a basis of  $\mathcal{H}_G^{J_p}$  is given by

$$|[\mathbf{g}]\rangle := \frac{1}{|[\mathbf{g}]|} \sum_{\mathbf{g}' \sim \mathbf{g}} |\mathbf{g}'\rangle, \quad (\text{D9})$$

where  $[\mathbf{g}]$  denotes the equivalence class of  $\mathbf{g}$  and  $|[\mathbf{g}]|$  its cardinality.

Next, we construct the common Hilbert space to connect both models. The Hilbert space of our blockade Hamiltonian  $H_G$  is given by

$$\mathcal{H}_G := \bigotimes_{l \in L_\circ} \mathcal{H}_l^G \otimes \bigotimes_{s \in S_\circ} \mathcal{H}_s^G. \quad (\text{D10})$$

where  $\mathcal{H}_l^G \simeq \mathbb{C}^{2^{|G|}}$  and  $\mathcal{H}_s^G \simeq \mathbb{C}^{2^{|G|^2}}$  denote the Hilbert spaces associated to a link and a site of the blockade model. By contrast, the Hilbert space associated to one link of the quantum double model is given by  $\mathcal{H}_l^G = \{|g\rangle \mid g \in G\}$ . We extend the Hilbert space  $\mathcal{H}_G$  by adding  $\mathcal{H}_l^G$  to every link. Thus we obtain the enlarged Hilbert space  $\mathcal{H}_{G \otimes G} := \mathcal{H}_G \otimes \bigotimes_{l \in L_\circ} \mathcal{H}_l^G$ . We can embed the states  $|\mathbf{g}\rangle \in \mathcal{H}_G$  of the quantum double model into this larger Hilbert space as

$$|\mathbf{0}\rangle |\mathbf{g}\rangle := \bigotimes_{l \in L_\circ} |\mathbf{0}\rangle_l |g_l\rangle_l \bigotimes_{s \in S_\circ} |\mathbf{0}\rangle_s. \quad (\text{D11})$$

In particular,  $|\mathbf{0}\rangle |\mathbf{g}\rangle$  is in the same quantum phase as  $|\mathbf{g}\rangle$  [76]. Let us define the following subspaces of embedded states:

$$\mathcal{H}_{G \otimes G}^0 := \text{span}\{|\mathbf{0}\rangle |\mathbf{g}\rangle \mid \mathbf{g} \in \mathcal{L}_G\}, \quad (\text{D12a})$$

$$\mathcal{H}_{G \otimes G}^1 := \text{span}\{|\mathbf{n}\rangle |\mathbf{1}\rangle \mid \mathbf{n} \in \mathcal{L}_G\}. \quad (\text{D12b})$$

We now construct an LU quantum circuit that maps  $\mathcal{H}_{G \otimes G}^0$  to  $\mathcal{H}_{G \otimes G}^1$ . Let  $\mathcal{L}_l^G$  ( $\mathcal{L}_s^G$ ) denote the set of ground state excitation patterns of  $H_G^0$  restricted to the link  $l \in L_\circ$  (the site  $s \in S_\circ$ ). By construction of  $\mathcal{G}$ , there exists a bijective map  $\eta_l : G \rightarrow \mathcal{L}_l^G$  which maps each group element to (the restriction of) a ground state excitation pattern on the link  $l$ . Moreover, the concatenation of all these excitation patterns  $\bigoplus_{l \in L_\circ} \eta_l(g_l)$  is part of a ground state pattern of  $H_G^0$  if and only if  $\mathbf{g} = (g_l)_{l \in L_\circ} \in \mathcal{L}_G$ . In particular, for every site  $s \in S_\circ$  with emanating links  $l_1, l_2, l_3 \in L_\circ$ , there exists a map  $\eta_s : (\mathcal{L}_{l_i}^G)^3 \rightarrow \mathcal{L}_s^G$  that maps  $\mathbf{n}_{l_i} := \eta_{l_i}(g_{l_i})$  (for  $i = 1, 2, 3$ ) to the unique pattern  $\eta_s(\mathbf{n}_{l_1}, \mathbf{n}_{l_2}, \mathbf{n}_{l_3}) \in \mathcal{L}_s^G$ .

Thus, for some  $l \in L_\circ$ , we can define the unitary  $U_l^{(1)}$  that acts on the link  $l$  as

$$U_l^{(1)} |\mathbf{0}\rangle_l |g\rangle_l = |\eta(g)\rangle_l |\mathbf{1}\rangle_l, \quad (\text{D13})$$

and trivially on all other links. Note that this does not define  $U_l^{(1)}$  on all of  $\mathcal{H}_{G \otimes G}$ ; it can be extended in an arbitrary way as we are only interested in its application to the subspace  $\mathcal{H}_{G \otimes G}^0$ .

Similarly, for a site  $s \in S_\circ$ , we define the unitary  $U_s^{(2)}$  that acts on  $s$  and its emanating links  $l_1, l_2, l_3$  as

$$\begin{aligned} U_s^{(2)} |\mathbf{0}\rangle_s |\mathbf{n}_1\rangle_{l_1} |\mathbf{n}_2\rangle_{l_2} |\mathbf{n}_3\rangle_{l_3} \\ = |\eta_s(\mathbf{n}_1, \mathbf{n}_2, \mathbf{n}_3)\rangle_s |\mathbf{n}_1\rangle_{l_1} |\mathbf{n}_2\rangle_{l_2} |\mathbf{n}_3\rangle_{l_3}, \end{aligned} \quad (\text{D14})$$



and trivially on all other parts of the tensor product. As before,  $U_s^{(2)}$  can be extended arbitrarily to a unitary on  $\mathcal{H}_{\mathcal{G} \otimes \mathcal{G}}$ .

As the honeycomb lattice  $\Lambda_{\circ}$  is bipartite, we can partition its sites  $S_{\circ}$  into two sublattices  $A$  and  $B$ , such that no two sites from  $A$  and  $B$  are connected by a link. Then,  $\{U_l^{(1)}\}_{l \in L_{\circ}}$ ,  $\{U_s^{(2)}\}_{s \in A}$  and  $\{U_s^{(2)}\}_{s \in B}$  are sets of unitary operators that act on non-overlapping regions of finite size. Thus  $U := \prod_{s \in B} U_s^{(2)} \prod_{s \in A} U_s^{(2)} \prod_l U_l^{(1)}$  defines a local unitary quantum circuit of constant depth (it has three layers). By construction, it constitutes the desired map from  $\mathcal{H}_{\mathcal{G} \otimes \mathcal{G}}^0$  to  $\mathcal{H}_{\mathcal{G} \otimes \mathcal{G}}^1$ . We define  $\eta : \mathcal{L}_{\mathcal{G}} \rightarrow \mathcal{L}_{\mathcal{G}}$  as the bijective map defined by  $U|\mathbf{0}\rangle|\mathbf{g}\rangle = |\eta(\mathbf{g})\rangle|\mathbf{1}\rangle$ .

Finally, we show that  $U$  maps the embedded ground states of the full quantum double Hamiltonian  $H_G$  to the embedded ground states of  $\tilde{H}_{\mathcal{G}}(0, \omega)$ . To this end, we define the subspaces

$$\mathcal{H}_{\mathcal{G} \otimes \mathcal{G}}^{0, J_p} := \text{span}\{|\mathbf{0}\rangle|\psi\rangle \mid |\psi\rangle \in \mathcal{H}_{\mathcal{G}}^{J_p}\}, \quad (\text{D15a})$$

$$\mathcal{H}_{\mathcal{G} \otimes \mathcal{G}}^{1, \omega} := \text{span}\{|\omega\rangle|\mathbf{1}\rangle \mid |\omega\rangle \in \mathcal{H}_{\mathcal{G}}^{\omega}\}. \quad (\text{D15b})$$

Note that by construction the plaquette operators satisfy

$$[\Theta_p(h)|\eta(\mathbf{g})\rangle] \otimes |\mathbf{1}\rangle = U\{|\mathbf{0}\rangle \otimes [A_p(h)|\mathbf{g}\rangle]\} \quad (\text{D16})$$

for all plaquettes  $p$  and group elements  $h \in G$ . Let  $|\psi\rangle \in \mathcal{H}_{\mathcal{G}}^{J_p}$  be a quantum double ground state. By construction of  $U$ , there exists a state  $|\omega(\psi)\rangle \in \mathcal{H}_{\mathcal{G}}^{\omega}$  such that  $U|\mathbf{0}\rangle|\psi\rangle = |\omega(\psi)\rangle|\mathbf{1}\rangle$ . By linearity, it follows that

$$[\Theta_p(h)|\omega(\psi)\rangle]|\mathbf{1}\rangle = U|\mathbf{0}\rangle[A_p(h)|\psi\rangle] \quad (\text{D17a})$$

$$= U|\mathbf{0}\rangle|\psi\rangle \quad (\text{D17b})$$

$$= |\omega(\psi)\rangle|\mathbf{1}\rangle \quad (\text{D17c})$$

which shows that  $|\omega(\psi)\rangle \in \mathcal{H}_{\mathcal{G}}^{\omega}$ . The proof for the converse direction is analogous.

In summary, this shows that  $U$  maps  $\mathcal{H}_{\mathcal{G} \otimes \mathcal{G}}^{0, J_p} = \text{span}\{|\mathbf{0}\rangle\} \otimes \mathcal{H}_{\mathcal{G}}^{J_p}$  unitarily to  $\mathcal{H}_{\mathcal{G} \otimes \mathcal{G}}^{1, \omega} = \mathcal{H}_{\mathcal{G}}^{\omega} \otimes \text{span}\{|\mathbf{1}\rangle\}$ . As  $U$  is a LU quantum circuit with finite depth, this transformation does not change the quantum phase represented by the states [76]. Moreover, adding and removing local degrees of freedom in form of tensor products also does not alter the topological order [76]. Thus we have constructed the desired generalized local unitary transformation. This shows that the Hamiltonians  $H_G$  and  $\tilde{H}_{\mathcal{G}}(0, \omega)$  describe the same quantum phase and thus that the states in  $\mathcal{H}_{\mathcal{G}}^{J_p}$  are topologically ordered.

Finally, we give a concrete basis of  $\mathcal{H}_{\mathcal{G}}^{\omega}$ . Let  $\sim_{\Theta}$  denote the equivalence relation on  $\mathcal{L}_{\mathcal{G}}$  defined by  $\mathbf{n} \sim_{\Theta} \mathbf{n}'$  if and only if  $\mathbf{n}$  can be transformed into  $\mathbf{n}'$  by plaquette operators  $\Theta_p(h)$ . Let  $[\mathbf{n}]_{\Theta}$  denote the equivalence class of  $\mathbf{n}$  under this equivalence relation and consider a set  $\{\mathbf{n}_k\}$  of representatives of all classes. Then from Eq. (D9) we obtain that

$$|\omega_k\rangle := \frac{1}{|[\mathbf{n}_k]_{\Theta}|} \sum_{\mathbf{n}' \sim_{\Theta} \mathbf{n}_k} |\mathbf{n}'\rangle \quad (\text{D18})$$

is a basis of  $\mathcal{H}_{\mathcal{G}}^{\omega}$ .

### b. Gap stability of $\tilde{H}_{\mathcal{G}}(0, \omega)$

a. *Conditions.* To establish the gap stability necessary for step 2 (**B**  $\rightarrow$  **C**), we utilize a result by Michalakis and Zwolak [74, Theorem 1]. A summary of these results and a detailed explanation of their application to the case  $G = \mathbb{Z}_2$  can be found in Ref. [56]. We start with a brief overview of the conditions that must be verified.

The systems considered by Michalakis and Zwolak are defined on a square lattice  $\Lambda_{\square} = (S_{\square}, L_{\square}, P_{\square})$  with sites  $S_{\square} = [0, L]^2 \subseteq \mathbb{Z}^2$ , where  $L$  denotes the system size. This lattice is endowed with an arbitrary norm  $\|\cdot\|$  (here we choose the  $\ell^{\infty}$ -norm). This norm defines balls centered at  $I \in \Lambda_{\square}$  of radius  $r$  by

$$B_r(I) := \{J \in S_{\square} \mid \|I - J\| \leq r\}. \quad (\text{D19})$$

Note that for the  $\ell^{\infty}$ -Norm,  $B_r(I)$  is a rectangular region. For each site  $I \in S_{\square}$ , there is an associated Hilbert space  $\mathcal{H}_I$ . The complete system Hilbert space is given by the tensor product  $\mathcal{H}_{\Lambda_{\square}} = \bigotimes_{I \in S_{\square}} \mathcal{H}_I$ .

The Hamiltonian of interest is of the form  $H = H_0 + V$ , where  $H_0$  denotes the unperturbed Hamiltonian and  $V$  the perturbation. The Hamiltonian  $H_0$  has to satisfy the following properties:

1.  $H_0$  has the form

$$H_0 = \sum_{I \in S_{\square}} Q_I, \quad (\text{D20})$$

such that  $Q_I$  has a constant range of support.

2. The Hamiltonian  $H_0$  satisfies periodic boundary conditions.
3. The Hamiltonian  $H_0$  is *frustration-free*, i.e., if  $P_0$  denotes the projector onto the ground state subspace of  $H_0$  and  $q_{I,0}$  denotes the minimal eigenvalue of  $Q_I$ , then

$$P_0 Q_I = q_{0,I} Q_I. \quad (\text{D21})$$

4. For  $L \geq 2$ , the Hamiltonian  $H_0$  has a spectral gap that is independent of the system size.

In addition,  $H_0$  must satisfy the conditions *local-gap* and *local-TQO*. For a set  $A \subseteq S_{\square}$ , define the localized Hamiltonian by

$$H_0^A := \sum_{\text{supp}(Q_I) \subseteq A} Q_I, \quad (\text{D22})$$

where  $\text{supp}(Q_I)$  denotes the support of the operator  $Q_I$ . Let  $E_0^A$  denote the ground state energy of  $H_0^A$ . For  $\epsilon \geq 0$ , let  $P_A(\epsilon)$  denote the projector onto the eigenstates of  $H_0^A$  with energy less or equal to  $E_0^A + \epsilon$ .

5. The *local-gap condition* then states that there exists a function  $\gamma(r) > 0$ , which decays at most polynomially, such that for all  $I_0 \in S_{\square}$ , it is  $P_{B_r(I_0)}(\gamma(r)) = P_{B_r(I_0)}(0)$ .

To define *local topological quantum order (local-TQO)*, let  $I_0 \in S_\square$  and define the two regions  $A = B_r(I_0)$  and  $A(l) = B_{r+l}(I_0)$  for some  $r \leq L^* < L$  and  $l \leq L - r$ . The parameter  $L^*$  is a cutoff of order  $L$ . For any two ground states  $|\psi_1\rangle$  and  $|\psi_2\rangle$  of  $H_0^{A(l)}$ , define  $\rho_i(A) := \text{Tr}_{\bar{A}}[|\psi_i\rangle\langle\psi_i|]$  (for  $i = 1, 2$ ) as their reduced density matrices when the complement of  $A$  (denoted as  $\bar{A}$ ) is traced out.

6. Then  $H_0$  satisfies local-TQO if and only if

$$\|\rho_1(A) - \rho_2(A)\|_1 \leq 2F(l), \quad (\text{D23})$$

where  $F$  is a decaying function and  $\|\cdot\|_1$  denotes the Schatten-1 norm. Intuitively, local-TQO formalizes the notion that different ground states cannot be distinguished by local observables.

Lastly, the perturbation  $V$  is assumed to have the form

$$V = \sum_{I \in S_\square} \sum_{r=0}^L V_I(r), \quad (\text{D24})$$

such that  $\text{supp}(V_I(r)) \subseteq B_r(I)$  and  $\|V_I(r)\| \leq Jf(r)$  for some constant  $J > 0$  and a rapidly decaying function  $f(r)$ . Here, the norm  $\|\cdot\|$  denotes the operator norm that is induced by the scalar product of  $\mathcal{H}_{\Lambda_\square}$ . A specification of the necessary decay rate of  $f$  is given in Ref. [74]. For our purposes this is irrelevant as we only consider perturbations of finite range (that is,  $f(r)$  can be chosen as 0 for  $r$  larger than some fixed threshold). We refer to a perturbation satisfying the aforementioned conditions as a  $(J, f)$ -perturbation.

This preparation allows us to formulate the gap stability result of Ref. [74].

**Theorem 2** (Michalakis and Zwolak [74]). *Let  $H_0$  be a Hamiltonian that satisfies conditions (1)-(6) and  $V$  be a  $(J, f)$ -perturbation. Then, there exist finite thresholds  $J_0 > 0$  and  $L_0 \geq 2$  such that the gap of  $H$  remains uniformly bounded from below for  $L \geq L_0$  and  $J \leq J_0$ .*

*b. Locality and frustration-freeness of  $\tilde{H}_G(0, \omega)$ .* To apply Theorem 2, we first have to define suitable local Hilbert spaces and a decomposition of the form (D20) of the unperturbed Hamiltonian

$$\tilde{H}_0 \equiv \tilde{H}_G(0, \omega) = H_G^0 + \omega \sum_p (\mathbb{1} - \Theta_p), \quad (\text{D25})$$

such that it is frustration-free. Note that due to the blockade interactions frustration-freeness is a nontrivial property.

To this end, we follow the same procedure as in Ref. [56]. We partition the vertex set  $V_G$  of the blockade graph  $\mathcal{G}$  into unit cells  $V_I$  as shown in Fig. 10. These unit cells consist of the vertex sets associated to two sites from  $S_\circ$  and three links from  $L_\circ$ ; as a consequence, these unit cells form a square-lattice  $\Lambda_\square = (S_\square, L_\square, P_\square)$ . We can view  $L_\square$  as a subset of  $L_\circ$ , where the (vertical) links

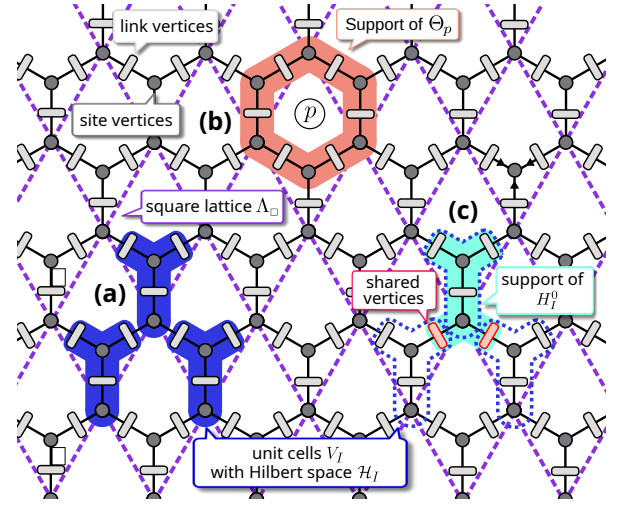


Figure 10. **Coarse graining of the Hamiltonian  $\tilde{H}_0$ .** Summary of the construction of a local, frustration-free decomposition of the Hamiltonian  $\tilde{H}_0$ . The blockade graph is represented by gray circles and light gray rectangles, connected by black lines. The gray circles represent the site vertices, the light gray rectangles represent the link vertices. (a) The vertex set of  $\mathcal{G}$  is partitioned into unit cells  $V_I$ , highlighted in dark blue. These unit cells form a square lattice, indicated by purple dashed lines. neighboring sites in the square lattice contain two-level systems that are in blockade. We associate a Hilbert space  $\mathcal{H}_I$  to each unit cell (the tensor product of the Hilbert spaces of the constituents of  $V_I$ ). (b) The support of the plaquette operator  $\Theta_p$  is highlighted in red. It overlaps with four unit cells. (c) The Hamiltonian  $H_G^0$  is partitioned into local terms  $H_I^0$ . The support of one such operator is highlighted in cyan. Note that the support of this operator contains vertices that belong to the neighboring unit cells of  $V_I$ . These shared vertices are highlighted in red. The blue dotted lines mark the unit cells affected by  $H_I^0$ .

connecting the sites that belong to the same unit cell are removed. Thus our orientation convention for the direction of links in  $L_\circ$  (see Fig. 1) induces an orientation convention for the direction of links in  $L_\square$ . To the unit cells we associate the local Hilbert spaces  $\mathcal{H}_I := \bigotimes_{i \in V_I} \mathcal{H}_i$ , where  $\mathcal{H}_i \simeq \mathbb{C}^2$  denotes the Hilbert space of one two-level-system. Next, we extend the square lattice  $\Lambda_\square$  to a finer lattice  $\tilde{\Lambda}_\square = (\tilde{S}_\square, \tilde{L}_\square, \tilde{P}_\square)$  that has one site for every edge, site and plaquette of  $\Lambda_\square$ . We refer to the set of sites that arise from plaquettes of  $\Lambda_\square$  as  $\tilde{S}_\square^P$ , and the to the set of sites that arise from links as  $\tilde{S}_\square^L$ . This lattice is again endowed with the  $\ell^\infty$ -norm. For  $I \in \tilde{S}_\square^L \cup \tilde{S}_\square^P$ , we associate the local Hilbert spaces  $\mathcal{H}_I \simeq \mathbb{C}$  (i.e., no degree of freedom). This construction is a formality needed to define the local decomposition for  $\tilde{H}_0$ . In summary, the Hilbert space of our system is decomposed as

$$\mathcal{H}_G = \bigotimes_{I \in \tilde{S}_\square} \mathcal{H}_I. \quad (\text{D26})$$

To obtain a local decomposition of the Hamiltonian  $H_G^0$ , we define the vertex set  $\text{Int}(V_I)$  as the subset of  $V_I$

consisting of the vertices on the sites  $s \in S_\square$  that are part of  $V_I$ , and the vertices on the link  $l \in L_\square$  that connects the two sites within  $V_I$ . Moreover, we define  $\partial V_I$  to consist of the vertices on the four links  $l \in L_\square$  that connect a site in  $V_I$  to a site not in  $V_I$ . Be aware that  $\partial V_I \not\subseteq V_I$ . In addition, we define  $\bar{V}_I := \text{Int}(V_I) \cup \partial V_I$ ; see Fig. 10. This allows us to define the local operators

$$H_I^0 := - \sum_{i \in \text{Int}(V_I)} \Delta_i n_i - \sum_{i \in \partial V_I} \frac{\Delta_i}{2} n_i + U_0 \sum_{\substack{i,j \in \bar{V}_I \\ i \sim j}} n_i n_j, \quad (\text{D27})$$

where the notation  $i \sim j$  denotes vertices in  $\mathcal{G}$  that are in blockade.

The induced subgraph of  $\bar{V}_I$  and the weights from Eq. (D27) define a blockade graph  $\mathcal{G}_I$ . The ground state excitation patterns of Eq. (D27), restricted to  $\bar{V}_I$ , are exactly the maximum-weight independent sets (MWIS) of  $\mathcal{G}_I$ . The Hamiltonians  $H_I^0$  are constructed such that the sum  $H_I^0 + H_J^0$  for two adjacent sites  $I, J \in S_\square$  is equivalent to the amalgamation of the blockade graphs  $\mathcal{G}_I$  and  $\mathcal{G}_J$ . Hence

$$H_{\mathcal{G}}^0 = \sum_{I \in S_\square} H_I^0 \quad (\text{D28})$$

is equivalent to the amalgamation of the blockade graphs  $\mathcal{G}_I$  for all  $I \in S_\square$ . Thus the decomposition (D28) is frustration-free if and only if there exists a globally consistent independent set on  $\mathcal{G}$  (see Appendix B 1). Since such sets exist (by construction), Eq. (D28) is a local, frustration-free decomposition of  $H_{\mathcal{G}}^0$ .

To obtain a decomposition of the full Hamiltonian  $\tilde{H}_0$ , we define the local operators

$$Q_I := \begin{cases} \omega(\mathbb{1} - \Theta_p), & I = p \in \tilde{S}_\square^P \\ H_I^0, & I \in S_\square \\ 0, & I \in \tilde{S}_\square^E \end{cases}, \quad (\text{D29})$$

such that

$$\tilde{H}_0 = \sum_{I \in \tilde{S}_\square} Q_I. \quad (\text{D30})$$

First, notice that for all  $I \in \tilde{S}$ ,  $\text{supp}(Q_I) \subseteq B_2(I)$ , i.e., each term has constant range of support. This establishes condition (1) [and (2)] from above.

To show frustration-freeness, note that the ground state energy  $E_0[\tilde{H}_0]$  of  $\tilde{H}_0$  is lower bounded by the sum of the smallest eigenvalues  $q_{0,I}$  of  $Q_I$ , i.e.,

$$E_0[\tilde{H}_0] \geq \sum_{I \in \tilde{S}_\square} q_{0,I}. \quad (\text{D31})$$

Further, note that the operators  $Q_I$  mutually commute, i.e.,  $[Q_I, Q_J] = 0$  for all  $I, J \in \tilde{S}_\square$ . Thus there exists a common eigenbasis for all operators  $Q_I$ . In particular, this implies that it suffices to construct one state that

saturates the bound (D31), because then any other state with  $Q_I |\psi\rangle = q_I |\psi\rangle$  and  $q_I > q_{0,I}$  has strictly larger energy. To this end, consider the state

$$|\omega\rangle := \frac{1}{|\mathcal{L}_{\mathcal{G}}|} \sum_{\mathbf{n} \in \mathcal{L}_{\mathcal{G}}} |\mathbf{n}\rangle. \quad (\text{D32})$$

The operators  $\Theta_p(h)$  define bijective maps  $\mathcal{L}_{\mathcal{G}} \rightarrow \mathcal{L}_{\mathcal{G}}$  for each  $h \in G$ . Hence, applying  $\Theta_p(h)$  to  $|\omega\rangle$  leads to a permutation of the summands, i.e.,  $\Theta_p(h) |\omega\rangle = |\omega\rangle$ . This shows that for every  $I = p \in \tilde{S}_\square^P$ ,  $|\omega\rangle$  satisfies  $Q_p |\omega\rangle = 0$ . As  $\mathbb{1} - \Theta_p$  is a projector, it has eigenvalues 0 and 1 and  $Q_p$  has eigenvalues 0 and  $\omega$ . It follows that  $|\omega\rangle$  is an eigenstate of  $Q_p$  with minimal eigenvalue. Moreover  $|\omega\rangle$  also is an eigenstate with minimal eigenvalue of  $H_I^0$  as it is a linear combination of states in  $\mathcal{H}_{\mathcal{G}}^0$ . Consequently,  $|\omega\rangle$  saturates Eq. (D31) which proves the frustration-freeness of the decomposition (D30); hence condition (3) from above is satisfied.

This construction also shows that  $\tilde{H}_0$  has a spectral gap. To this end, note that for  $I \in S_\square$ ,  $H_I^0$  has a spectral gap of at least  $\min_i(\Delta_i)/2$  [we assume  $\max_i(\Delta_i) \ll U_0$ ] and for  $p \in \tilde{S}_\square^P$ ,  $Q_p$  has a spectral gap of  $\omega$ . Hence if one of the common eigenvectors of the operators  $Q_I$  fails to be a ground state of some operator  $Q_I$ , its energy is increased by at least  $\min\{\min_i(\Delta_i)/2, \omega\}$ , independent of the system size; this establishes condition (4) from above.

The local-gap condition (5) from above can be verified with a similar argument. Here, for  $A = B_r(I_0)$  with  $I_0 \in \tilde{\Lambda}_\square$  and  $r \geq 0$ , we must consider the localized Hamiltonian

$$\tilde{H}_0^A := \sum_{\text{supp}(Q_I) \subseteq A} Q_I. \quad (\text{D33})$$

Moreover, we define the localized Hamiltonian without plaquette fluctuations

$$H_0^A := \sum_{\text{supp}(H_I^0) \subseteq A} H_I^0. \quad (\text{D34})$$

If we denote the set of ground state configurations of  $H_0^A$  as  $\mathcal{L}_{\mathcal{G}}^A$ , the same arguments as above shows that the state

$$|\omega\rangle_A := \frac{1}{|\mathcal{L}_{\mathcal{G}}^A|} \sum_{\mathbf{n} \in \mathcal{L}_{\mathcal{G}}^A} |\mathbf{n}\rangle \quad (\text{D35})$$

is a ground state minimizing the eigenvalue of all operators  $Q_I$  with  $\text{supp}(Q_I) \subseteq A$ , and that the spectral gap is lower bounded by  $\min\{\min_i(\Delta_i)/2, \omega\}$ .

*c. Local-TQO.* To verify the local-TQO condition (6), we show a stronger condition, namely that there exists an  $r$ -independent bound  $l^*$  such that for  $l \geq l^*$ , the reduced density matrices [Eq. (D43) below] are equal. We follow the proof of Cui *et al.* [68, Theorem 3.1] (who proved this condition for the original quantum double models).

Let  $A = B_r(I_0)$  for some  $I_0 \in \tilde{S}_\square$  and  $r \geq 0$ . Moreover, let  $A(l) = B_{r+l}(I_0)$  for  $l \geq 4 =: l^*$ ; these regions are

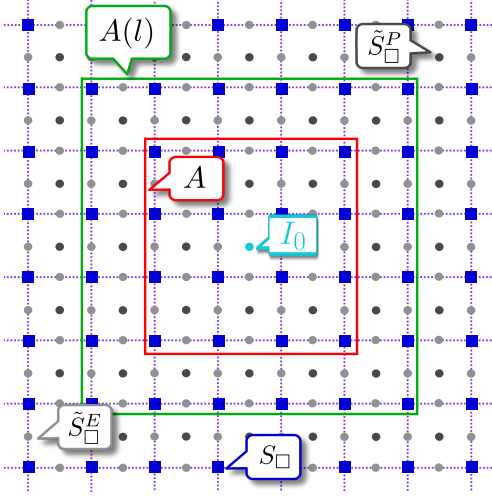


Figure 11. **Setting for local-TQO.** Summary of the construction to verify local-TQO. The blue squares represent the sites of the square lattice  $\Lambda_\square$  and the purple dotted lines its edges. The dark gray (light gray) circles represent the sites of the extended lattice  $\tilde{\Lambda}_\square$  that correspond to plaquettes (edges) of  $\Lambda_\square$ . The boundary of the rectangular region  $A = B_r(I_0)$  is highlighted by a red square, the central site  $I_0$  is highlighted cyan. The boundary of the region  $A(l) = B_{r+l}(I_0)$  is highlighted by a green square. The figure shows the configuration for  $r = 3$  and  $l = 2$ .

shown in Fig. 11. As before,  $\tilde{H}_0^{A(l)}$  denotes the localized Hamiltonian and  $\mathcal{H}_G^{A(l),0}$  its classical ground state manifold for  $\omega = 0$ , spanned by excitation patterns in  $\mathcal{L}_G^{A(l)}$ . For an excitation pattern  $\mathbf{n}$ , we denote its restriction to vertices that are part of some set  $X \subseteq S_\square$  as  $\mathbf{n}|_X$ . This allows us to define the set  $\mathcal{L}_{G,A}^{A(l)} := \{\mathbf{n}|_A \mid \mathbf{n} \in \mathcal{L}_G^{A(l)}\}$ . We indicate excitation patterns of vertices in  $X \subseteq S_\square$  by writing  $\mathbf{n}_X$ .

With these conventions, we find that an arbitrary ground state  $|\omega\rangle \in \mathcal{H}_G^{A(l),\omega}$  can be written as

$$|\omega\rangle = \sum_{\mathbf{n} \in \mathcal{L}_G^{A(l)}} C(\mathbf{n}) |\mathbf{n}\rangle \quad (\text{D36a})$$

$$= \sum_{\mathbf{n}_A \in \mathcal{L}_{G,A}^{A(l)}} |\mathbf{n}_A\rangle_A |\omega_{\bar{A}}(\mathbf{n}_A)\rangle_{\bar{A}}, \quad (\text{D36b})$$

with some coefficients  $C(\mathbf{n}) \in \mathbb{C}$ . These coefficients cannot be arbitrary but have to be chosen such that  $\Theta_p(h)|\omega\rangle = |\omega\rangle$  is satisfied for every plaquette  $p \in A(l)$  and  $h \in G$ . Note that the implicitly defined states  $|\omega_{\bar{A}}(\mathbf{n}_A)\rangle$  are not normalized.

We use Eq. (D36b) to construct a Schmidt decomposition of  $|\omega\rangle$ . To this end, let  $L_{\square,A}$  denote the set of links emanating from sites in  $S_\square \cap A$ . On this finite patch of the square lattice, we can define the quantum double Hilbert space  $\mathcal{H}_{\square G}$  and operators  $A_p(h)$  and  $B_I$  for  $h \in G$  as usual (see Ref. [68]; the  $\square$  in  $\mathcal{H}_{\square G}$  indicates that this is a quantum double on the square lattice). To define

these operators, we use the orientation conventions of  $L_\square$  as induced by our orientation convention on  $L_\square$  (recall Paragraph D 2 b b). For plaquettes with boundary edges that do not belong to  $L_{\square,A}$ , the operators  $A_p(h)$  are still defined as usual on the edges that are part of  $L_{\square,A}$ .

Let  $\mathcal{H}_{\square G,A}^0$  denote the ground state manifold of the quantum double Hamiltonian  $H_{\square G}$  on the square lattice for  $J_p = 0$ . As this Hamiltonian is diagonal in the group basis, we can define  $\mathcal{L}_{\square G,A}$  such that  $\mathcal{H}_{\square G,A}^0 = \text{span}\{|\mathbf{g}_A\rangle \mid \mathbf{g}_A \in \mathcal{L}_{\square G,A}\}$ . The operators  $A_p(h)$  are permutation matrices when represented in the group basis. Thus they induce a group action on  $\mathcal{L}_{\square G,A}$  by  $A_p(h)|\mathbf{g}_A\rangle = |A_p(h) \cdot \mathbf{g}_A\rangle$ . By abuse of notation, we use the same symbol for the operator  $A_p(h)$  and its induced group action on  $\mathcal{L}_{\square G,A}$ .

From the condition  $l \geq 4$  it follows that  $\text{supp}(H_I^0) \subseteq A(l)$  for all  $I \in A$ . Thus the excitation patterns  $\mathbf{n}_A$  are maximum-weight independent sets of the amalgamation of all site structures  $\mathcal{G}_s$  where the site  $s \in S_\square$  is part of a site  $I \in A$ . Hence, by construction, they can be mapped bijectively to ground state configurations of the quantum double on  $L_\square$ . For such configurations on  $L_\square$ , the group elements on the edges in  $L_\square$  uniquely determine the group elements on the remaining (vertical) edges. Thus there exists a bijection  $\zeta : \mathcal{L}_{G,A}^{A(l)} \rightarrow \mathcal{L}_{\square G,A}$ . This bijection satisfies

$$\zeta(\Theta_p(h) \cdot \mathbf{n}_A) = A_p(h) \cdot \zeta(\mathbf{n}_A), \quad (\text{D37})$$

for all  $\mathbf{n}_A \in \mathcal{L}_{G,A}^{A(l)}$ ,  $h \in G$  and  $p \in A(l)$ .

For  $\mathbf{g}_A \in \mathcal{L}_{\square G,A}$ , we denote by  $\mathbf{g}_A|_{\partial A}$  the restriction of this configuration to the links in  $L_{\square,A}$  that cross the boundary between  $A$  and  $\bar{A}$ . Cui *et al.* [68] showed that for any two configurations  $\mathbf{g}_A, \mathbf{g}'_A \in \mathcal{L}_{\square G,A}$  with  $\mathbf{g}_A|_{\partial A} = \mathbf{g}'_A|_{\partial A}$ , there exists  $h_p \in G$ , such that  $A_{\text{int}} := \prod_{p \in A} A_p(h_p)$  satisfies  $\mathbf{g}'_A = A_{\text{int}} \cdot \mathbf{g}_A$ . Note that  $A_{\text{int}}$  acts trivially on the group elements on the boundary of  $A$ . It follows that for any  $\mathbf{n}_A, \mathbf{n}'_A \in \mathcal{L}_{G,A}^{A(l)}$  with  $\zeta(\mathbf{n}_A)|_{\partial A} = \zeta(\mathbf{n}'_A)|_{\partial A}$ , there exists  $h_p \in G$  for  $p \in A$ , such that  $\Phi_{\text{int}} := \prod_{p \in A} \Theta_p(h_p)$  satisfies  $\mathbf{n}'_A = \Phi_{\text{int}} \cdot \mathbf{n}_A$ . As  $|\omega\rangle$  is invariant under  $\Theta_p(h)$  for all  $h \in G$ , it follows that

$$|\omega_{\bar{A}}(\mathbf{n}_A)\rangle_{\bar{A}} = \langle \mathbf{n}_A|_A |\omega\rangle \quad (\text{D38a})$$

$$= \langle \mathbf{n}_A|_A \Phi_{\text{int}}^\dagger |\omega\rangle \quad (\text{D38b})$$

$$= \langle \mathbf{n}'_A|_A |\omega\rangle \quad (\text{D38c})$$

$$= |\omega_{\bar{A}}(\mathbf{n}'_A)\rangle_{\bar{A}}. \quad (\text{D38d})$$

Thus the state  $|\omega_{\bar{A}}(\mathbf{n}_A)\rangle_{\bar{A}}$  only depends on  $\zeta(\mathbf{n}_A)|_{\partial A}$ . Define  $\zeta_{\partial A}(\mathbf{n}_A) := \zeta(\mathbf{n}_A)|_{\partial A}$ , then by abuse of notation, we can denote this state as  $|\omega_{\bar{A}}(\zeta_{\partial A}(\mathbf{n}_A))\rangle_{\bar{A}}$ .

Define the set  $\mathcal{L}_{\square G,\partial A} := \zeta_{\partial A}(\mathcal{L}_{\square G,A}^{A(l)})$  and for  $\mathbf{g}_{\partial A} \in \mathcal{L}_{\square G,\partial A}$ , define  $\mathcal{L}_{G,A}^{A(l)}(\mathbf{g}_{\partial A}) := \{\mathbf{n}_A \in \mathcal{L}_{G,A}^{A(l)} \mid \zeta_{\partial A}(\mathbf{n}_A) = \mathbf{g}_{\partial A}\}$ . Then Eq. (D36b) becomes

$$|\omega\rangle = \sum_{\mathbf{g}_{\partial A} \in \mathcal{L}_{\square G,\partial A}} \mathcal{N}_1(\mathbf{g}_{\partial A}) |\xi_A(\mathbf{g}_{\partial A})\rangle_A |\omega_{\bar{A}}(\mathbf{g}_{\partial A})\rangle_{\bar{A}} \quad (\text{D39})$$

where

$$|\xi_A(\mathbf{g}_{\partial A})\rangle_A := \frac{1}{\mathcal{N}_1(\mathbf{g}_{\partial A})} \sum_{\mathbf{n}_A \in \mathcal{L}_{\mathcal{G},A}^{A(l)}(\mathbf{g}_{\partial A})} |\mathbf{n}_A\rangle_A \quad (\text{D40})$$

and  $\mathcal{N}_1(\mathbf{g}_{\partial A}) := \sqrt{|\mathcal{L}_{\mathcal{G},A}^{A(l)}(\mathbf{g}_{\partial A})|}$ .

We now show that Eq. (D39) is a Schmidt decomposition of  $|\omega\rangle$ . To this end, we must show that the states  $|\omega_{\bar{A}}(\mathbf{g}_{\partial A})\rangle_{\bar{A}}$  are orthogonal and have the same norm.

For orthogonality, suppose that  $\mathbf{g}_{\partial A}$  and  $\mathbf{g}'_{\partial A}$  differ in link  $l$ , i.e.,  $g_l \neq g'_l$ . Let  $I \in S_{\square}$  be the unique site in  $\bar{A}$  from which  $l$  emanates. As  $l \geq 4 = l^*$  (be aware, that this "l" refers to the length that is used to define  $A(l)$  and not to a link.),  $\text{supp}(H_I^0) \subseteq A(l)$ , and therefore every excitation pattern from  $\mathcal{L}_{\mathcal{G}}^{A(l)}$  restricted to  $I$  can be mapped bijectively to group elements on the links emanating from  $I$ . For every excitation pattern  $\mathbf{n} \in \mathcal{L}_{\mathcal{G}}^{A(l)}$ , both  $\mathbf{n}|_A$  and  $\mathbf{n}|_I$  must associate the same group element to link  $l$ , otherwise  $\mathbf{n}$  cannot be a ground state pattern. Suppose  $\mathbf{n}_{\bar{A}}$  is an excitation pattern in the expansion of  $|\omega_{\bar{A}}(\mathbf{g}_{\partial A})\rangle_{\bar{A}}$  and  $\mathbf{n}'_{\bar{A}}$  is an excitation pattern in the expansion of  $|\omega_{\bar{A}}(\mathbf{g}'_{\partial A})\rangle_{\bar{A}}$ . Then  $g_l \neq g'_l$  implies that  $\mathbf{n}_{\bar{A}}|_I \neq \mathbf{n}'_{\bar{A}}|_I$  and thus  $\langle \mathbf{n}_{\bar{A}}|_{\bar{A}} | \mathbf{n}'_{\bar{A}} \rangle_{\bar{A}} = 0$ . As this holds for all excitation patterns in the expansions of the respective states, we have shown the desired orthogonality.

Now we show that all states  $|\omega_{\bar{A}}(\mathbf{g}_{\partial A})\rangle_{\bar{A}}$  for  $\mathbf{g}_{\partial A} \in \mathcal{L}_{\square G, \partial A}$  have the same norm. Cui *et al.* [68] showed that for any two configurations  $\mathbf{g}_{\partial A}, \mathbf{g}'_{\partial A} \in \mathcal{L}_{\square G, \partial A}$ , there exist group elements  $h_p \in G$  such that  $A_{\partial A} := \prod_{p \in \partial A} A_p(h_p)$  satisfies  $A_{\partial A} \cdot \mathbf{g}'_{\partial A} = \mathbf{g}_{\partial A}$ . Here,  $p \in \partial A$  denotes the condition that  $p$  is neither contained in  $A$  nor in  $\bar{A}$ . Eq. (D37), together with the previous paragraph, implies that there exist group elements  $h_p \in G$  such that for  $\mathbf{g}_{\partial A}, \mathbf{g}'_{\partial A} \in \mathcal{L}_{\square G, \partial A}$ , the automorphism  $\Phi_{\partial A} := \prod_{p \in \partial A} \Theta_p(h_p)$  satisfies

$$\mathcal{L}_{\mathcal{G},A}^{A(l)}(\mathbf{g}_{\partial A}) = \Phi_{\partial A} \cdot \mathcal{L}_{\mathcal{G},A}^{A(l)}(\mathbf{g}'_{\partial A}). \quad (\text{D41})$$

We can factor  $\Phi_{\partial A} = \Phi_{\partial A}^A \Phi_{\partial A}^{\bar{A}}$ , where  $\Phi_{\partial A}^A$  acts trivially on vertices in  $\bar{A}$  and  $\Phi_{\partial A}^{\bar{A}}$  acts trivially on vertices in  $A$ . Both of these permutations induce unitary operators on  $\mathcal{H}_{\mathcal{G},A}$  and  $\mathcal{H}_{\mathcal{G},\bar{A}}$  respectively. By abuse of notation, we denote them with the same symbols  $\Phi_{\partial A}^A$  and  $\Phi_{\partial A}^{\bar{A}}$ . Eq. (D41) then implies that  $\Phi_{\partial A}^A |\xi_A(\mathbf{g}'_{\partial A})\rangle = |\xi_A(\mathbf{g}_{\partial A})\rangle$ . In particular, this shows that  $\mathcal{N}_1 \equiv \mathcal{N}_1(\mathbf{g}_{\partial A})$ . Moreover, from  $\Phi_{\partial A} |\omega\rangle = |\omega\rangle$  it follows that

$$|\omega_{\bar{A}}(\mathbf{g}'_{\partial A})\rangle_{\bar{A}} = \langle \xi_A(\mathbf{g}'_{\partial A})|_A |\omega\rangle \quad (\text{D42a})$$

$$= \langle \xi_A(\mathbf{g}'_{\partial A})|_A \Phi_{\partial A}^{\dagger} |\omega\rangle \quad (\text{D42b})$$

$$= \langle \xi_A(\mathbf{g}'_{\partial A})|_A (\Phi_{\partial A}^A)^{\dagger} (\Phi_{\partial A}^{\bar{A}})^{\dagger} |\omega\rangle \quad (\text{D42c})$$

$$= (\Phi_{\partial A}^{\bar{A}})^{\dagger} \langle \xi_A(\mathbf{g}_{\partial A})|_A |\omega\rangle \quad (\text{D42d})$$

$$= (\Phi_{\partial A}^{\bar{A}})^{\dagger} |\omega_{\bar{A}}(\mathbf{g}_{\partial A})\rangle_{\bar{A}}. \quad (\text{D42e})$$

Since  $(\Phi_{\partial A}^{\bar{A}})^{\dagger}$  is unitary, the states  $|\omega_{\bar{A}}(\mathbf{g}_{\partial A})\rangle_{\bar{A}}$  and  $|\omega_{\bar{A}}(\mathbf{g}'_{\partial A})\rangle_{\bar{A}}$  have the same norm; we denote this norm as  $\mathcal{N}_2$  and the states  $1/\mathcal{N}_2 |\omega_{\bar{A}}(\mathbf{g}_{\partial A})\rangle_{\bar{A}}$  are orthonormal.

Consequently, taking the partial trace of Eq. (D39) over  $\bar{A}$  yields

$$\rho_A = (\mathcal{N}_1 \mathcal{N}_2)^2 \sum_{\mathbf{g}_{\partial A} \in \mathcal{L}_{\square G, \partial A}} |\xi_A(\mathbf{g}_{\partial A})\rangle_A \langle \xi_A(\mathbf{g}_{\partial A})|_A. \quad (\text{D43})$$

The only terms in Eq. (D43) that could depend on the state  $|\omega\rangle$  are the normalization constants  $\mathcal{N}_1$  and  $\mathcal{N}_2$ . However, since all states  $|\xi_A(\mathbf{g}_{\partial A})\rangle_A$  are normalized, the condition  $1 = \text{Tr}[\rho_A]$  implies that  $(\mathcal{N}_1 \mathcal{N}_2)^2 = |\mathcal{L}_{\square G, \partial A}|$ , which is independent of  $|\omega\rangle$ .

Thus we have shown that the reduced density matrix  $\rho_A$  is the same for all states  $|\omega\rangle \in \mathcal{H}_{\mathcal{G}}^{A(l), \omega}$ , as desired.

## Appendix E: Wilson loops

In Section III we used the Wilson loop (operator) (13) of the quantum double model

$$\hat{W}^R(\gamma) := \sum_{|\mathbf{g}\rangle \in \mathcal{H}_G} \chi_R(g_\gamma) |\mathbf{g}\rangle \langle \mathbf{g}| \quad (\text{E1})$$

with product  $g_\gamma := \prod_{l \in \gamma} g_l^{\sigma_l}$  along a closed, oriented loop  $\gamma$  on the dual lattice; the sign functions  $\sigma_l$  are defined in Section III (see also Fig. 3).  $\chi_R$  denotes the character of the irreducible representation (irrep)  $R$  of the group  $G$ . Note that in Section III we work with the matrix elements of the operator (E1) in the product basis  $|\mathbf{g}\rangle$  for simplicity.

At the fixpoint of the quantum double phase, the measurement of the Wilson loop operators over all irreps  $\hat{G}$  of the group  $G$  uniquely determines the enclosed flux, independent of the shape of the loop. Here we demonstrate this property by explicitly performing the discrete Fourier transform for class functions

$$\hat{W}^C(\gamma) := \frac{1}{|Z_G(r_C)|} \sum_{R \in \hat{G}} \chi_R^*(r_C) \hat{W}^R(\gamma) \quad (\text{E2})$$

where  $Z_G(r_C)$  is the centralizer of the representative  $r_C \in C$  of conjugacy class  $C \in \text{Cl}(G)$ . Note that  $|Z_G(\cdot)|$  is a class function since centralizers of different representatives are isomorphic via conjugation. By the orbit-stabilizer theorem, we can rewrite the cardinality of the centralizer  $|Z_G(r_C)| = |G|/|C|$  for any  $r_C \in C$ , this makes Eq. (14a) and Eq. (E2) equivalent.

The *completeness* of the character on the set of class functions can be formulated as

$$\sum_{R \in \hat{G}} \chi_R^*(g) \chi_R(h) = |Z_G(g)| \delta_{g \sim h}, \quad (\text{E3})$$

where  $\delta_{g \sim h} = 1$  if  $g$  and  $h$  are conjugate and  $\delta_{g \sim h} = 0$  otherwise. This allows us to rewrite the Fourier transform (E2) as

$$\hat{W}^C(\gamma) = \sum_{|\mathbf{g}\rangle \in \mathcal{H}_G} \delta_{r_C \sim g_\gamma} |\mathbf{g}\rangle \langle \mathbf{g}|; \quad (\text{E4})$$

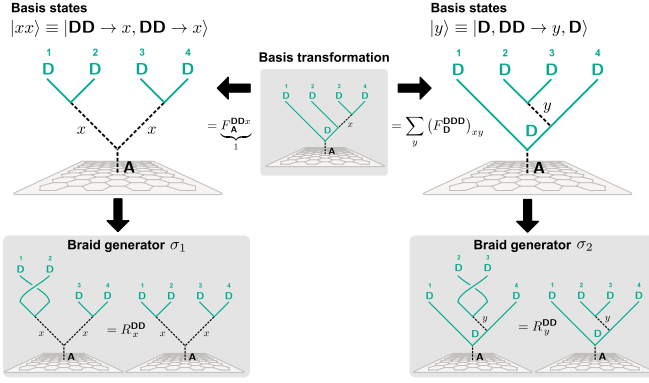


Figure 12. **Basis states and braid group generators.** The fusion basis  $|xx\rangle \equiv |\mathbf{D}\mathbf{D} \rightarrow x, \mathbf{D}\mathbf{D} \rightarrow x\rangle$  of  $\mathcal{H}_{\mathbf{A}}^{\mathbf{D}\mathbf{D}\mathbf{D}\mathbf{D}}$ , which describes four  $\mathbf{D}$ -anyons that fuse into the vacuum  $\mathbf{A}$ , is shown on the left as a splitting diagram. In this basis, the braid generators  $\sigma_1$  and  $\sigma_3$  are diagonal with  $R_x^{\mathbf{D}\mathbf{D}}$ . Another basis  $|y\rangle \equiv |\mathbf{D}, \mathbf{D}\mathbf{D} \rightarrow y, \mathbf{D}\rangle$  is shown on the right. In this basis, the braid generator  $\sigma_2$  is diagonal with  $R_y^{\mathbf{D}\mathbf{D}}$ . The basis transformation between  $|xx\rangle$  and  $|y\rangle$  is performed via two  $F$ -moves: The first is trivial (since  $F_{\mathbf{A}}^{\mathbf{D}\mathbf{D}x} = 1$ ) and the second gives rise to a non-trivial basis transformation via  $F_{\mathbf{D}}^{\mathbf{D}\mathbf{D}\mathbf{D}}$ .

where  $\delta_{r_C \sim g_\gamma} = 1$  if  $g_\gamma \in C$  and zero otherwise; this shows Eq. (14b).

As an example, consider a state  $|C_s\rangle \in \mathcal{H}_{\tilde{G}}^0 \cap \mathcal{H}_{\tilde{G}}^S$  where one flux anyon  $[C, E]$  is pinned on site  $s$ . We consider loops  $\gamma$  that enclose  $s$ . Note that the product  $g_\gamma$  is conserved when reshaping the loop such that it traverses a site without flux anyon (since then  $g_0 g_1 g_2 = 1$  for the group elements on the three emanating links). This allows us to contract the loop  $\gamma$  to enclose only the site  $s$  with the flux anyon. Then  $g_\gamma$  is just the product of the three group elements of its emanating links, which is in  $C$  for all states  $|g\rangle$  in  $|C_s\rangle$ . Then  $\langle C_s | \hat{W}^R(\gamma) | C_s \rangle = \chi_R(r_C)$  for some representative  $r_C \in C$  (as proposed in Section III) and  $\langle C_s | \hat{W}^{C'}(\gamma) | C_s \rangle = \delta_{C', C}$  is nonzero only for  $C' = C$ .

## Appendix F: Braiding in $\mathcal{D}(S_3)$

The braid group  $B_4$ , which describes the world lines of four anyons that start and end aligned on a row at fixed positions, is generated by three operations:  $\sigma_1$  exchanges the first anyon with the second,  $\sigma_2$  the second anyon with the third, and  $\sigma_3$  the third with the fourth. We define these exchanges with an anti-clockwise orientation, as shown in Figs. 5 and 12. In Section IV we introduced the basis  $|xx\rangle \equiv |\mathbf{D}\mathbf{D} \rightarrow x, \mathbf{D}\mathbf{D} \rightarrow x\rangle$  of the fusion space  $\mathcal{H}_{\mathbf{A}}^{\mathbf{D}\mathbf{D}\mathbf{D}\mathbf{D}}$  which contains the states with four  $\mathbf{D}$ -anyons that fuse into the vacuum  $\mathbf{A}$ . The fusion algebra of  $\mathcal{D}(S_3)$  allows for  $x \in \{\mathbf{A}, \mathbf{C}, \mathbf{F}, \mathbf{G}, \mathbf{H}\}$ , i.e., the first two anyons fuse into  $x$  and the remaining two anyons also fuse into  $x$ , which finally fuse into the vacuum  $\mathbf{A}$ , see Fig. 12. The fusion outcome of both pairs must be equal because those fuse into the vacuum and in  $\mathcal{D}(S_3)$  all anyons are their

own antiparticle. It follows that  $\dim \mathcal{H}_{\mathbf{A}}^{\mathbf{D}\mathbf{D}\mathbf{D}\mathbf{D}} = 5$ , which reflects the non-abelian nature of the  $\mathcal{D}(S_3)$  anyon theory.

Braiding anyons effects unitary operations on  $\mathcal{H}_{\mathbf{A}}^{\mathbf{D}\mathbf{D}\mathbf{D}\mathbf{D}}$ . Due to locality, the representations of the two braid generators  $\sigma_1$  and  $\sigma_3$  are diagonal in the basis  $|xx\rangle$  (braiding two anyons cannot change their fusion channel):

$$\sigma_1 : |xx\rangle \mapsto R_x^{\mathbf{D}\mathbf{D}} |xx\rangle, \quad (\text{F1a})$$

$$\sigma_3 : |xx\rangle \mapsto R_x^{\mathbf{D}\mathbf{D}} |xx\rangle, \quad (\text{F1b})$$

with  $R_x^{\mathbf{D}\mathbf{D}} \in \mathbb{C}$  the  $R$ -matrices (phases) for braiding two  $\mathbf{D}$ -anyons that are in fusion channel  $x$ . For the quantum double  $\mathcal{D}(S_3)$ , one finds [66]

$$R_{\mathbf{A}}^{\mathbf{D}\mathbf{D}} = R_{\mathbf{C}}^{\mathbf{D}\mathbf{D}} = R_{\mathbf{F}}^{\mathbf{D}\mathbf{D}} = -1, \quad (\text{F2a})$$

$$R_{\mathbf{G}}^{\mathbf{D}\mathbf{D}} = -\bar{\omega}^2, \quad (\text{F2b})$$

$$R_{\mathbf{H}}^{\mathbf{D}\mathbf{D}} = -\bar{\omega}, \quad (\text{F2c})$$

with  $\bar{\omega} = e^{2\pi i/3}$ . Note that the last two equations implicitly define which anyons we call  $\mathbf{G}$  and  $\mathbf{H}$ . This was not yet fixed since we did not specify the representations  $\Gamma_{R_1}$  and  $\Gamma_{R_2}$  in Section IV.

The braid generator that allows us to probe the non-abelian statistics is  $\sigma_2$  – which is *not* diagonal in the  $|xx\rangle$  basis since the fusion channel of anyon 2 and 3 is not determined in this basis. We denote the basis of  $\mathcal{H}_{\mathbf{A}}^{\mathbf{D}\mathbf{D}\mathbf{D}\mathbf{D}}$  in which anyon 2 and 3 fuse into  $y \in \{\mathbf{A}, \mathbf{C}, \mathbf{F}, \mathbf{G}, \mathbf{H}\}$  as  $|y\rangle \equiv |\mathbf{D}, \mathbf{D}\mathbf{D} \rightarrow y, \mathbf{D}\rangle$ . The anyon  $y$  then fuses with the fourth  $\mathbf{D}$ -anyon into  $\mathbf{D}$ , which finally fuses with the first  $\mathbf{D}$ -anyon into the vacuum, see Fig. 12. (The fusion channel of  $y$  with the fourth  $\mathbf{D}$ -anyon must be  $\mathbf{D}$  because this is the only way to fuse the first  $\mathbf{D}$ -anyon into the vacuum  $\mathbf{A}$ .)

Again due to locality, in this basis the unitary representation of the braid generator  $\sigma_2$  is diagonal:

$$\sigma_2 : |y\rangle \mapsto R_y^{\mathbf{D}\mathbf{D}} |y\rangle. \quad (\text{F3})$$

The basis change from  $|xx\rangle$  to  $|y\rangle$  is achieved by two  $F$ -moves, see Fig. 12, where the first move is trivial because  $F_{\mathbf{A}}^{\mathbf{D}\mathbf{D}x} = 1$ . Consequently, the basis transformation is determined by the matrix  $F_{\mathbf{D}}^{\mathbf{D}\mathbf{D}\mathbf{D}}$ ,

$$|xx\rangle = \sum_y (F_{\mathbf{D}}^{\mathbf{D}\mathbf{D}\mathbf{D}})_{xy} |y\rangle, \quad (\text{F4})$$

with  $F$ -matrix given by [66]

$$F_{\mathbf{D}}^{\mathbf{D}\mathbf{D}\mathbf{D}} = \frac{1}{3} \begin{pmatrix} 1 & \sqrt{2} & \sqrt{2} & \sqrt{2} & \sqrt{2} \\ \sqrt{2} & 2 & -1 & -1 & -1 \\ \sqrt{2} & -1 & 2 & -1 & -1 \\ \sqrt{2} & -1 & -1 & -1 & 2 \\ \sqrt{2} & -1 & -1 & 2 & -1 \end{pmatrix}. \quad (\text{F5})$$

Here, the order of the basis states is given by  $\{\mathbf{A}, \mathbf{C}, \mathbf{F}, \mathbf{G}, \mathbf{H}\}$ . Note that  $(F_{\mathbf{D}}^{\mathbf{D}\mathbf{D}\mathbf{D}})^2 = \mathbb{1}$ , so that the inverse transformation from basis  $|y\rangle$  to  $|xx\rangle$  is also given by  $F_{\mathbf{D}}^{\mathbf{D}\mathbf{D}\mathbf{D}}$ .

This allows us to express the matrix  $U_{\sigma_2}$ , which represents the braid generator  $\sigma_2$  in the basis  $|xx\rangle$ , by first changing to the basis  $|y\rangle$ , then performing the braid  $R_y^{\mathbf{DD}}$ , and finally switching back to the basis  $|xx\rangle$ :

$$U_{\sigma_2} = F_{\mathbf{D}}^{\mathbf{DDD}} \cdot R^{\mathbf{DD}} \cdot F_{\mathbf{D}}^{\mathbf{DDD}} \quad (\text{F6})$$

with the diagonal matrix  $(R^{\mathbf{DD}})_{xy} = \delta_{xy} R_y^{\mathbf{DD}}$ ; this yields [66]

$$U_{\sigma_2} = -\frac{1}{3} \begin{pmatrix} 1 & \sqrt{2} & \sqrt{2} & \sqrt{2}\bar{\omega} & \sqrt{2}\bar{\omega}^2 \\ \sqrt{2} & 2 & -1 & -\bar{\omega} & -\bar{\omega}^2 \\ \sqrt{2} & -1 & 2 & -\bar{\omega} & -\bar{\omega}^2 \\ \sqrt{2}\bar{\omega} & -\bar{\omega} & -\bar{\omega} & -\bar{\omega}^2 & 2 \\ \sqrt{2}\bar{\omega}^2 & -\bar{\omega}^2 & -\bar{\omega}^2 & 2 & -\bar{\omega} \end{pmatrix}. \quad (\text{F7})$$

Applying this operation on our initial state

$$\langle xx|AA\rangle = (1 \ 0 \ 0 \ 0 \ 0)^T \quad (\text{F8})$$

leads to the result in Eq. (22) of the main text (up to a global phase).